ATF Report 2020

Alexander Aryshev[3], Philip Bambade[2], Douglas Bett[5], Laurent Brunetti[4], Philip Burrows[5], Vera Cilento[1], Angeles Faus-Golfe[2], Pavel Karataev[6], Pierre Korysko[5], Kiyoshi Kubo[3], Shigeru Kuroda[3], Andrea Latina[1], Alexey Lyapin[6], Takashi Naito[3], Toshiyuki Okugi[3], Andrii Pastushenko[1], Rebecca Ramjiawan[5], Nobuhiro Terunuma[3], Rogelio Tomas Garcia[1], and Renjun Yang[1]

On behalf of the ATF International Collaboration

[1]CERN, European Organization for Nuclear Research, Geneva, Switzerland
[2]IJCLab, Laboratoire de Physique des 2 infinis Irène Joliot-Curie, Orsay, France
[3]KEK, High Energy Accelerator Research Organization, Tsukuba, Japan
[4]LAPP, Laboratoire d'Annecy de Physique des Particules, Annecy, France
[5]John Adams Institute, University of Oxford, Oxford, UK
[6]John Adams Institute, Royal Holloway University of London, Egham, UK

Abstract

The KEK accelerator test faciliry (ATF) conducts R&D on a beam for the Linear Collider. The damping ring provides a low emittance electron beam and the final focus test beamline (ATF2) provides studies on small beam of nanometer level by utilizing a low emittance beam. These R&D are conducted under the ATF international collaboration with many contributions of graduate students around the world.

A review meeting to discuss the further studies at ATF will be held on September 29, 2020 as a short tele-conference. This report provides the information necessary for discussion.

We summarize the remaining studies that will be done in the coming years and ILC preparatory period for further improvements of nanometer beam technology, and the use of ATF facility as a test bench for ILC subsystem in the preparatory period and after. The possible utilizations of the ATF/ATF2 beams for R&D beyond Linear Colliders are also presented.

Submitted on August 31, 2020 as material for the ATF Review Meeting.

Contents

1 Introduction

1.1 Overview of ATF/ATF2

In linear colliders (LCs), e.g., the International Linear Collider (ILC) [1, 2] and the Compact Linear Collider (CLIC) [3–5], beams collide only once at the Interaction Point (IP), unlike circular accelerators where beams intersect every turn. Therefore, it is very important for linear colliders to make the collision beam size as small as possible to increase the luminosity. There are two essential systems to achieve this small beam sizes. The first is a damping ring (DR) that produces a low emittance beam, and the second is a final focus system (FFS) just before the IP. It is very important to investigate the beam optics for the FFS and its tuning procedures in the presence of realistic imperfections. In order to explore these technologies, the Accelerator Test Facility (ATF) with DR was constructed in KEK [6], and upgraded to incorporate the FFS test beamline (ATF2) [7, 8]. Therefore, in general, ATF is the name of the entire facility, but when used in distinction from ATF2, for convenience, ATF refers to the upstream part containing the DR, and ATF2 refers to the part after the DR, especially the final focus test beamline. The focal point of ATF2 is also referred to as "IP" in relation to LCs.

ATF is a very unique facility internationally, providing low emittance beam for R&D and developing nanometer beam technology. Figure 1 shows the current configuration of ATF.
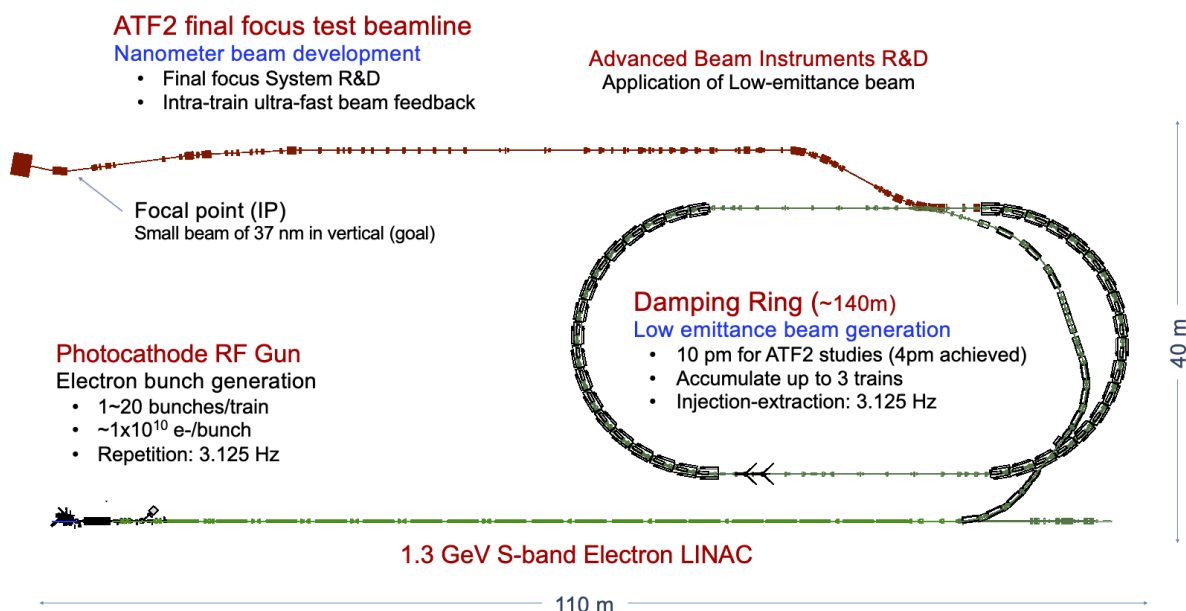
Figure 1: Schematic configuration of the KEK accelerator test facility.

The ATF was designed and constructed in the early 1990s to investigate the issues associated with the multi-bunch beam for the normal conducting linear colliders of the time. It started operation in 1996 with a thermionic gun electron source, 1.3 GeV S-band linac, damping ring (DR) and extraction line. Here, the design emittance of the DR is comparable to that of the current ILC and is still being used effectively. In the construction and upgrade of the ATF, SLAC and FNAL have made significant in-kind contributions to the DR injection/extraction kicker system and the DR high resolution BPM readout system, respectively, through the US-Japan Science and Technology Cooperation Program in High Energy Physics. In 2002, a thermionic gun was replaced by a photocathode RF gun. It improved the beam injection to the DR significantly, then enabled an effective development of the low emittance beam. The low emittance beam of 4 pm in vertical had been successfully demonstrated in 2003. Details of the DR emittance tuning are described in Sec. 4.1. This low emittance property at ATF is a valuable

tool for advanced R&D; i.e., it leads the development of sub-micron resolution beam-size and beam-position monitors, and also enables studies on the FFS.

In 2001, a local chromaticity correction scheme for the final focus system of future linear colliders was proposed [9]. It has advantages of a shorter beamline and wider energy bandwidth compared to that of previous studies at FFTB [10]. The ILC FFS is designed using this local chromaticity correction optics. Since the ILC uses superconducting technology for beam acceleration to efficiently accelerate more than 1000 bunches with one RF pulse, the RF frequency used for the ILC beam acceleration is 1.3 GHz, and the effective bunch length for the beam acceleration is several hundreds of microns (300 μm for ILC design). The β function at the collision point is specified to be comparable to the bunch length to minimise luminosity reduction by the hourglass effect. The ATF2 beamline has the same magnet arrangement as the ILC FFS, targeting similar tuning difficulties by keeping the same chromaticity and excluding effects from synchrotron radiation (details in Sec. 4.2.1.2). On the other hand, the CLIC is considering beam acceleration using normal conducting technology at high frequency RF (12 GHz) to achieve a high accelerating gradient. Therefore, the bunch length for efficient beam acceleration in CLIC is several tens of microns (44 μm for 3 TeV operation), which is shorter than ILC, and the β function at the IP can be smaller than ILC. However, the smaller β function at the IP increases aberrations like chromaticity and it makes the beam tuning more difficult. Hence, the ATF is also testing the beam optics with larger aberrations than ILC to study the beam optics tuning for CLIC (details in Sec. 4.2.1.4). The techniques for the larger aberration control are of interest also for the ILC for a robust IP beam size control and to allow for a possible reduction of the β^* from the current 410 μm closer to the bunch length value of 300 μm. Parameters of the final focus system for ATF2, ILC and CLIC are listed in Table 1.

Table 1: The major FFS parameters for ATF2, in comparison with the ILC and CLIC designs. L^* is the distance between the last quadrupole and IP, ξ_y the vertical chromaticity, ε_y the vertical emittance, σ_E the energy spread and σ_y^* the IP vertical beam size.

	ATF2 nominal	ATF2 ultra-low β^*	ILC (500 GeV)	CLIC (3 TeV)
L^* [m]	1	1	$(3.5/4.5)^a$	6
β_x^* [mm]	4 $(40)^b$	4 $(100)^c$	11	7
β_y^* [mm]	0.1	0.025	0.48	0.12
$\xi_y \sim L^*/\beta_y^*$	10000	40000	$(7300/9400)^a$	50000
ε_y [pm.rad]	12	12	0.07	0.003
σ_E [%]	0.08	0.08	$(0.07/0.12)^d$	0.3
$\sigma_{y,\text{design}}^*$ [nm]	37	23	5.9	0.9
$\sigma_{y,\text{measured}}^*$ [nm]	$42.3\pm2.7^b/41.1\pm0.7^{b,e}$	50.1 ± 0.6^c	-	-

[a] SiD/ILD detector configurations.

[b] Optics with loosen β_x, $10\beta_x^*$.

[c] Optics with loosen β_x, $25\beta_x^*$.

[d] Positron/electron beam of ILC.

[e] Results achieved with beam stabilization in two-bunch mode.

In 2005, the ATF International Collaboration was established to cooperate in the technical research and development of the final focus system of the future linear collider [8]. Details of the Collaboration are described in Appendix A. Under this collaboration, the ATF2 beamline was constructed based on the design of the ILC final focus system, and the beam size at the focus point was targeted to be 37 nm. KEK led the construction and was in charge of the base components, such as floor refurbishment, cooling system, radiation shields, beam dump, beampipes including stripline BPMs and so on. The extraction line was reconstructed and connected to the ATF2 final focus beamline. Alignment of the entire beamline was also done by KEK. The nanometer beam size monitor at the IP (IPBSM in Sec. 4.2.1.2) was

installed by the Unversity of Tokyo and KEK. Overseas institutes provided a number of valuable in-kind contributions for the ATF2. SLAC provided readout electronics for the stripline BPMs and Cavity BPMs, sextupole magnets, quadrupole magnets with cooperation from IHEP, magnet movers used at FFTB, and the power supply system for the final focus magnets. Here for the cavity BPMs (in Sec. 4.4.2.1), PAL provided all BPMs and RHUL contributed the development of the readout system. IHEP also provided dipole magnets. CERN provided octupole magnets. A special honeycomb table and rigid supports to minimise mechanical vibration of the final double magnets, and ground motion sensors 4.3.3) were provided by LAPP. A movable low impedance collimator was provided by IFIC and LAL (in Sec. 4.4.3). Several types of beam profile monitors have been installed, for example, multi-OTR system by IFIC and SLAC, Laser wire monitor by RHUL (in Sec. 4.4.4), OTR/ODR/ChDR monitor by RHUL and CERN (in Sec. 4.4.5). For the study of beam position stabilization, the intra-train feedback system was installed by the University of Oxford (in Sec. 4.2.3), and the cavity BPM equipment for IP was provided by Korea University and LAL (in Sec. 4.4.2.2).

The ATF2 started commissioning in 2009 but suffered interruptions following an accident in the Linac modulator and the Great East Japan Earthquake in 2011. Beam operation resumed at ATF/ATF2 in 2012 thanks to major efforts at KEK together with its international collaborators. The progress of the ATF2 beamline commissioning was dependent on the commissioning of several beam monitors, e.g. the cavity BPMs distributed along the beamline and the nanometer beam size monitor at the IP (IPBSM). In particular, the capability to achieve small beams at the IP was closely linked to the progress developing the IPBSM, and vice versa.

Through small beam studies, it was found that the beam size at the IP has a large beam intensity dependence in ATF2. An international review of the ATF2 program was held in 2013 and proposed to distinguish between beam focusing studies and wakefields. The latter is produced by a change in the internal cross section of the beam pipe in the beamline and is independent of the focusing optics. The minimum beam size of 41 nm, obtained as the upper limit by the IPBSM, was achieved at a beam intensity of 0.7×10^9 electrons/bunch in 2016 in cooperation with the position stabilization by an intra-train feedback system (See Sec.4.2.1.3), while the design value is 37 nm with 1×10^{10} electrons/bunch. Numerous studies of wakefield effects on the small beam have been conducted to evaluate and understand the effect for LCs (details in Sec. 4.2.2). In parallel to the optics and the tuning method studies for ILC, the ultra-low beta* optics studies have been conducted for CLIC [11] (details in Sec. 4.2.1.4). These studies are complementary both for ILC and CLIC.

1.2 Goals

The ATF/ATF2 had been designed and constructed to provide a test bed for development of instrumentation and accelerator physics ideas, train the next generation of accelerator physicists and promote truly international collaboration building and operating a facility. In the ATF2 proposal, two major goals were defined as follows:

- I. Achievement of 37 nm beam size
  - Demonstration of a compact final focus system based on local chromaticity correction
  - Maintenance of the small beam size
- II. Control of beam position
  - Demonstration of beam orbit stabilization with nano-meter precision at the IP
  - Establishment of beam jitter controlling techniques at the nano-meter level with an ILC-like beam

The small beam size of 41 nm at the ATF2 IP was successfully achieved with an intra-train orbit feedback (FONT) in 2016 (see Sec. 4.2.1.3). This demonstrates the functionality of a compact final

focus system based on local chromaticity correction and the practical effectiveness of intra-train orbit feedback. This small beam was realized under lower beam intensity because of the significant impact of wakefields on the IP beam size. Since the wakefields depend on the internal geometric structure of the beamline, it was suggested to distinguish the wakefield issues of the ATF2 beamline from the proof of the final focus system [12]. The wakefield effect on small beam becomes the important study target as like "the third goal" of ATF2.

– (III.) Investigate wakefield effects on the small beam

The second goal, control of the beam position, aims at a direct measurement of beam position stabilization at the IP. To realize this resolution at ATF2 IP, the higher bunch intensity about 1×10^{10} electrons/bunch is required while it is limited for a small beam by wakefield. In addition, the development of nanometer BPM with a fast signal decay for multi-bunch beam is also required. However, this challenging BPM is needed only for studies aimed at the direct monitoring of stabilization at the ATF2 IP, and is not required for ILC. Although the development of the nanometer resolution BPM has been continued step by step, it is a challenging task and not easy to reach the desired resolution in a timely manner. A complementary approach to beam position stabilization has been conducted using the FONT feedback setups located upstream in the ATF2 beamline and at the IP. These show acceptable stabilization performance for ILC.

1.3 Contribution to education of young researchers

Education for graduate students and young staff is one of the important roles of the ATF international Collaboration. Since many research and development activities such as beam diagnostic equipment and beam control technology are being carried out at ATF, a significant number of people including graduate students have been participated. They visit KEK several times a year, repeat it for years, and carry out research and development in doctoral programs. Over 60 students earned a PhD through ATF research. Figure 2 shows the number of PhDs by year and country of institution. Most of them are based at KEK and overseas research institutes and universities. The ATF international Collaboration makes a significant contribution to the education of young researchers.
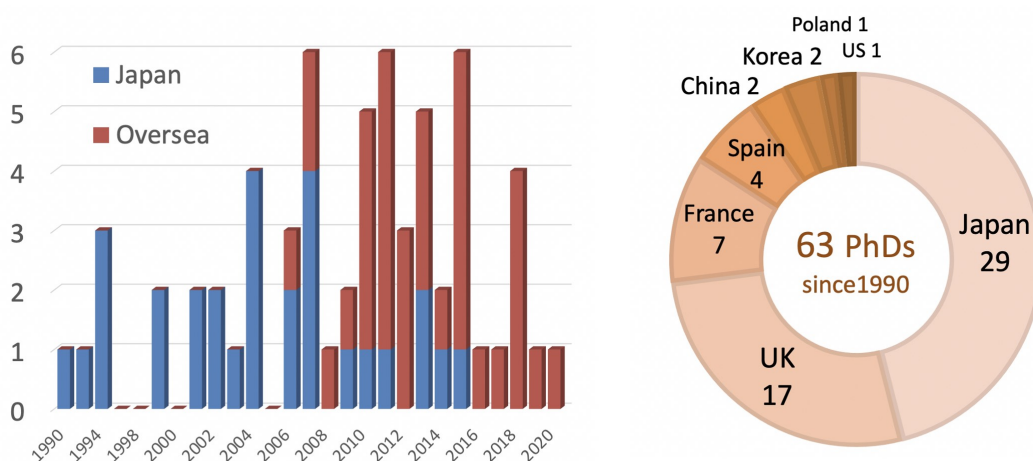

Figure 2: Number of PhDs from ATF research activities.

1.4 Availability of ATF beams

The ATF has been operated with the series of a few beam-weeks and a maintenance week, except for a longer summer shutdown from July to September. This interlaced maintenance week is effective for the preparatory work of R&D, i.e., installation and improvement of devices for the coming beam studies. Every beam week starts from Monday afternoon or evening and continues to Friday evening. There is no beam on weekends due to the limited number of ATF staff responsible for safety and hardware maintenance during beam operation. Weekends are used to prepare for next week studies.

In recent years, the number of beam operation weeks has been limited due to the rise of electricity prices resulting from the 2011 Great East Japan Earthquake, while it was about 21 weeks per year until then. A significant decrease happened since 2014 as shown in Fig. 3. To ameliorate this difficulty, CERN contributed to the operation of ATF with the cooperation of the budget through the collaborative research contract between CERN and KEK. The contribution was repeated in four fiscal years and could extend the beam operations by about two weeks each year. In 2019, the situation became even more difficult as operations were limited to 10 weeks. In this year, 2020, five weeks are approved so far, with additional beam weeks possible by the end of March 2021 will be determined, taking into account the recommendation of this ATF review.
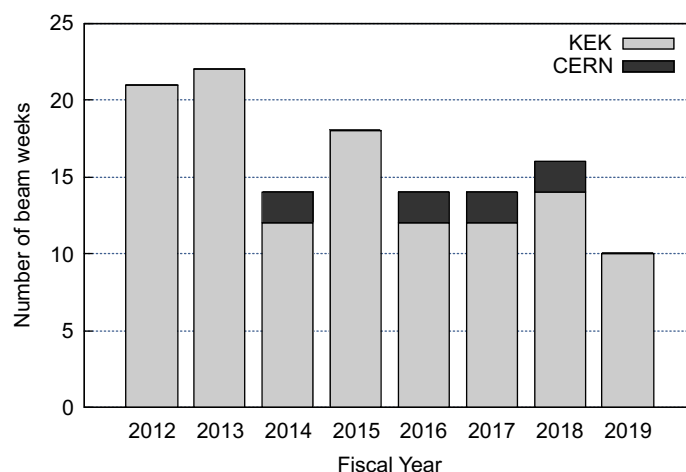

Figure 3: History of ATF operation weeks.

The history of the number of people who have visited ATF and participated in R&D is shown in Figure 4 (a). It represents a major contribution to the construction of the ATF2 beamline by 2009, and subsequent commissioning in 2010. In 2011, the number of visiting researchers decreased because of the completion of the setting-up the beamline devices, and in addition, a suspension of operations due to the Great East Japan Earthquake. The beam operation was fully resumed in 2012 by the collaborative recovery with overseas researchers. Most Japanese researchers shown in Fig. 4 (a) are graduate students from Japanese universities. Unfortunately the number has decreased with time because of lower availability of students from the universities. Although the number of Japanese students has reduced, the number of participants from overseas did not change so much until 2016, but after that it has decreased as the beam operation period has reduced.

Figure 4 (b) shows the history of FTE per day of the staff supporting ATF operations. The FTE of KEK staff dedicated to ATF is almost constant but it is not sufficient to manage the whole ATF accelerator system which consists of the LINAC, DR and ATF2 beamline. Therefore the support by outsourced staff is essential to keep ATF running; however it is becoming increasingly difficult to keep the number of such staff because of budget limitations. In addition, contributions by KEK staff from other LC subgroups are also decreasing because of the work increasing at the Superconducting RF Test Facility (STF) at KEK.

8

Keeping the current manpower is an important and serious issue for future ATF operations.

(a) Researchers visiting for ATF programs

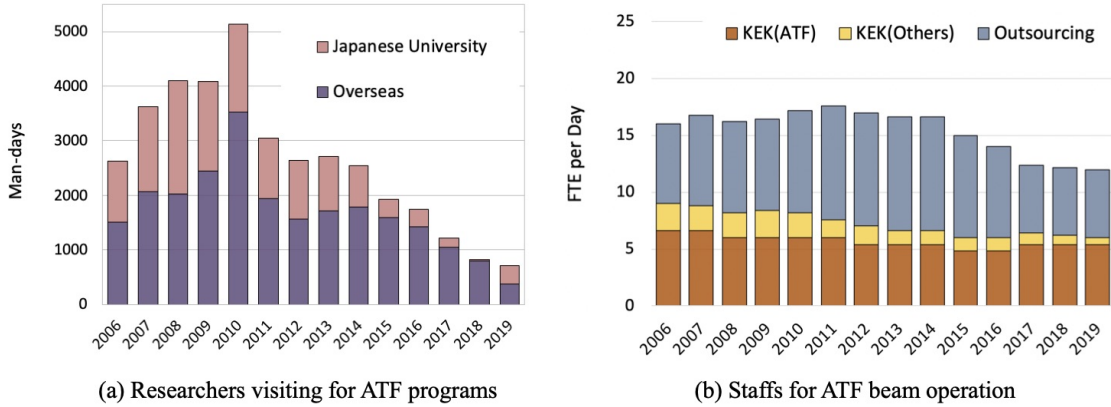(b) Staffs for ATF beam operation

Figure 4: Manpower profile for the ATF beam operation.

The ATF has a history of more than 25 years since its construction, and it is essential to deal with aging. However, it is difficult to secure all of the maintenance cost and the reduced budget limits the operating time. At this point, in the unlikely event of a serious failure, the beam will be out of service for half a year to a year. The procurement of particularly expensive and long-lead-time key components such as the LINAC high power RF source (Klystron) is a top priority but has been postponed in recent years. Also, some specialized devices are out of production due to outdated technology or low demand, requiring not only component replacements, but complete system updates including power supplies and control system. It also includes critical systems such as damping ring RF power source, and beam injection/extraction kicker systems. Assuming that the ATF will be operational for several years, these measures should be done with the help of experts from other accelerator groups, as was done during the construction of the ATF.

1.5 Beam structure for R&D

Here we describe the beam structure at ATF for discussions in later sections. A beam available at ATF/ATF2 is generated by the photocathode RF gun. It consists of multi-bunches (train) from single to 10 bunches with 5.6 ns spacing by controlling the number of laser pulses generated by the 178.5 MHz laser system. The bunch intensity up to 1×10^{10} electrons/bunch, which is controlled by the laser power, is provided in recent studies. Another multi-bunch beam up to 20 bunches with 2.8 ns spacing is available when the 357-MHz laser system is used. A beam is accelerated by the S-band Linac up to 1.3 GeV, then injected into the DR, and finally extracted and delivered to the ATF2 beamline. The repetition rate of this process is 3.1 Hz. Most of ATF2 studies are carried out with a single bunch and an intensity between 0.1 and 1×10^{10} electrons/bunch.

Another beam structure for ATF2 is a train comprising up to three bunches with a bunch spacing of up to c. 150 ns (the ILC bunch spacing is 554 ns) is provided for intra-train feedback studies (FONT). In this scheme, up to three bunches are stored in the DR and extracted to the ATF2 beamline simultaneously by using a 300 ns-long kicker pulse. The beam extraction rate of this scheme is 1.56 and 1.04 Hz for 2 and 3 bunch modes, respectively.

Further, we have a special multi-bunch beam extraction scheme from the DR by using the fast kicker system which is described in Sec. 4.4.1. In this scheme, the extraction of 30 bunches with 308 ns bunch spacing had been successfully demonstrated. However, the beam current stored in the DR had to be reduced because of a limitation caused by the configuration of the fast kicker system which is

geometrically constrained by the design for the original conventional kicker magnet. This intensity does not suit other studies so that this configuration is used only for the fast kicker study.

2 Remaining studies planned for the next few years

Our main study items in the near future are:

– Study of higher order aberrations and corrections (non-linear knobs)
– Study of intensity dependence (wakefield)
– Improvement of IPBSM laser system
– Stabilizing beam orbit and reducing beam jitter

2.1 Study of 2nd order aberrations and corrections

We have established a tuning procedure for the linear optics using a set of "linear knobs" and been able to confirm small beam sizes at the IP of about 40 nm in 2014-2016, which is almost the original design value (37 nm). However, this has been achieved with the $10 \times \beta_x^*$ optics, which is less sensitive to higher order aberrations than the nominal. While dedicated "non-linear knobs", defined in terms of orthogonal sets of strength changes of both regular and skew sextupole magnets, were successfully integrated into the experimental tuning procedure used to produce very small beam sizes at ATF2, systematic measurement and correction of the main higher order aberrations have not been fully demonstrated yet. Since it is hard to predict higher order magnetic field errors in the ILC final focus beam line, confirming the effectiveness of such non linear corrections is a very important task.

Also, the energy bandwidth of the final focus, which is an important quantity characterising the performance of the system, should be measured accurately and compared with calculations to enable a reliable assessment of the expected performance of ILC.

Moreover, there are different optics that enhance the effects of aberrations and that could be the subject of future studies. These are, besides the nominal ATF2 design with a nominal β_x^* value, the ultra-low β^* optics and an alternative lattice with longer L^* (the drift between the last quadrupole and the IP). The latter has the advantage of increased aberration levels for the same vertical beam size, which would be interesting in case of limitations of the IPBSM for beam sizes lower than 40 nm.

(See 4.2.1.3 for details.)

2.2 Study of intensity dependence (wakefield)

Though the wakefield effect at the ILC final focus is expected to be much weaker than at ATF, further investigation of the intensity dependence of the beam size is necessary. Experimental study at ATF will improve the reliability of our calculations of wakefields and their effects. Also it will give important information for the design of the ILC beamline.

Studies so far have shown qualitative agreement of our observations and simulations/calculations. However, quantitatively, the observed intensity dependence is significantly stronger than the expectation. We will investigate possible, yet unknown, wakefield sources in the beam line. For example, accurate data of correlations between beam orbit, intensity and beam size at IP will be used to specify major wakefield sources.

It should be noted that the possibility of other effects causing beam size intensity dependence has not been completely excluded. For example, higher order chromatic or/and geometric aberrations should also be studied as possible causes of the intensity dependence.

(See 4.2.2.8 for details of the intensity dependence studies.)

2.3 Stability

Studies described above have not completed yet, because after 2016, conditions eventually deteriorated and we have not been able to reproduce the smallest beam size. For these studies, beam size dependence on various conditions should be measured precisely. The stability of the incoming beam and beam position/size monitors is crucial for such measurements.

We have often experienced unstable, fluctuating measured beam sizes, affecting the beam tuning performance. Unstable condition of the laser for the beam size monitor at IP (IPBSM) is suspected to be one of the major reasons. We also observed beam orbit drift and orbit jitters which could affect the stability and accuracy of measurements.

2.3.1 Stabilizing IPBSM

For precise beam size measurement, a new laser system may be needed, which requires a significant budget. However, it is worthwhile trying to stabilize the present laser. We have also started testing another available laser this year (2020). The IPBSM performance will be tested and confirmed using small and stable beam. (See sections 4.2.1.2 for details of IPBSM.)

2.3.2 Stabilizing beam orbit and reducing beam jitter

2.3.2.1 Slow orbit drift

(See 4.3.4 for details): The stability of magnets in the beam line was checked and some problems of magnet power supplies were cured. However, correlation between monitored applied currents to magnets and the beam orbit could not be clearly seen. And we have not specified the main source of the orbit drift yet and further investigation is necessary. Since the beam orbit is highly sensitive to the magnetic field distortions, satisfactory stability will be able to be confirmed only using the beam.

2.3.2.2 FONT intra-train feedback system

(See 4.2.3 for details): The performance specifications of the ILC IP intra-train feedback system have been demonstrated with the upstream FONT system [13]. In addition, in dual-phase operation the system has provided beam jitter reduction in both vertical position and angle by a factor of 4, showing the potential for beam stabilisation at the ATF2 IP to the 1nm level [14]. Additional beam operations are required for a systematic study of the feedback-loop gains so as to optimise the performance.

For the dedicated FONT system using cavity BPMs at the IP, further studies are needed in order to optimize the performance. Given the achieved best real-time BPM resolution of 19nm (Table 9), it is possible to improve beam position stabilization from the achieved 41nm (Table 11) to as low as 25nm.

The upstream FONT system also has been shown [14] to yield almost a factor-2 reduction in the beam-size dependence on beam intensity (Section 4.2.2), implying significant reduction in wakefield effects resulting from the beam jitter reduction by the orbit feedback. Future small-beamsize studies would hence benefit from routine operation of the upstream FONT system.

2.3.2.3 Ground motion monitoring studies

Taking into account the successful implementation in SuperKEKB of a "permanent GM monitoring" (http://lappweb.in2p3.fr/SuperKEKB/), acquired via a real-time setup on site and then synchronized on a cloud system to be saved in a local server and automatically treated to provide spectral analysis, with ATF2 type of GM sensors, in the short term we will plan to implement a similar permanent GM monitoring system in ATF2. For doing this we will use the already installed GM sensors at various strategic locations that will be chosen by experiments and simulations, along with the already known sensitive locations as the FD magnets (QF1 and QD0). This permanent GM monitoring will allow to evaluate more efficiently the vibrations sources in time. (See 4.3.3 for details).

3 Technical preparation for ILC

3.1 ILC project implementation plan

"Recommendations for the implementation of the ILC project" were published by KEK in October 2019 [16]. It defines the current phase as the pre-preparatory phase. A positive signal by the Japanese government expressing its intent to host the ILC as part of the critical decision process will trigger the project transition into the main preparatory phase, we call it simply "preparatory phase" here after, which is expected to complete in about four years. The key activities in the preparatory phase will be the technical preparations for ILC construction and the inter-governmental negotiations. The technical preparations will be led and coordinated by a preparatory laboratory ("Pre-Lab"). A budget estimate for the preparatory phase, including the technical preparations by ATF, has been provided with that of the ILC construction and operation. Therefore, it is assumed that a dedicated budget will be allocated during the preparation phase. The inter-governmental negotiations during the preparatory phase are expected to culminate in an inter-governmental agreement, signaling the official launch of the ILC project. This agreement will trigger the transition of the Pre-Lab structure into a full ILC Laboratory, which will mark the start of the construction phase of the ILC project.

In order to plan the Pre-Lab, the International Development Team (IDT) of ILC, the successor to Linear Collider Collaboration (LCC), was organized by ICFA in August 2020. The term of the IDT is supposed to last until the end of 2021, and then the preparatory phase is expected to begin shortly thereafter. The creation of the Pre-Lab will be based on a mutual understanding of the Pre-Lab mandate and organizational structure by participating laboratories with the consent of their respective governmental authorities, to be established during the pre-preparatory phase.

3.2 Importance of continuous improvement of ATF/ATF2

ATF/ATF2 is expected to play a definitely important role in technical preparation. The preparatory phase is expected to be approximately four years, so it is important to maintain current activity and improve the beam status of ATF2 in order to get effective performance from the beginning of the preparatory phase. Therefore, it is essential to continue the efforts to upgrade and test the ATF in the current pre-preparatory phase, eliminating as much as possible the known difficulties in conducting the current studies (described in Sec. 2.3). A particularly important overhaul of the IPBSM needs to be done in conjunction with the generation of nanometer-sized beams. These efforts will be maintained under the currently limited manpower which is described in Sec. 1.4. Improving the current beam situation and keeping or increasing the manpower are essential issues to be considered. Furthermore, it should be mentioned that the ATF can be used as a beam test bench for ILC components and as an education/training machine for young researchers who contribute to ILC.

3.3 Upgrade of ATF2 for technical preparations of ILC

Building on the achievements of the ATF2 project a follow-on, upgraded facility ('ATF3') for pursuing R&D aimed at maximising the luminosity potential of ILC is necessary. ATF3 would comprise an overhaul and upgrade of the existing ATF2 beamline so as to model more accurately the energy-scaled ILC final-focus system. Beamline sections and components that act as wakefield sources and currently limit the achieved beam size at beam intensities above 1×10^9 electrons would be removed and replaced. Improved, ILC-style diagnostic devices (BPMs etc.) could be installed, and the IP BSM laser could be upgraded to provide for stable, long-term operations. This upgraded facility would provide a test bench for beam tuning and stabilisation techniques aimed at achieving small and stable beam spots consistent with the (energy-scaled) ILC requirements.

In addition, if commissioned and tested nearby at a dedicated SC magnet test stand in the ATF hall, a SC final-focus QD0/QF1 magnet system could be installed at the ATF3 IP. This would allow in situ studies of a prototype ILC SC final-doublet system, including study and control of multipole field

components and cold-mass vibrations, as well as deployment and testing of alignment, passive damping, and beam-based feedback systems.

The ATF3 beamline would also provide a test facility environment for prototyping, deploying and commissioning with beam other ILC systems, including: a modern high-polarisation electron source, non-invasive beam emittance measurement systems, BPMs, feedback/feed-forward stabilisation systems, and a SC crab-cavity prototype.

ATF3 would hence provide the opportunity to attract additional resources from overseas collaborating institutes to deliver the programme described above in a modular and sensibly time-ordered fashion. Installation and commissioning of ATF3 would proceed in the ILC Preparation Phase, and operations would continue during the ILC construction phase, providing a dedicated test facility for the instruments, devices and techniques required for achieving the ILC design luminosity. ATF3 would also provide a state-of-the-art test facility for other users of high-quality, stable, ultra-low-emittance electron beams.

3.4 Technical preparations at ATF/ATF2 in the ILC preparatory phase

The technical preparations at the ATF facility in the ILC preparation phase, which are not performed yet during the current R&D at ATF, are expected and summarized as follows.

- Long term stability of fast injection and extraction systems.
- Long term stability of beam size and orbit at the ATF2 interaction point.

The need to confirm long term stability at ATF was mentioned both in the revised KEK-ILC action plan in 2018 [15] and in the Recommendation on ILC Implementation by the KEK International Working Group in 2019 [16]. It was also pointed out as specific technical issue by the ILC Advisory Panel of MEXT [17] and by the ILC committee in the Science Council of Japan (SCJ) [18].

For the achievement of long term stability of beam size and orbit at ATF2, it will moreover be important to establish a suitable organisation to support efficient continuous beam operation over longer periods.

3.4.1 *Long term stability of fast injection and extraction system*

We planned the long-term operation of the fast injection and extraction kicker system. The system consisting a strip-line kicker and a fast pulsed power source was developed and successfully demonstrated multiple systems using beams at ATF (details in Sec. 4.4.1). The remaining task is to ensure the stability and reliability over long-term operation.

The beam operation test of the fast kicker system was performed in the ATF damping ring (DR) in 2011. The fast kicker system was installed in the extraction point of the DR by replacing the conventional pulsed kicker magnet. The multiple bunch extraction was successfully demonstrated, however the heating problem on the strip-line kicker occurred. It was caused by the Synchrotron radiation from the circulating electron beam, because the extraction point of DR was located at the end of the arc section of the ATF DR. It is a problem unique to ATF and not relevant for ILC. However, it was difficult to keep the fast kicker system in the ATF damping ring for the heating problem, and the devices were removed just after the performance test. Therefore, the long-term stability test was postponed, and not yet performed.

In order to investigate the long-term stability of the fast kicker system, we are planning to install the test stand at a location different from the present extraction kicker (*i.e.* in the ATF extraction line) to avoid the heating problem from synchrotron radiation in DR. The fast kicker test stand is expected to be constructed when the ILC preparatory phase starts.

Furthermore, stripline kickers with low impedance mismatches have been developed for the CLIC DR [19, 20]. The wakefield of the kicker devices will be tested throughout the ATF's operation over this

few years. The kicker power supplies with higher output voltage have also been developed. This device R&D will be continued into the ILC preparatory phase.

3.4.2 *Long term stability of beam size and orbit at the ATF2 interaction point*

We aim to do significant long-term stability studies of the beam focusing and position control at the ATF2 virtual interaction point (ATF2 IP). Beam focusing for the ILC final focus system was already successfully pursued at ATF2, achieving a beam size of 41 nm, which is close to the target beam size of 37 nm (details in Sec. 4.2.1.3). The ILC prototype feedback system was also validated to satisfy all ILC requirements for position control at the interaction point (details in Sec. 4.2.3). The foreseen long-term stability studies will be conducted by the KEK staff in close collaboration with its international partners, based on their accumulated experience doing R&D at ATF2.

The FONT intra-train feedback system is an essential tool not only to stabilize the IP beam position, but also to reduce the intensity dependence of the beam size for the ATF2 IP (details in Sec. 4.2.2). The FONT intra-train feedback was developed mainly by Oxford university as their own operating system, and the performance test was also performed only when the scientists of the Oxford University was come to ATF for the test. We have to expand the FONT intra-train feedback system from the specific system of the Oxford University to the ATF operation system to operate every time when we will be able to use the FONT intra-train feedback. A stable IP beam size monitor is essential for the long-term stability study (details in Sec. 4.2.1.2). In order to update the present IP beam size monitor to be stable, we must replace the present multi-mode laser system of IPBSM to a stable single mode laser system seeded by a mode lock laser. Furthermore, the development and investigation of the online beam monitor system (*i.e.* dispersion measurement by using SVD analysis) will be carried out in coming years beam operation.

In the ILC preparation period, we will integrate the FONT intra-train feedback system, the stable IP beam size monitor and the online beam monitor system to the ATF control system in order to perform the long-term stability test of the beam focusing and the position control at ATF2 IP.

3.4.3 *Planning for long term beam operation*

While a number of R&D activities have been independently conducted successfully over the years by teams of scientists from Japan and abroad using the beam at ATF or ATF2 , achieving long term stability of strongly focused beams at the ATF2 IP calls for well-prepared and relatively long periods of continuous beam operation, typically of at least a week. Such rather long continuous periods are needed to prepare excellent beam conditions at injection to the highly non-linear final focus optics, to ensure sufficient orbit stability using feedback, and to perform the large number of iterative adjustments of the many optical tuning knobs involved in producing and maintaining small beam sizes in a real system with imperfections.

The success of such long periods of operation will require participation of a sufficient number of scientists working together on a succession of beam tuning tasks defined in advance, with efficient coordination by senior experts. Typically, the team will combine students and postdocs both from Japan and abroad, who will in the process acquire precious educational experience with the operation of a real ILC-like final focus.

In the past, several such periods were organised successfully at ATF2. The first continuous beam operation period in 2013 led to the achievement of the first beam sizes smaller than 50 nm.

During the preparation for ILC, such joint operation by an international team working towards a common goal for extended periods will become even more important, both in terms of training and technical achievement. An organisation to manage such operation periods will need to be defined involving senior accelerator scientists from KEK and from the institutes abroad who will be sending staff.

3.5 Possible use of ATF for ILC preparation other than final focus system

The ATF facility can be used not only in the ILC preparatory phase but also in the construction phase to provide a platform for beam testing and to verify the performance of key ILC components. Up to now, the development of many ILC components has been advanced, and demonstration tests have been completed. However, technology is evolving day by day, and it will take approximately 8-10 years for ILC construction. The best technology should be selected at the time of construction, and a technology development facility for that purpose is necessary. ATF can hence serve as both a test stand for key accelerator components and a platform for long-term stability tests with beam.

The Superconducting RF Test Facility (STF) also serves as a test accelerator for ILC at KEK. Since the STF is a superconducting accelerator, it takes time to prepare for operation, whereas the normal-conducting ATF can set up for versatile operation quickly as required. During the ILC preparation and construction periods, it will be essential to pursue component development, final design and testing by taking advantage of the complementary capabilities of both ATF and STF. This will enable a smooth transition of final components to the ILC construction, as well as human resource development and efficient skills transfer at the beginning of ILC operation. The ATF facility can provide the following platforms:

3.5.1 Permanent magnet test bench

The application of permanent magnets (PMs) to accelerators is progressing, especially for the low emittance light sources. Further considerations to reduce the total power consumption of large scaled accelerators have also been done. For example, tunable high-gradient PM quadrupoles for CLIC drive-beam accelerator has been developed [21]. PM will be one of the effective technology choices for ILC, and ATF will be able to serve as the performance test bench for PM.

In addition, PM contributes to improved beam stability because of the static magnetic field. It is suitable for ATF2 research. Another benefit for ATF will be expected on the improvement of the beam extraction from DR. The aparture of the extraction septum region at ATF is as narrow as 14 mm, the length is 5 m and includes a series of three septum magnets. Controlling the beam passing here is somewhat difficult and it gives constraints on ATF2 beam tuning. Application of PM to the ATF septum magnets will have a possibility to improve the physical aperture around the extraction section.

3.5.2 Superconducting magnet test bench

A refrigeration facility will be placed in the ATF facility and a superconducting magnet test base will be constructed. We would like to fabricate and test the superconducting magnets, such as the ILC final focus magnets, the crab cavities, and the helical undulator for polarized positron generation.

The ILC superconducting final focus magnets were designed by BNL, and the prototype of the final focus magnets will be fabricated to install to the ATF2 beamline by using same technology. Since the magnet arrangement of the ATF2 beamline has exactly the same layout as ILC, it is possible to focus the beam using the similar scheme of the ILC final focus system.

The ILC crab cavities are based on the Fermilab design for a 9-cell 3.9 GHz cavity, and the a 3-cell prototype of this cavity has been manufactured and achieved a gradient of 7.5 MV/m in cold tests [22]. a proof-of-principle test of a 7-cell 1.5 GHz cavity at the JLab ERL facility has demonstrated the phase control and the feasibility [23]. It is very useful experience to fabricate a prototype crab cavities designed by Fermilab (9-cell 3.9 GHz), and a beam test using the fabricated cavities at the ATF facility.

A prototype of a helical undulator for polarized positron production for ILC was manufactured and tested at Daresbury Laboratory [24]. The prototype consisted of two superconducting magnets and a cryostat, and both of them achieved the magnetic field strength required for ILC. By making a new magnet at the ATF facility, it is possible to further improve the magnet production technologies and demonstrate the orbit tuning for the narrow aperture of the undulators.

3.5.3 *Polarized electron source test bench*

A cathode for an electron gun with a quantum efficiency of more than 1 % and a polarity of approximately 85 % has already been developed at Nagoya University [25]. Further optimization of the cathode will be able to carried out based on this technology, and the development of a laser system for electron excitation will be promoted. Finally, it will be incorporated into the ATF or STF accelerators to evaluate the long-term stability for the polarized electron beam generation, including the laser performance.

3.5.4 *Preparation of additional devices*

ILC intends to use permanent electromagnets for the beamlines of Ring to Mail Linac (RTML) and Damping Ring (DR). Since investigating the magnetic field damages of permanent magnets under a radiation environment is useful for ILC, we think it is useful to put these magnets in an accelerator and test them as long as possible. Furthermore, it is necessary for ILC to develop L-band normal conduction standing wave RF cavities and a rotating target used for a polarized positron source. We think it can also be used as test benches for the additional developed elements, if there is an ATF facility during the ILC preparation and construction period.

3.6 Other studies in the ILC preparation period

Since the ATF is a test accelerator for technology development, which is flexible in operation and can provide the opportunity to perform R&D not only for LC technology development but also for other technology development using electron beam, we consulted with the Japanese accelerator community to investigate the potential demand for beam utilization by ATF electron beams. Several proposals have been collected and are described in Sec. 5.2.

4 Results and current status of studies

This section describes the detail of the R&D at ATF2 for the beam control and metrology techniques needed to produce and maintain focused and stable beams with vertical beam sizes of tens of nanometers.

4.1 DR low emittance

The ATF Damping Ring (DR) was designed and constructed as a prototype DR of Linear Colliders (LCs). It has racetrack shape with superperiod of 2. The arc sections consist of periodic FOBO cell with combined functioned bending magnets. Design horizontal equilibrium emittance $\gamma\epsilon_x$ is 3×10^{-6} m. The goal vertical emittance is less than 1% of the horizontal one, namely, less than 12 pm in physical emittance at the energy of 1.3 GeV. For that low emittance, good magnets (including their alignment), good monitors and sophisticated corrections are required. The very low vertical emittance had been studied for years [26, 27], and in early 2000's low emittance of about 4 pm had been achieved [28]. A laser wire monitor (LW) was used as a beam size monitor there. After that, ATF2 project had started utilizing the low emittace beam from the DR. It studies final focus system of LCs, and required vertical emittance is 12 pm or less. In the followings, recent status of a low emittance in the ATF DR is described.

Low Emittance Tuning

Vertical dispersion correction and coupling correction are performed routinely at the start-up shift of each beam period. Usually with these corrections, the vertical emittance of around 12 pm can be realized.

- **Vertical Dispersion Correction:** Vertical dispersion is measured and is fit by a few vertical correctors. The dispersion is corrected by applying the reverse current to the correctors. This correction is iterated a few times.

- **Coupling Correction:** This correction minimizes the vertical orbit leakage when a horizontal corrector's current is changed. The correction is done with skew quadrupoles, which are special trim winding coil of sextupole magnets.

Emittance Measurement

Emittance can be calculated with beam size and the beta function there. For beam size measurement, LW monitors which measured the 4 pm emittance has already uninstalled. Instead profile monitor using Synchrotron Radiation (SR) light is used in X-ray region, that can measure small beam size down to about 4 μm in single shot. Beta function at quadrupole magnet is measured as tune slope when the magnet strength is changed. Beta functions of several quadrupole magnet around the SR emission point are measured. By fitting them, the beta function at the SR emission point can be obtained. By the routine emittance tuning, vertical emittance of about 12 pm is quickly achieved at the start-up shift.

Stabilities

The ATF DR can be operated with electron intensity up to 1×10^{10}/bunch. Not only the intensity but also the emittance can be kept stably for a week. Recently we are understanding the effect of air and cooling water temperature deeply, and those setting can be knobs for stabilization. Finally, works checking magnet alignment done is the shutdown period also contribute the operation stability.

4.2 Final Focus Study

4.2.1 IP beam size focusing

4.2.1.1 Optics design of ATF2 beamline

The ILC final focus system is designed based on the Local Chromaticity Correction technique [9]. This scheme has many advantageous properties over previously studied focusing schemes, including being significantly shorter for a given energy and having a significantly better energy bandwidth. The main purpose of the ATF2 beamline is to demonstrate beam focusing with the Local Chromaticity Correction scheme, and to establish a beam tuning method for ILC final focus system.

The IP horizontal and vertical beta-functions (β_x^*, β_y^*) of ATF2 were originally designed to generate the same horizontal and vertical chromaticities as ILC (1×1 optics). However, since the ATF2 beam energy is much smaller than ILC, the geometrical aberrations of ATF2 are much larger than ILC, and the effect of the multipole errors is larger than ILC. Therefore, in recent ATF2 beam operation, the ATF2 beamline was operated with a 10 times larger horizontal IP beta-function than that of original optics in order to reduce sensitivity to the multipole errors. We call this optics as 10×1 optics. The beam optics for the final focus system of ILC and ATF2 are shown in Fig. 5, and the beam and optics parameters are listed in Table 2. The multipole field error tolerances of IP vertical beam size for ILC and ATF2 final doublet (QF1, QD0) are shown in Fig. 6. The tolerances are defined as the error which induces a 2% of IP vertical beam size growth. Figure 6 shows that the tolerances of the multipole field errors in ATF2 10×1 optics are comparable with those of ILC.

4.2.1.2 IP beam size monitor

A nanometer scale beam size monitor (proposed in [29]) was demonstrated at SLAC FFTB in the 1990s [10], measuring a beam size of approximately 70 nm. This beam size monitor used at FFTB was modified for ATF2 and installed at the ATF2 IP. The beam size at the ILC interaction point will be measured by using not this type of beam size monitor, but the luminosity monitor (*i.e.* incoherent pair monitor) by colliding two beams. Unlike ILC, IPBSM is the only monitor that can measure nanometer beam size in a single beamline FFTB or ATF2.
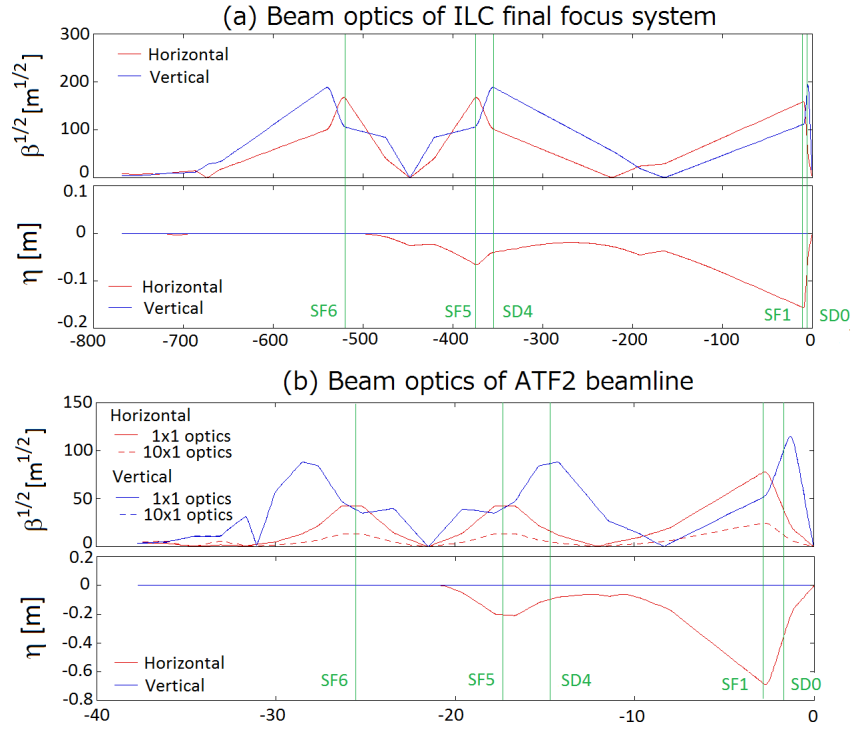
Figure 5: Beam optics of the ILC final focus beamline (a) and the ATF2 beamline (b). Both the 1×1 optics and the 10×1 optics are shown.
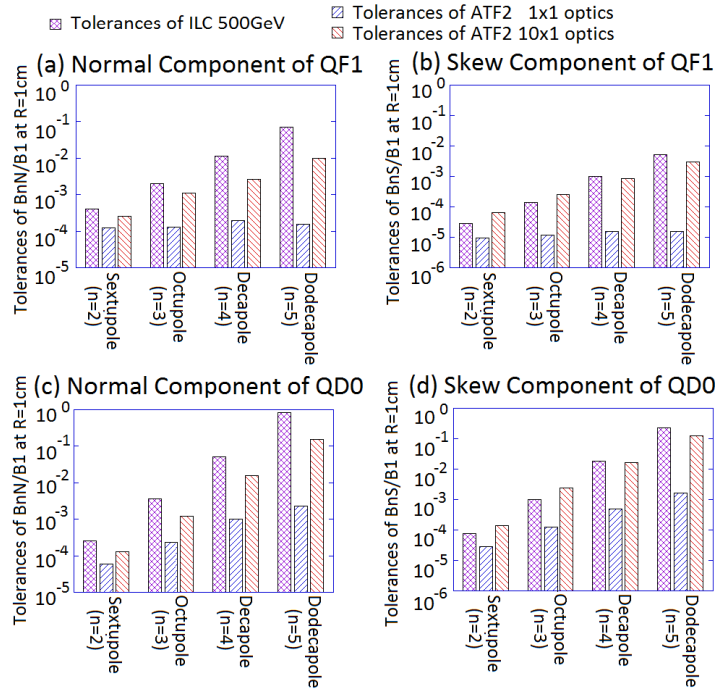

Figure 6: Tolerances of multipole field errors for the final doublet (QF1 and QD0) of the ILC and ATF2 final focus beamlines.

Table 2: Beam and optics parameters for the ILC and ATF2 final focus beamlines (10×1 optics).

		ILC250	ATF2(10×1)
Beam energy	E	125 GeV	1.28 GeV
Distance between final quad. and IP	L^*	4.1 m	1.0 m
Phycical emittance	$\varepsilon_x/ \varepsilon_y$	0.02 nm / 0.14 pm	2 nm /12 pm
Normalized emittance	$\gamma\varepsilon_x / \gamma\varepsilon_y$	5 μm / 0.035 μm	5 μm /0.030 μm
IP beta functions	β_x^*/β_y^*	13 mm / 0.41 mm	40 mm /0.10 mm
IP beam sizes	σ_x^*/σ_y^*	0.51 μm / 7.6 nm	8.9 μm /37 nm
Bunch length	σ_z	0.3 mm	7.0 mm
Momentum spread	σ_p/p	0.19%	0.07%

The IPBSM uses a fringe pattern formed by two interfering laser beams. The schematic drawing of the IPBSM is shown in Fig. 7. The laser fringe pitch is defined by the wavelength (λ) and crossing angle of the two laser paths (θ): $d = \lambda/2\sin(\theta/2)$.
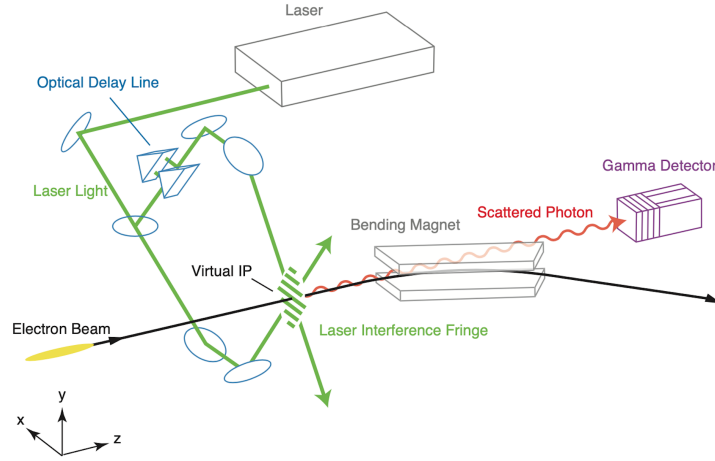

Figure 7: The schematic drawing of the IPBSM. [30]

Compton scattered photons from the transverse overlap of the laser fringe pattern with the beam are measured downstream of the IP. The modulation depth of the Compton signal obtained by moving the fringe pattern with respect to the beam is written as a function of IP vertical beam size (σ_y):

$$M = C\,|\cos\theta|\exp\left(-2k_y^2\sigma_y^2\right), k_y = \pi/d, \tag{1}$$

where C expresses the contrast reduction of the laser fringe pattern. Reduction of the laser fringe contrast is caused by deteriorated laser spatial coherency, mismatch in the overlap of the two laser beams *etc.*. Since the modulation depth of the Compton signal is also reduced by C, this is referred to as the modulation reduction factor. From Eq. (1), the beam size is expressed as a function of the modulation depth:

$$\sigma_y = \frac{d}{2\pi}\sqrt{\frac{1}{2}\ln\left(\frac{C\,|\cos\theta|}{M}\right)}. \tag{2}$$

We can measure the modulation depth of the Compton signal by measuring its strength for various relative beam positions with respect to the laser fringe. Then, we can evaluate the IP beam size from the measured modulation depth using Eq. (2). For ATF2, the laser wavelength used in the IPBSM was changed from 1064 nm to 532 nm to reduce the laser fringe pitch, and three laser crossing modes (2-8

degree mode, 30 degree mode, 174 degree mode) were prepared to increase the range of possible beam size measurements [31]. The dynamic ranges of the IPBSM at ATF2 are shown in Fig. 8.
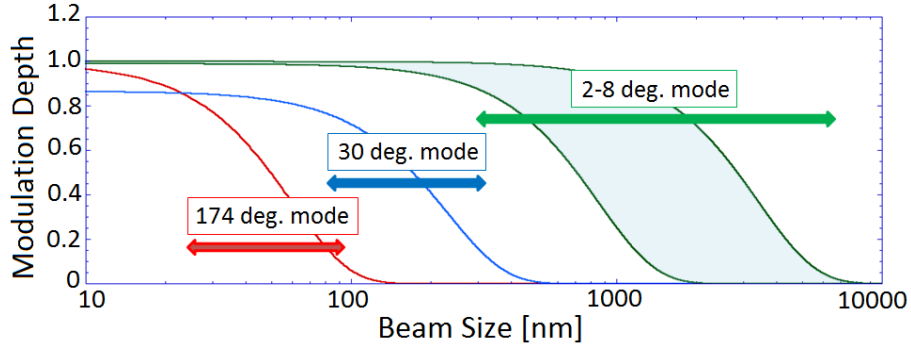

Figure 8: Dynamic ranges of the IPBSM at the ATF2 IP. Dynamic ranges for 3 laser crossing modes are plotted in the figure.

The laser of the IPBSM is a seeded multi-mode Nd:YAG laser (Spectra-Physics Quanta-Ray PRO 350). The transverse laser profile is not Gaussian (see Fig. 9(a)), and the M^2 of the laser light is approximately 2. The measured IP laser spot size as a function of the focal lens position is shown in Fig. 9(b). The minimum laser spot size for vertical and longitudinal directions are different, and the laser beam waist positions are also different each other. Since the transverse profile of the laser light is quite different from the Gaussion, the IP laser profile is deformed a lot through the aberrations of the final focal lens, when the laser light is not on the center of the final focal lens. Furthermore, the laser position on the final focal lens is drifted through the laser transport line of approximately 20 m.
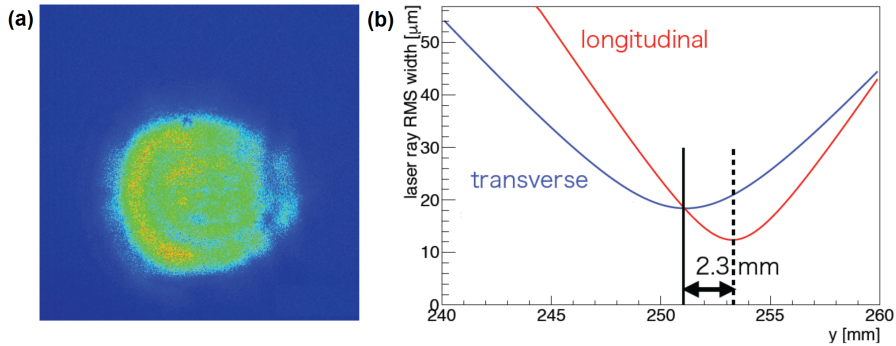

Figure 9: (a) IPBSM laser profile, measured at the laser table. (b) The evaluated IP laser spot size as a function of the focal lens position. The laser spot size was measured by the optical system with long focal lens, and the laser spot size was converted to the IP spot size. [32]

Figure 10(a) shows the laser position drift, measured by the laser profile monitor near by the final focal lens. The laser position drifts during the laser warming-up, and changes during the day and night were also observed. Since the laser positions are different for two laser paths, the IP laser profiles are also different through the optical aberrations of the final focal lenses. It makes the contract of the laser fringe pattern worse, and it reduces the measured IPBSM modulation depth (the beam size is over-estimated). Figure 10(b) shows the IPBSM modulation depths of 30 degree mode before and after the laser path realignment, as a function of the focal lens position for the lower path. Here, the initial alignment of the laser path was done just before starting the beam operation. The small beam tuning was carried out four days and the beam size was evaluated to be smaller than 85 nm by IPBSM 174 degree mode. This beam size should give a modulation depth greater than 0.76 when we switch the IPBSM measurement mode to
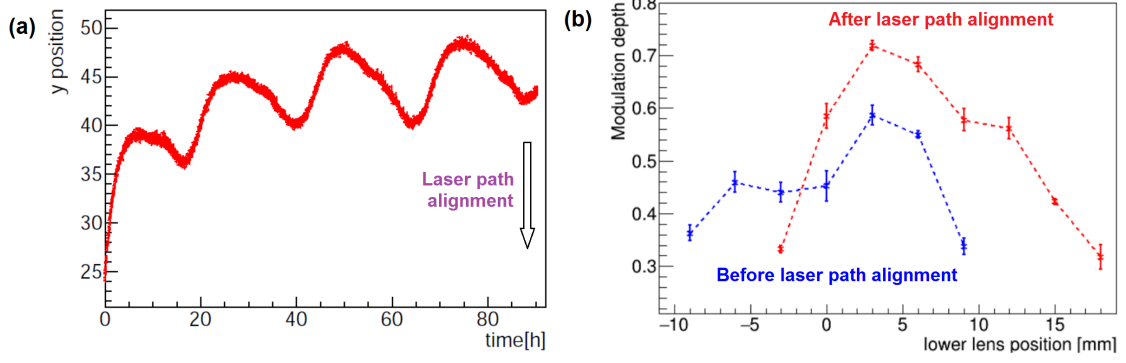
Figure 10: (a) the laser position drift near by the final focal lens. (b) IPBSM modulation depths of 30 degree mode before and after the laser path alignment. The IPBSM modulation depths were plotted as a function of the final focal lens position for the lower path. [32]

the 30 degree mode with no modulation reduction ($C=1$ in Eq. (2)). However the maximum modulation depth was obtained about 0.6 when we switched back to the 30 degree mode without changing a beam condition. Just after that, the laser path alignment was performed again and it brought an improved modulation depth of 0.7. The laser path alignment strongly affects to the beam size evaluation by the IPBSM. We normally align the laser path twice a week, just before the beam operation and the middle of the week. Then, important measurements are performed at the second half of the operation week. Since the modulation reduction caused by the current multi-mode Nd:YAG laser is difficult to estimate, the beam size at ATF2 IP have been evaluated by omitting this modulation reduction. Therefore, the beam size is determined larger and is understand as the upper limit.

4.2.1.3   IP beam size tuning for 10×1 optics

There are five sextupole magnets (SF6FF, SF5FF, SD4FF, SF1FF and SD0FF) in the ATF2 beamline. The transverse positions of all the sextupole magnets are controlled using magnet movers. When a sextupole magnet is moved horizontally, a quadrupole field is generated. The strength of the generated quadrupole field is proportional to the horizontal offset and changes the horizontal and vertical beam waists (α_x and α_y), IP horizontal dispersion η_x and its derivative η'_x. The linear optics tuning knobs of α_x (AX knob), α_y (AY knob), η_x (EX knob) and η'_x (EPX knob) are calculated as orthogonal sets of horizontal offsets of the sextupole magnets, only individually changing α_x, α_y, η_x and η'_x, respectively [33].

When a sextupole magnet is moved vertically, a skew quadrupole field is generated. The strength of the generated skew quadrupole field is proportional to the vertical offset and changes the vertical dispersion η_y, the derivative η'_y and xy coupling components at the IP, especially $< x'y >_{IP}$. The linear optics tuning knobs of η_y (EY knob), η'_y (EPY knob) and $< x'y >_{IP}$ ($Coup2$ knob) are calculated as orthogonal sets of the vertical offsets of the sextupole magnets, only individually changing η_y, η'_y and $< x'y >_{IP}$, respectively.

The IP vertical beam size is sensitive to the beam waist position offset (α_y), the IP vertical dispersion (η_y) and the amount of xy coupling at the IP ($< x'y >_{IP}$) and are used for IP vertical beam size tuning during ATF2 beam operations. The IP vertical beam size can be expressed as:

$$\sigma_y^{*2} = \varepsilon_y \beta_y^* + \left(AY + \alpha_y \sqrt{\varepsilon_y/\beta_y^*} \right)^2 + (EY + \eta_y \delta)^2 + \left(Coup2 + < x'y >_{IP} \sqrt{\varepsilon_x/\beta_x^*} \right)^2 + \Delta\sigma_{y,MP}^2$$
(3)

where AY, EY and $Coup2$ are amplitudes of the beam waist knob, the vertical dispersion knob and the xy coupling knobs $< x'y >_{IP}$, respectively. $\Delta\sigma_{y,MP}^2$ is the IP beam size contribution due to multipole

21

field errors. Inserting Eq. (3) into Eq. (1), the modulation depth can be expanded as:

$$M = C \left| \cos \theta \right| \exp \left[-2k_y^2 (\varepsilon_y \beta_y^* + \Delta \sigma_{y,MP}^2) \right]$$

$$\exp \left[-2k_y^2 \left(AY + \alpha_y \sqrt{\varepsilon_y / \beta_y^*} \right)^2 \right]$$

$$\exp \left[-2k_y^2 \left(EY + \eta_y \delta \right)^2 \right] \tag{4}$$

$$\exp \left[-2k_y^2 \left(Coup2+ <x'y>_{IP} \sqrt{\varepsilon_x / \beta_x^*} \right)^2 \right]$$

The 1st line of Eq. (4) is the maximum amplitude of the modulation depth, corresponding to the minimum achievable beam size after application of the linear knob corrections. The 2nd to 4th lines of Eq. (4) are the responses of the linear knobs. Examples of IP beam size tuning with the linear knobs are shown in Fig. 11. The modulation depth exhibits a Gaussian response to the linear knobs, as can be seen from Eq. (4). The optimum setting of a linear knob corresponds to the peak of the fitted Gaussian function.
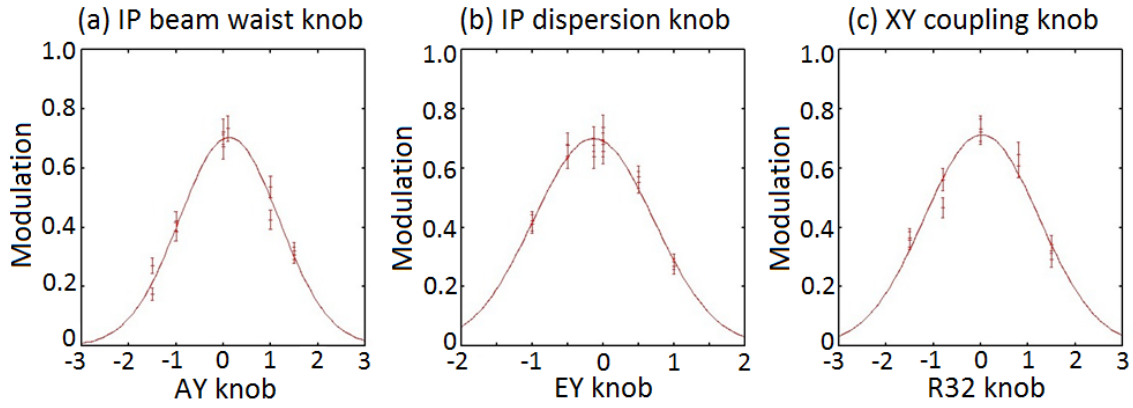

Figure 11: Example of IP beam size tuning using linear knobs. The beam size tuning was done with IPBSM 2-8 degree mode.

The strengths of the sextupole magnets in the final focus beamline are set for cancelling chromatic and geometrical aberrations [9]. Other 2nd order aberrations can also be generated, for example, if there are sextupole field errors present in any magnets. When there is a sextupole field error (ΔK_{2N}), the IP horizontal and vertical position is changed as a function of the particle positions at the sextupole magnet Δx, Δy and the momentum offset δ:

$$\Delta x_{IP} = \frac{R_{12} \Delta K_{2N}}{2} \left(\Delta x^2 + 2 \eta_x \Delta x \delta + \eta_x^2 \delta^2 - \Delta y^2 \right) \tag{5}$$

$$\Delta y_{IP} = R_{34} \Delta K_{2N} \left(\Delta x \Delta y + \eta_x \Delta y \, \delta \right). \tag{6}$$

Furthermore, when the sextupole error sources are located at the large beta function region from where the betatron phase advances to the IP are almost $(n+1/2)\pi(n; \text{integer})$, the horizontal and vertical positions at the error sources are strongly correlated to the horizontal and vertical angles at the IP, x'_{IP} and y'_{IP} as $\Delta x = -R_{12} x'_{IP}$ and $\Delta y = -R_{34} y'_{IP}$. Therefore, the horizontal and vertical position change at the IP by the sextupole field errors can be expressed as:

$$\Delta x_{IP} = P_{X22} x'^2_{IP} + P_{X26} x'_{IP} \delta + P_{X66} \delta^2 + P_{X44} y'^2_{IP}, \tag{7}$$

$$\Delta y_{IP} = P_{Y24} x'_{IP} y'_{IP} + P_{Y46} y'_{IP} \delta, \tag{8}$$

$$P_{X22} = + \sum \frac{\Delta K_{2N} R_{12}^3}{2}, \quad P_{Y26} = - \sum \Delta K_{2N} R_{12}^2 \eta_x,$$

$$P_{X66} = +\sum \frac{\Delta K_{2N} R_{12} \eta_x^2}{2}, P_{X44} = -\sum \frac{\Delta K_{2N} R_{12} R_{34}^2}{2},$$
$$P_{Y24} = +\sum \Delta K_{2N} R_{12} R_{34}^2, P_{Y46} = -\sum \Delta K_{2N} R_{34}^2 \eta_x.$$

In order to correct the 2nd order optics errors, tuning knobs to correct 2nd order aberrations were prepared [33]. There are five normal sextupole magnets in the ATF2 final focus beamline. On the other hand, the number of parameters that affect the horizontal and vertical beam size growth at the IP is six (P_{X22}, P_{X26}, P_{X66}, P_{X44}, P_{Y24} and P_{Y46}), from Eqs. (7), (8). Therefore, P_{X44} is ignored to make the ATF2 IP beam size tuning knobs because the effect of P_{X44} is expected to be insignificant. Tuning knobs to correct sextupole field error components (X_{22}, X_{26}, X_{66}, Y_{24} and X_{46}) are calculated as orthogonal sets of strength changes of five sextupole magnets changing only P_{X22}, P_{X26}, P_{X66}, P_{Y24} and P_{Y46}, respectively.

Horizontal beam size change due to the skew sextupole fields is expected to be small and ignored here. Vertical beam size growth at the IP due to the skew sextupole field errors (ΔK_{2S}) can be expressed as:

$$\Delta y_{IP} = P_{Y22} y_{IP}'^2 + P_{Y26} y_{IP}' \delta + P_{Y66} \delta^2 + P_{X44} y_{IP}'^2, \tag{9}$$
$$P_{Y22} = +\sum \frac{\Delta K_{2S} R_{12}^2 R_{34}}{2}, P_{Y26} = -\sum \Delta K_{2S} R_{12} R_{34} \eta_x,$$
$$P_{Y44} = -\sum \frac{\Delta K_{2S} R_{34}^3}{2}, P_{Y66} = +\sum \frac{\Delta K_{2S} R_{34} \eta_x^2}{2}.$$

Four skew sextupole magnets (SK1FF-SK4FF) installed into the beamline to correct the 2nd order field errors. The tuning knobs to correct skew sextupole field error components (P_{Y22}, P_{Y26}, P_{Y66} and P_{Y44}) are calculated as orthogonal sets of strength changes of four sextupole magnets changing only P_{Y22}, P_{Y26}, P_{Y66} and P_{Y44}, respectively.

At the beginning of ATF2 beamline tuning, all of the sextupoles are turned off. Then, the orbit tuning is carried out. The corrected beam orbit is kept by using an orbit drift feedback. Since the vertical beta-function is reached up to approximately 10,000 m in ATF2 beamline, the feedback corrector must be controlled within the accuracy of 0.01 Gauss·m. Therefore, the air core correctors are used for the orbit feedback. After the orbit tuning, the IP horizontal and vertical beam divergences are set to the design values. The beam waists are also set to the ATF2 IP.

The magnetic centres of the sextupoles must be aligned with respect to the corrected beam orbit in order to avoid the linear optics deformation by the sextupoles. The offsets are measured by beam based alignment (BBA) techniques. The skew sextupoles must be aligned within 100 μm accuracies in order to make 2nd order knobs effective [34]. The sextupoles are turned on after the magnetic centre positions are moved with respect to the beam orbit. Then, the IP beam size is minimized by using the linear and 2nd order knobs with IPBSM monitor.

Figure 12 shows history of minimum beam size, measured at ATF2 IP. The plotted beam sizes are calculated by assuming to $C = 1$ in Eq. (2) [34–37]. The electron beam intensity in this period is approximately 1×10^9 per bunch, and emittance measured in the damping ring is around 10 pm. Improvement of IPBSM is one of the important contribution to the progress, including laser stabilization. Since it was turned out that one of the sextupole magnet coils was shorted in January 2013, this magnet had been used as one with the weakest strength setting. The new sextupole magnet setting was calculated so that the troubled magnet was turned off. From August 2015, the troubled sextupole magnet was replaced to the magnet, which was used in quantum beam experiment in STF. After the replacement, the second order optics correction was performed by using five sextupole magnets.

Figure 13(a) shows the IPBSM modulation, and Figure 13(b) shows the evaluated beam size by assuming no modulation reduction of the IPBSM monitor ($C = 1$ in Eq. (2)) in February 2016. The bunch population was $N = 1 \times 10^9$. The beam tuning was followed by the tuning procedure of the
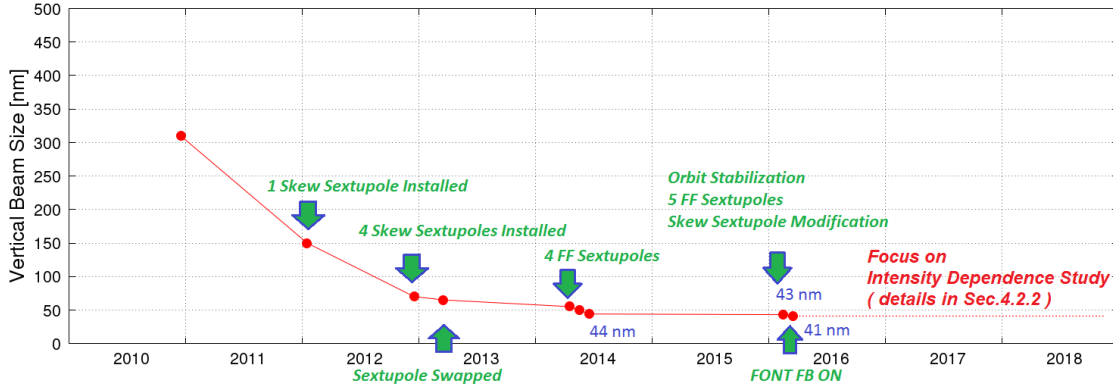
Figure 12: Trend of the measured minimum beam size at ATF2 IP. The beam size was evaluated as $C = 1$ in Eq. (2).

previous section. Two iterations of 2nd order knob tuning (Y_{24}, Y_{46}, Y_{22}, Y_{26}, Y_{66} and Y_{44}) were applied to minimize the IP vertical beam size. The linear knob tuning was also carried out in between each set of 2nd order knob tunings. The average modulation of 15 measurements was 0.592, and it corresponds to 43.2 nm vertical beam size with no modulation reduction. The IPBSM modulation and the evaluated beam size without skew sextupoles was also measured just after the measurement. Results are shown in Fig. 13(c),(d). The average beam size was increased to be 63.7 nm. It shows the skew sextupole field to correct the 2nd order optics errors of T_{322}, T_{326}, T_{366} and T_{344} were effective to focus the beam at ATF2 IP. Although a number of systematic studies remain to be done, in particular to fully measure and correct all higher order optical aberrations in the system, a basic tuning procedure was successfully developed to focus the ATF2 IP beam to very small sizes, close to the nominal value. Since the linear and 2nd order optics are exactly the same at ATF2 and ILC, the tuning procedure developed at ATF2 can serve as basis for the tuning of the ILC final focus.

The highest modulation at ATF2 IP is 0.622, and it corresponds to 41.1 nm vertical beam size for $C = 1$ in Eq. (2). The modulation was measured at $N = 0.7 \times 10^9$ electrons/bunch in March 2016 with a beam position stabilization by FONT feedback [38–40]. The achieved beam size is close to the ATF2 target value of 37 nm.

4.2.1.4 *Ultra-low beta* optics studies*

To explore the feasibility of a FFS with a higher chromaticity, being comparable to that of the CLIC FFS, the ultra-low beta* optics has been proposed with four-times smaller IP vertical beta-function than the nominal and a target vertical beam size of 23 nm [41–46]. The ultra-low beta* optics intends to explore the uncharted chromatic territory and push the limits of ATF2. Tuning both the 10×1 optics and the ultra-low beta* optics in the presence of realistic imperfections is of great difficulty, but the latter is much more challenging. To avoid the detrimental effect of multipolar and fringe field errors [47] to the IP vertical beam size, two scenarios have been proposed: insertion of a pair of octupoles to correct third-order aberrations and modifying the optics by increasing β_x^*. In consequence, two octupoles have been fabricated at CERN and installed at ATF2 in 2016 [48], as shown in Fig. 14. The position of the two octupoles has been recently swapped, which can increase the probability of reducing the IP vertical beam size below 30 nm [49]. Following this study, it has been developed a different approach to align the stronger octupole, which does not require the use of high-resolution BPMs around IP and is based on the waist shift information from the IPBSM. On the other hand, the value of β_x^* has been optimized to be 100 mm, 25 times larger than the design.

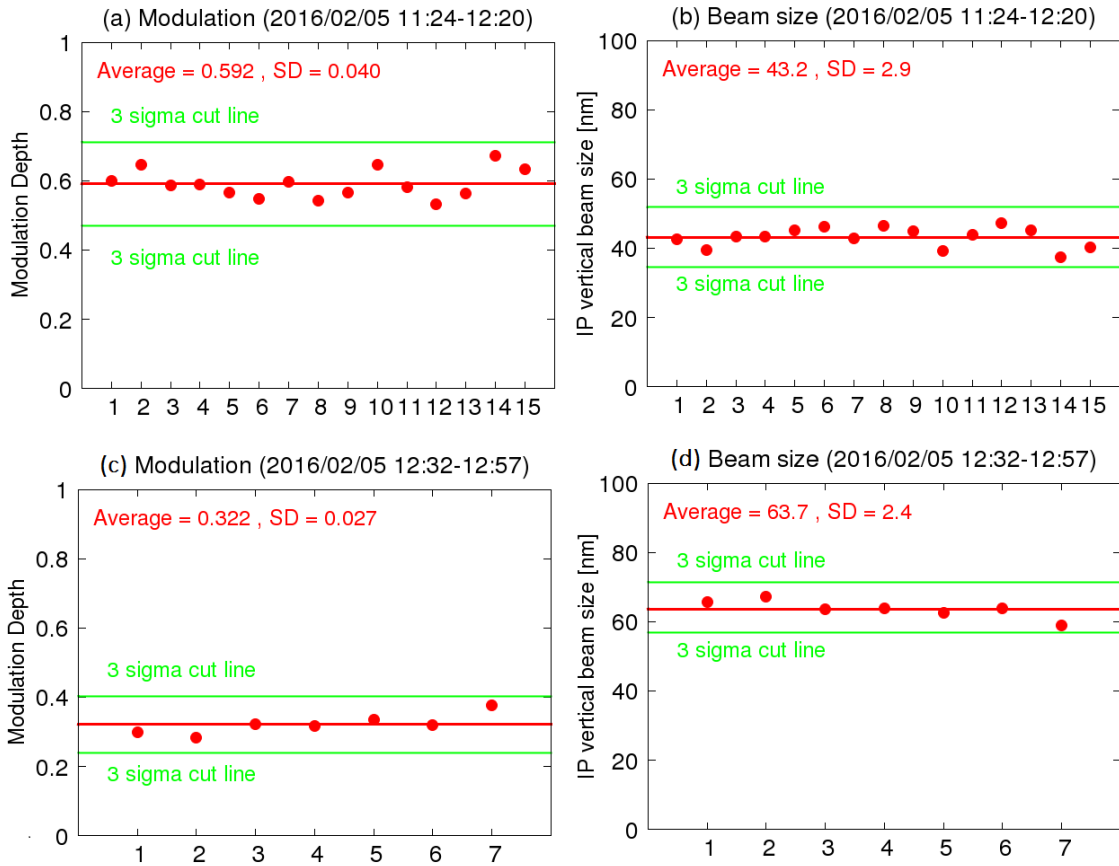To verify the optics design, tuning simulations in the presence of statics and dynamic errors have

Figure 13: (a) IPBSM modulation and (b) the beam size after the IP beam size tuning in 2016 February. (c) IPBSM modulation and (d) the beam size without skew sextupoles. The beam size was evaluated by assuming no modulation reduction of the IPBSM monitor ($C = 1$ in Eq. (2)).

been carried out using a script developed in SAD [50]. The static errors mainly include transverse misalignments, rotation and strength errors of magnets, BPM readout errors and mover accuracy. The dynamic errors contain beam jitters at the extraction point, mechanical vibration of the final-doublet quadrupoles, and ground motion. Following the tuning procedures validated in the 10×1 optics, the simulated IP vertical beam size converges to less than 100 nm after the first iteration of linear aberration corrections, and finally reaches 32.2 ± 4.5 nm after another few iterations of linear and non-linear knob corrections, as shown in Fig. 15. These dedicated tuning knobs are constructed orthogonally using the sextupoles and skew-sextupoles distributed in the FFS. Moreover, the IP vertical position jitter has been accessed to be 20.8 ± 3.4 nm, which increases the multi-shot beam size to 38.3 ± 3.8 nm, for initial beam jitters of 10% of beam sizes. Including the upstream FONT feedback system, which can mitigate vertical beam jitters before the FFS, a probable lower limit of the IP vertical position jitter is evaluated to be about 18 nm. However, on the other hand, the IP position jitter might be worsened by a higher vibration of QF1 during summer operation period [51].

In the past four years, a few dedicated weeks of ultra-low beta* operation have been allocated for consecutive tuning of the ultra-low beta* optics, during which the IP vertical beam size has been successfully squeezed from about 100 nm to 50 nm. In June 2019, the IP beam size was stabilized at about 60 nm for a couple of days with a minimum of 50.1 ± 0.6 nm, about 20 nm above the simulation predictions, as shown in Figs. 16. The gap between the observed and the predicted IP vertical beam sizes has been attributed to the beam size growth due to multipolar errors, beam jitter, wakefield effects and the IPBSM diagnostics errors. Contributions from these systematic effects have been quantified through
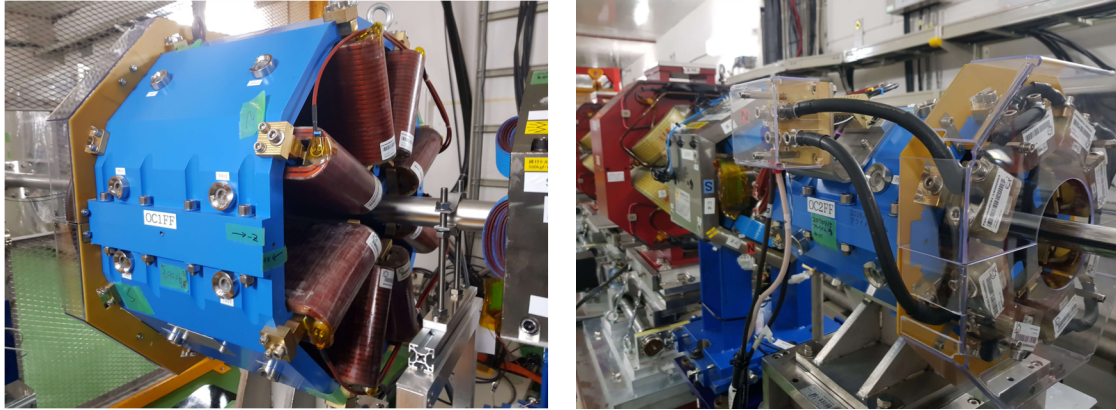
Figure 14: The two Octupoles, OCT1 (left) and OCT2 (right) installed in the ATF2 beam line.
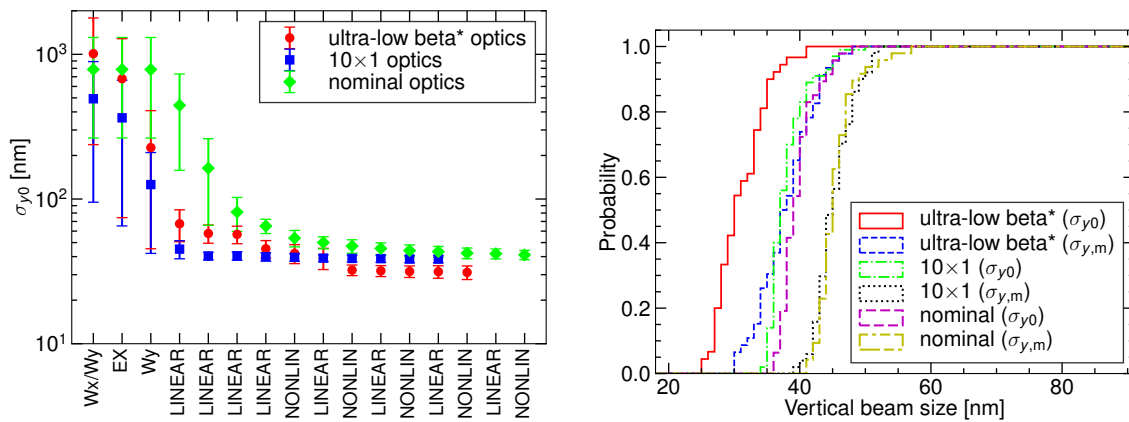

Figure 15: Vertical beam size throughout tuning procedure (left) and cumulative histogram of the final single-shot and multi-shot beam sizes (right). The horizontal labels in (a) are: Wx and Wy, the horizontal and vertical beam waist adjustments using the FD quadrupoles; EX, the IP horizontal dispersion correction; LINEAR, correction of vertical waist, dispersion and coupling from horizontal momentum employing the linear knobs; and NONLIN, correction of residual chromaticity and second-order aberrations applying the non-linear knobs.

simulations and measurements, and are further used to evaluate single-shot beam size from IPBSM measurements. For the obtained 50.1±0.6 nm beam size, a single-shot wakefield-free beam size of about 35.5 nm, consistent with the simulation predictions (32.2±4.5 nm), has been estimated.

A new alignment technique was tested with Ultra-low β_y^* optics in December 2019 and March 2020 operations using IPBSM@30 deg, see Fig. 17. It is based on the waist shift information from the IPBSM. The vertical IP waist shift produced by the misaligned octupole is $\propto (\Delta x^2 - \Delta y^2)$ and can be observed directly on the AY knob scan. The peak of such a scan would be at non zero location, assuming the beam is well-tuned beforehand in either 30 or 174-degree mode. Both measurements agree well and indicate excellent installation precision.

For the near future, tuning with optimal octupole configuration and the FONT upstream beam stabilization have been proposed. The near-term goal is to achieve an IP vertical beam size of less than 40 nm, after which beam tuning with smaller β_x^*, e.g., $10\beta_x^*$ and below, should be explored at ATF2. Sufficient consecutive machine time in stable machine conditions will be favorable for these proposals. Integration of fast beam stabilization system, robust wakefield mitigation strategies, and optimizations of the IPBSM for measuring a beam size of less than 30 nm are also essential. Besides, further online
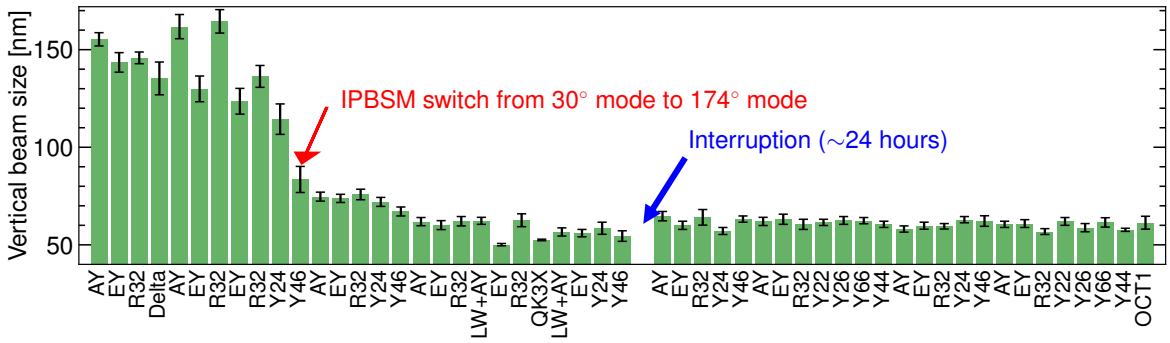
Figure 16: IP vertical beam size versus the beam tuning in the ultra-low beta* optics.

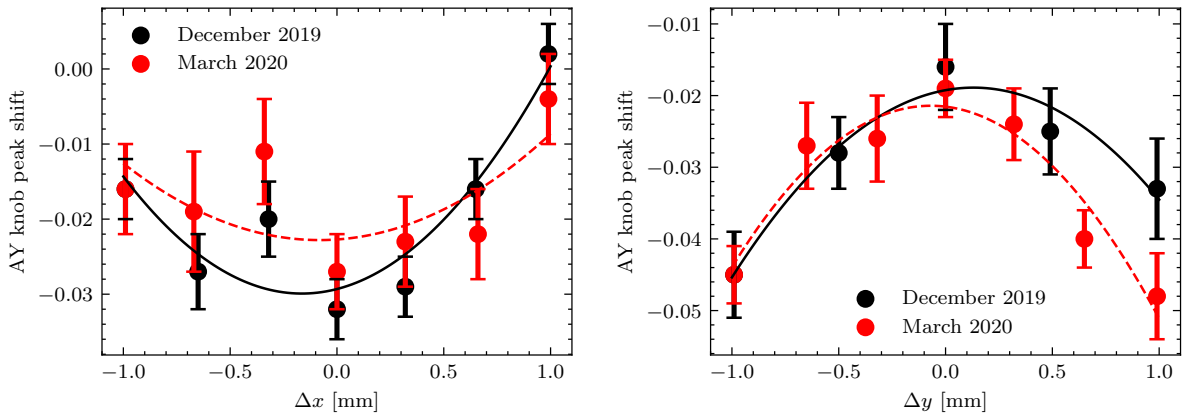measurements and corrections of the exotic vibration of QF1 is recommended.

Figure 17: Measurements of the horizontal (left) and vertical (right) magnetic center of the OCT2 in December 2019 and March 2020 Ultra-low β_y^* runs using IPBSM@30 deg.

4.2.2 Wakefield, intensity dependence of IP beam size

The small beam size at IP could be measured only with low bunch intensity (around $N = 1 \times 10^9$), and we observed strong intensity dependence of the beam size. An example of the dependence is shown in Fig.18, modulation of IPBSM (30 deg. mode) as a function of bunch population. The dashed line is from fitting according to

$$\sigma_y^2 = \sigma_{y,0}^2 + w^2 N^2, \tag{10}$$

where N is the bunch population. $\sigma_{y,0}$ and w are two fitting parameters, the beam size at zero intensity and strength of intensity dependence, respectively.

Wakefield was suspected to be the main reason of the intensity dependence. Though it will not be significant at ILC, it was found that the wakefield cannot be ignored at ATF2 final focus beam line, and we have conducted substantial efforts for studying the effects. [52–55]

Major wakefield sources in the beam line are considered to be C-band cavity type beam position monitors (CBPM), the reference cavity of the CBPM system (RefCav), bellows and flange gaps.

We consider vertical wakefield effects in one bunch. Particles are kicked vertically by wakefield induced by preceding particles in the same bunch. Such transverse kicks cause orbit difference of paticles depending on the longitudinal position, then beam size growth.
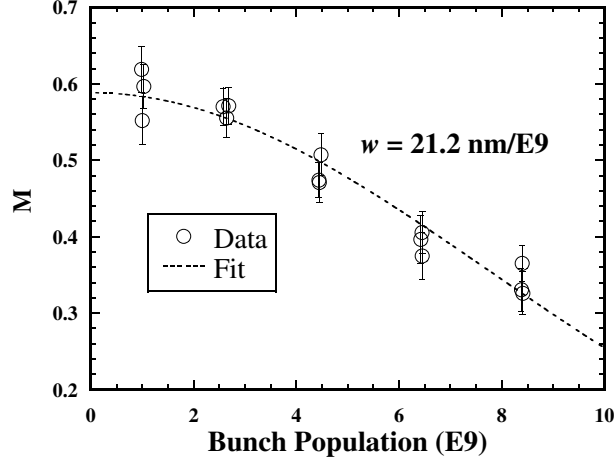
Figure 18: Measured modulation of IPBSM as function of bunch population. The line is fitting result assuming the dependence as Eq.(10). (Measured on Oct. 26, 2016)

We define wake potential, $W(z)$, of a certain structure in the beam line which gives orbit angle change (strength of kick) depending on the relative longitudinal position in a bunch (distance from the bunch center), z, as

$$\Delta y' = eq(y - y_a)W(z)/E \tag{11}$$

where y is the mean vertical position of the beam, y_a the vertical offset of the structure, q the charge of the bunch and E the beam energy. We assume the structure has cylindrical symmetry and the angle change is proportional to $(y - y_a)$, which is the relative offset between the center of the structure and the beam.

Wake potentials of major components in the final focus line were calculated using GdfidL [56], as shown in Fig.19. Here, the bunch is assumed to have Gaussian shape with $\sigma =$ 7 mm.
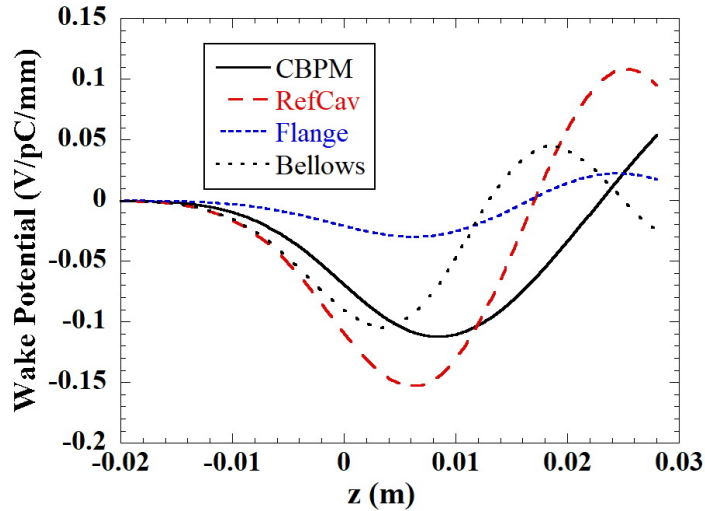

Figure 19: Calculated Wakepotentials of CBPM, RefCav, Bellows and Flange.

There are many wakefield sources in the beam line and the position change at IP can be expressed as

$$y_{IP}(z) = eq\sum_i (y_i - y_{a,i})\sqrt{\beta_i\beta_{IP}} \sin\phi_i W_i(z)/E. \tag{12}$$

where i is the index for wakefield sources. $\sqrt{\beta_i \beta_{IP}} \sin \phi_i$ is the 3-4 component of transfer matrix (R_{34}) from the i-th source to IP, where β_i and β_{IP} are betafunctions at the i-th structure and IP, respectively, and ϕ_i the phase advance between them.

The effect to the position change at IP is proportional to square-root of the beta-function. It should be noted that phase advances to IP are very close to $(n + 1/2)\pi$ (n is integer) from anywhere in the final focus beam line, except for short regions with very small beta-function. This is shown in Fig. 20, the vertical beta function and the phase to IP along the final focus beam line.
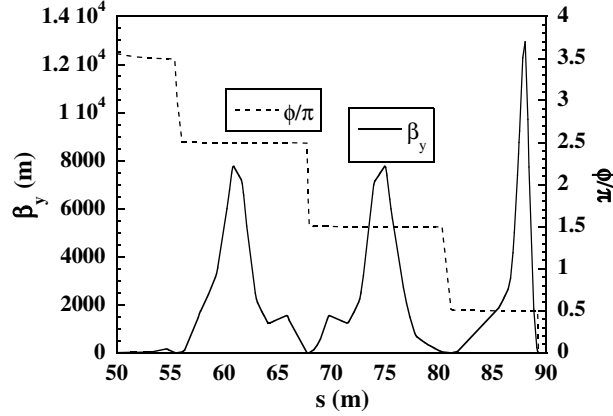

Figure 20: beta-function (solid line) and phase advance to IP (dashed line) along the final focus beam line of ATF.

For studying the wakefield, we installed mover, on which a wakefield source was put and the transverse positions could be remotely controlled. It was in the region of large vertical beta-function to make its wakefield effect large.

4.2.2.1 *orbit change study using wakefield source on mover*

Wakefield changes beam orbit (orbit of center of mass of a bunch) downstream of the wakefield source. The orbit along the beam line was measured using cavity BPMs (CBPMs) changing the vertical position of a wakefield source (in this case RefCav) on the mover, with various bunch charge. For precisely evaluating beam position response at downstream CBPMs, effects of pulse to pulse jitters were eliminated by subtracting propagating orbit using data of upstream CBPMs. Wakefield of the structure depending on the mover positions were carefully calculated. Fig. 21 shows the orbit responses agreed with the calculations within a factor of 1.2. In spite of the complex shape change of the movable structures (e.g. distorted bellows), this is a good agreement. Details were reported in the reference [57].

4.2.2.2 *Static effects to beam size and compensation by wakefield source on mover*

We performed simulations including randomly misaligned CBPM and bellows, with normal distribution with RMS 0.3 mm, and, for a particular random number, Figs 22 (a), (b) and (c) show simulated vertically projected beam profiles at IP for bunch population 0 (no wakefield), 4×10^9 and 8×10^9, respectively.

We used RefCav on mover for correcting and studying the wakefield effects to beam size too. By controlling the vertical position of RefCav, kicks by other wakefield sources can be reduced. Since z (relative longitudinal position in a bunch) dependence of $W(z)$ is different for different types of structures, it cannot be exactly zero for all z. However, if shapes of $W(z)$ of major wakefield sources are similar to the structure on mover, most of the static wakefield effects can be canceled by adjusting the position of the structure.

The effectiveness of the compensation is shown by simulations as in Fig 23(A), the RMS beam size as function of the vertical position of RefCav. The modulations of IPBSM with 30 degrees mode
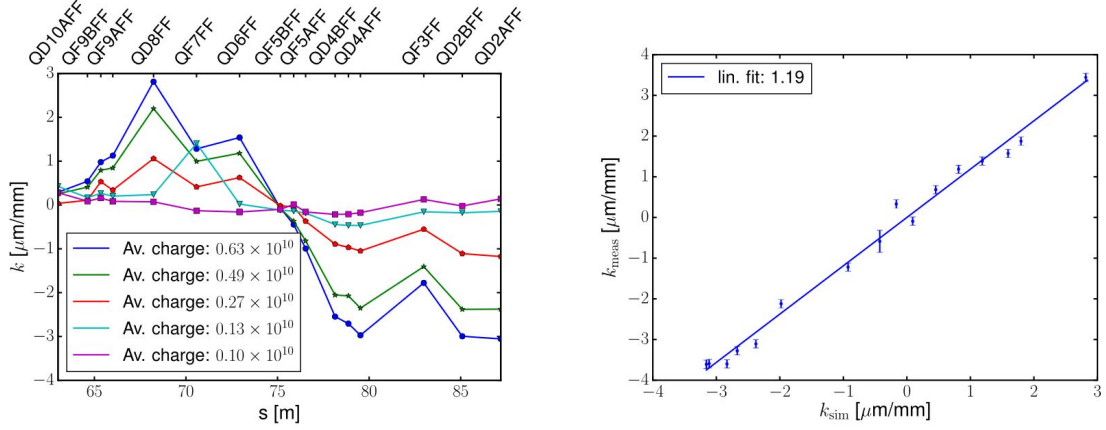
Figure 21: (Left) The measured vertical orbit response for each CBPM with respect to the movable section position for different bunch intensities after pulse averaging and jitters subtraction. (Right) The measurement and simulation are compared for an average bunch charge of 0.75×10^{10} particles. A linear fit is shown as well. [57]
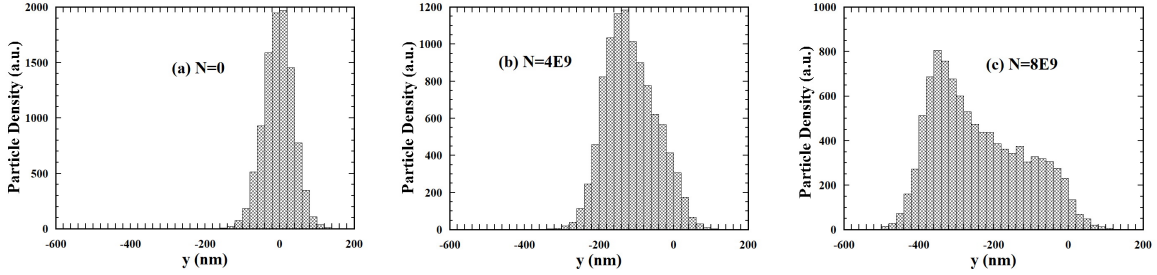

Figure 22: Simulated vertically projected beam profiles at IP for bunch population (a) 0 (no wakefield), (b) 4×10^9 and (c) 8×10^9.

are also shown as a function of the vertical position of RefCav in Fig 23(B). The bunch population was set as 8×10^9. There are four lines in each plot: (a) only CBPMs are misaligned, (b) only bellows are misaligned, (c) only flanges are misaligned and (d) no misalignment.

For each of (a), (b) and (c), amount of the misalignment was chosen to make the resulted beam size about 105 nm (meaning w about 13 nm/10^9) with the RefCav position zero. By adjusting the RefCav position, the beam size can be reduced to 64 nm, 55 nm and 44 nm for the cases (a), (b) and (c), respectively. This means w can be reduced to 6.3 nm/10^9, 4.7 nm/10^9 and 2.3 nm/10^9, respectively. The difference between three cases can be explained from the different shapes of the wakepotentials, $W(z)$ (see Fig.19).

One example of experimental data of such compensation is shown in Fig 24, the modulation of IPBSM with 30 degrees mode as function of the vertical position of RefCav. The bunch population was 8×10^9 during the experiment.

After setting the RefCav position at the peak of the modulation, the intensity dependence of the beam size reduced.

For studying the compensation effects further, another mover was installed and other types of structures have been installed, C-band pillbox (a simplified model of C-band cavity BPMs, CBPM) and bellows. The experiments using these wakefield sources on mover have suggested that wakefield compensation with two different structures (e.g. CBPM and bellows) is better than that using only one of these structures, as expected.
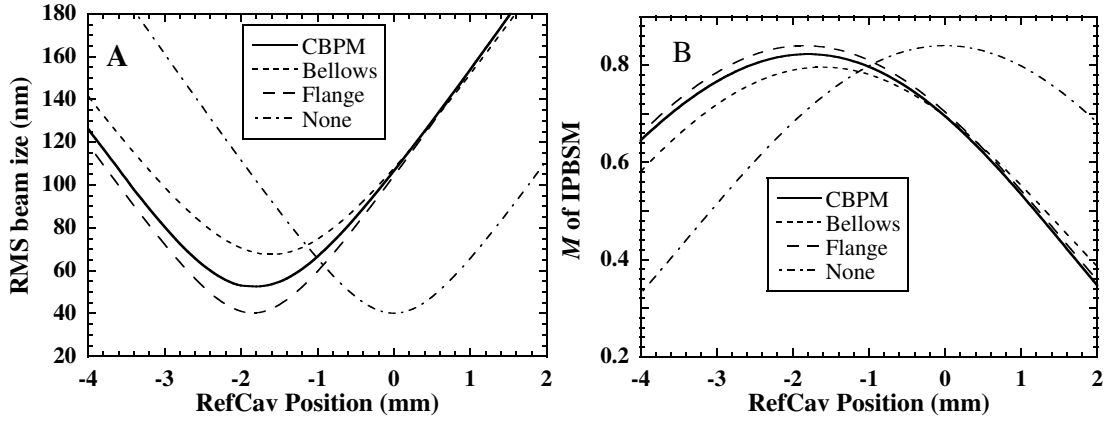
Figure 23: Simulation results of wakefield compensation by a wakefield source on a mover. (A) RMS beam size at IP and Bb) IPBSM modulation as functions of position of RefCav. Four lines correspond to different misalignment: (a) only CBPMs are misaligned, (b) only bellows are misaligned, (c) only flanges are misaligned, and (d) no misalignment.
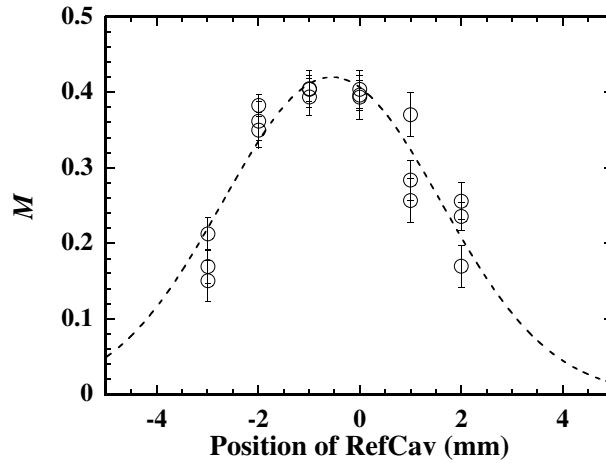

Figure 24: An example of experiments of wakefield compensation by a wakefield source on a mover. IPBSM modulation as function of position of RefCav. (Measured on Oct. 25, 2016.)

4.2.2.3 *Reduction of wakefield sources*

In November 2016, we changed the vaccum chamber configuration of the final focus beam line. Some of cavity BPMs, bellows and flange connections were removed. RF contacts were inserted to most of the remained bellows.

The total wakefield strengths in the final focus beam line, before and after the above change (October and November 2016), were experimentaly compared as follows.

The vertical beam size at IP was minimized by changing vertical position of the wakefield source (RefCav) on a mover, for each of different vertical beam orbits in the final focus beam line. The orbit was changed by using a vertical steering magnet, from which the phase advance to IP was set as 3π, so that only the angle at IP phase orbit was changed.

The measured modulations of IPBSM (30 deg. mode) are shown in Fig. 25 (a) and (b) as functions of the mover position for different beam orbits, and the correlations between the orbit and the optimum RefCav position are shown in Fig. 25 (c).

The optimum position of RefCav is result of compensation of wakefield in the whole beam line,

which is changed according to the orbit change. Then, the correlation slopes in Fig. 25 (c) are strengths of wakefield in the final focus beam line in unit of the strength of wakefield of RefCav. Therefore, the experiments indicate the wakefield in the final focus beam line was reduced to about $1/3$ by the modification of the beam line (removal of structures) in November 2016.

Simulation including cavity BPMs, RefCav, un-masked bellows and flange gaps showed reduction of wakefield to about $1/2$, which agrees with the experiment within estimated errors.
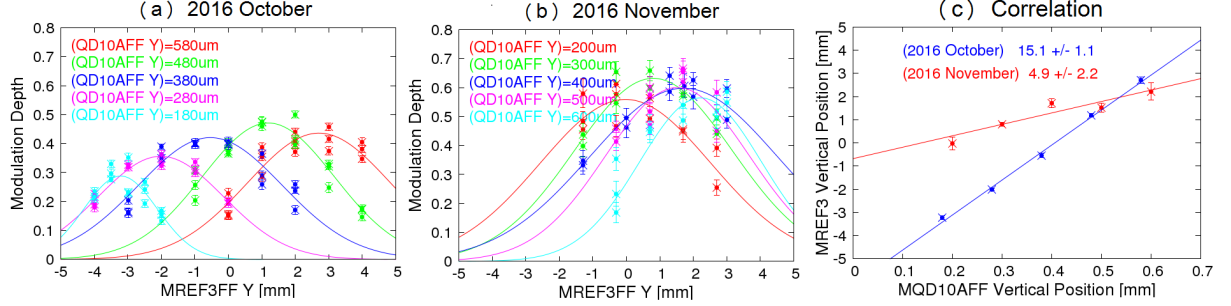

Figure 25: The IP vertical beam size optimization by optimizing the RefCav position optimization for several FD phase beam orbit. The bunch population was $N = 7 \sim 8 \times 10^9$ in the measurement. (a) 2016 October, (b) 2016 November, (c) correlation between orbit and the optimum RefCav mover position. The orbit change is shown as change of beam position at a CBPM named MQD10AFF. [52]

4.2.2.4 Dynamic wakefiled effect

Here, wakefield effect to apparent beam size with beam orbit distortion is discussed.

Beam orbit can be divided into two different phases, 'position at IP' (position orbit) and 'angle at IP' (angle orbit). For an orbit with amplitude of the 'position at IP' a_{position} and amplitude of the 'angle at IP' a_{angle}, the beam position at a certain location in the beam line is expressed as

$$y = a_{\mathrm{position}}\sqrt{\beta\epsilon}\cos\phi - a_{\mathrm{angle}}\sqrt{\beta\epsilon}\sin\phi, \tag{13}$$

whehe β is the beta-function of the location, ϵ the nominal emittance and ϕ the phase advance from the location to IP. The amplitude a_{position} and a_{angle} are normalized with nominal beam size and angular divergence at IP, respectively.

Consider perfectly aligned wakefield sources with beta-function β_i and phase ϕ_i to IP. Then, using Eq. (12) and Eq. (13), position change at IP due to wakefield is

$$y_{IP}(z) = eq\sqrt{\beta_{IP}\epsilon}\sum_i \beta_i(a_{\mathrm{position}}\sin\phi_i\cos\phi_i$$
$$-a_{\mathrm{angle}}\sin^2\phi_i)W_i(z)/E \tag{14}$$

Since at all important wakefield sources, $\phi_i \approx (n+1/2)\pi$, and $\cos\phi_i \approx 0$ and $\sin^2\phi_i \approx 1$, the effect of the 'Position at IP' phase orbit can be ignored and

$$y_{IP}(z) = -eqa_{\mathrm{angle}}\sqrt{\beta_{IP}\epsilon}\sum_i \beta_i W_i(z)/E. \tag{15}$$

Note that effects of all wakefield sources are added with the same sign.

Wakefield effect of static orbit distortion can be mostly compensated as same as the effect of misalignment discussed in the previous section. However, when orbit is changing, the beam shape is

changing pulse by pulse and apparent beam size will be increased. Note that our beam size monitor measures projected beam size of many pulses.

We observed beam orbit jitter in the final focus line, usually from 0.1 to 0.3σ of the nominal beam size, depending on conditions. The direct effect of the 'Position at IP' phase orbit is very small even with 0.3σ. It will only change the apparent beam size from 1σ to $\sqrt{1+0.3^2}\sigma$ (difference is 0.044σ), which is much smaller than typically observed beam size growth.

Simulations were performed to show the effects of the orbit jitter. 'Angle at IP' phase orbit is randomly set as normal distribution with RMS 0.3σ. All wakefield sources (CBPMS, bellows, flanges and RefCav) are aligned perfectly. Fig. 26 shows RMS beam size (sum of 100 random orbits) as function of bunch population for orbit jitter with RMS 0.3σ. It also shows apparent beam size, which is calculated from the modulation of IPBSM with 30 degree mode. From the fitting (Eq.(10)), the intensity dependence is evaluated as 17.1 nm/10^9 for 0.3σ orbit jitter. This result suggests that significant part of the observed intensity dependence can be explained as the wakefield effect with orbit jitter.
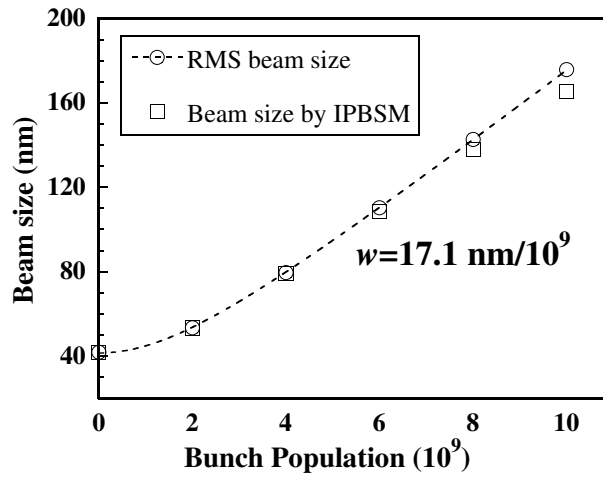

Figure 26: Simulated RMS beam size as function of bunch population for orbit jitter with RMS 0.3σ.

4.2.2.5   reduction of jitter effect by orbit feedback

For studying the dynamic wakefield effect, intensity dependence of beam size was measured with and without fast orbit feedback (upstream FONT) on June 22, 2018. In two-bunch operation, orbit information of the first bunch is used for correcting the second bunch orbit. The system is located upstream of the final focus beam line. The beam size of the second bunch was measured. For making the feedback effect clearer, the angle at IP phase jitters were increased by setting an optics with small β_y^* (0.025 mm), by changing strengths of the quadrupole magnets in the upstream of the final focus beam line.

The RMS of the angle jitter at IP of 2nd bunch was evaluated from BPM data as 215 μrad without feedback, and it was reduced to 50.6 μrad with feedback (Fig. 27(a)). Fig. 27(b) shows the results of intensity dependence of 2nd bunch with and without orbit feedback. Table 3 shows the summary of the vertical angle jitters at IP and the evaluated intensity dependence of the 2nd bunch beam size. It was confirmed that the dynamic component of the intensity dependence can be reduced by reducing the angle jitter by using the feedback.

4.2.2.6   data selection for jitter effect study

Since synchronized data of BPM and IPBSM were saved for each beam pulse, we can effectively reduce the angle jitter by selecting data of small $|y_{IP}'|$. Analysis of IPBSM data selected as $|y_{IP}'| < y_{cut}'$ with various y_{cut}' were performed for data of single bunch operation (no feedback) with small β_y^* optics.
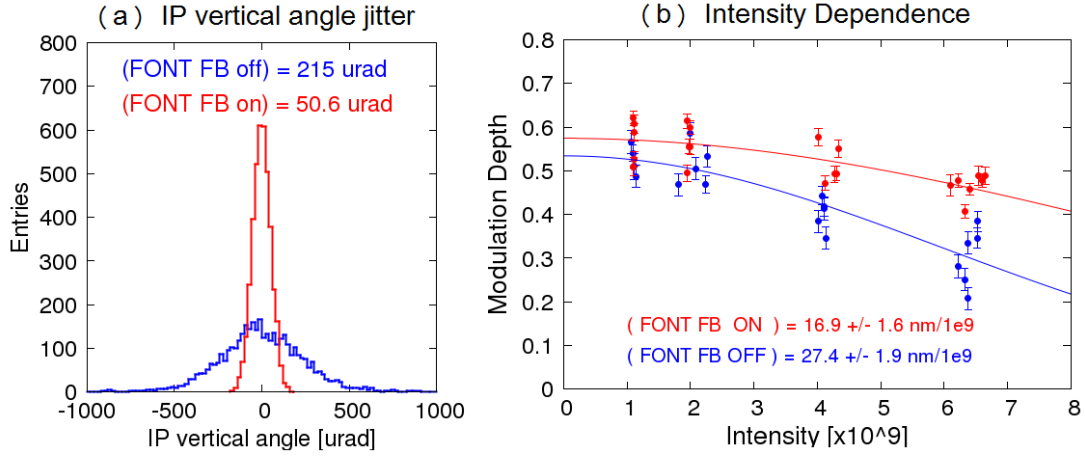
Figure 27: Vertical angle jitter at IP and intensity dependence for 2 bunch operation with/without orbit feedback. [52]

Table 3: Summary of intensity dependence for 2 bunch operation.

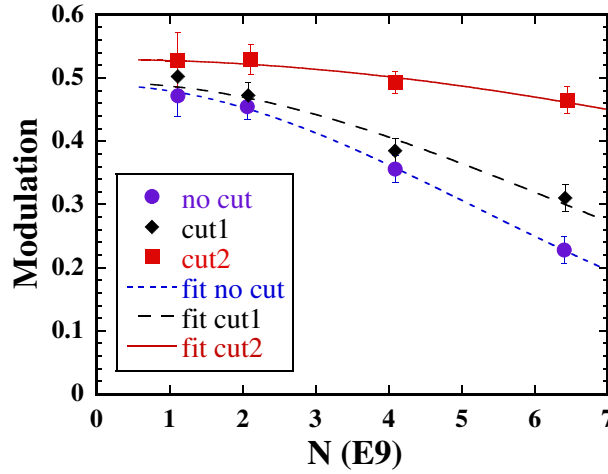|	Angle jitter at IP	Intensity dependence
without feedback	215 μrad	27.4$\pm$1.9 nm/$10^9 e$
with feedback	50.6 μrad	16.9$\pm$1.6 nm/$10^9 e$

Figure 28: Modulation of IPBSM (with 30 degree mode) as function of bunch intensity with three different data selections by angle at IP, no cut: all data used, cut1: $|y'| < 520\mu$rad, cut2: $|y'| < 173\mu$rad, The lines of fitting for estimating intensity dependence are also shown.

Fig. 28 shows modulation of IPBSM (with 30 degree mode) as function of bunch intensity with three different data selections; all data used, $|y'_{IP}| < 520\,\mu$rad and $|y'_{IP}| < 173\,\mu$rad. The lines are from fitting by the function

$$M = M_0 e^{-\left(\frac{\sqrt{2}\pi w N}{d}\right)^2} \tag{16}$$

for estimating intensity dependence. Here, N is the bunch intensity, d the pitch of the laser interference. M_0 and w are the fitting parameters, the modulation at zero intensity and the intensity dependence parameter.

34

w was evaluated for each of selected data set with the angle at IP limit (y'_{cut}). Fig.29 shows w as function of the RMS of y'_{IP} of the selected data. From the fitting, w is expressed as

$$w[\text{nm}/10^9] = (0.110 \pm 0.0308)\sigma_{y'}[\mu\text{rad}] + (3.07 \pm 6.41) \tag{17}$$
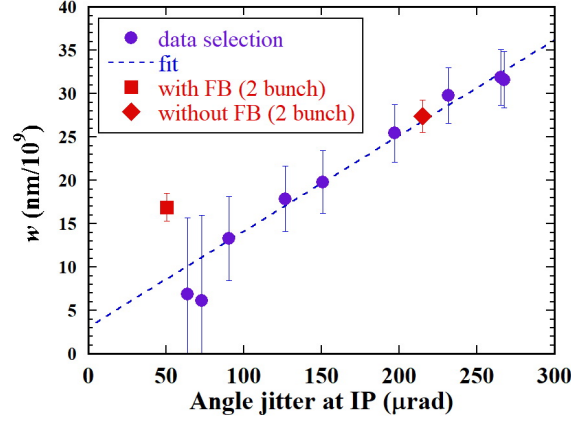

Figure 29: Intensity dependence parameter as function of RMS angle jitter. Each point was evaluated as the intensity dependence parameter with a certain limit of angle at IP (y'_{cut}). The RMS angle jitter was from distribution of y'_{IP} at high intensity ($N \approx 6.5 \times 10^9$), while apparent RMS jitter was larger for lower intensities due to intensity dependence of BPM resolution.

Fig.29 also shows the data with and without the fast orbit feedback in two-bunch operation. Though the result without feedback well agrees with the result of data selection, the result with feedback is not on the fitting line. The reason of the discrepancy has not been understood yet.

Beam size measurement data in 2016 for three different β_y^* optics were also analyzed with three different angle jitter selections for each optics. Fig. 30 shows intensity dependence parameter (w) as function of the RMS of y'_{IP}, These data points are not on one single line, suggesting significant static effects remained, which depend on optics.

These data were taken before the wakefield source reduction in November 2016, the dependence was much larger than that in 2018. However, the slopes of the dependence (effect of the orbit jitters) are not large compared with that in Fig. 29. This discrepancy has not been explained yet.

4.2.2.7 Comparison between ILC and ATF

Rough comparison of expected effects of wakefield in the final focus beam line at ILC and ATF can be evaluated from simple scaling as follows. [58]

We assume there are the same wakefield sources distributed at every magnet (number of sources is proportional to the number of magnets). For effects of random misalignment, assume the same accuracy of component alignment. For effects of beam orbit jitter, assume the same jitter amplitude relative to the nominal beam size. Then, expected effects to the beam size relative to the nominal beam size are compared.

There are four factors considered as follow.

– Because of the higher beam energy, ILC beam will be more rigid than ATF.
– Different bunch lengths, 300 μm at ILC and ≈ 7 mm at ATF, also gives different effects. For rough scaling, the difference factor due to the bunch lengths was evaluated as 0.5 (smaller effect at ILC) from wakepotential calculation of C-band cavity BPM with different bunch lengths.
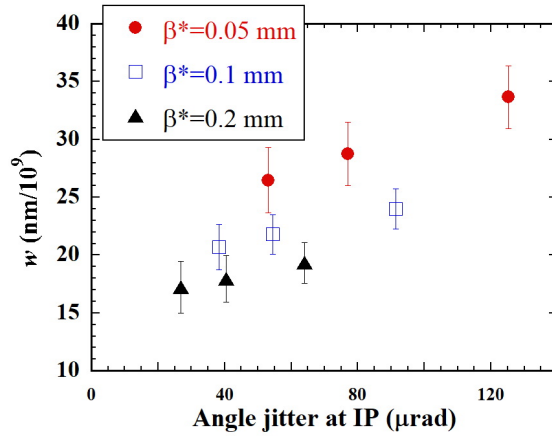
35

Figure 30: Intensity dependence parameter (w) as function of the RMS of y'_{IP} for three different optics, with three different data selections each.

Table 4: Relative effect of misalignment and orbit jitter at ILC and ATF2

	ILC	ATF	Ratio of effect (ILC/ATF)	
			misalignment	orbit jitter
Beam Energy	125 GeV	1.3 GeV	0.01	0.01
Bunch Length	0.3 mm	7.0 mm	0.5	0.5
Emittance	0.16 pm	12 pm	8.7	1
Sum of β_y	390 km	61 km	2.5	6.7
Total			0.11	0.032

– The misalignment effect scales as inverse of square-root of the emittance (the nominal beam size). The orbit jitter effect does not depend on emittance, because jitter amplitude is assumed to be proportional to the square-root of emittance and the effect is compared with the nominal beam size which is also proportional to square-root of emittance.

– The misalignment effect scales as square-root of total summation of betafunctions at wakefield sources ($\propto R_{34}$ to IP) . The orbit jitter effect scales as total summation of betafunctions at wakefield sources, since beam position offset is also proportional to square-root of betafunctions at wakefield sources.

Table 4 summarizes the comparison, depending on beam energy, bunch length, emittance and beta-function.

As conclusion, assuming the same bunch charge, relative wakefield effect at ILC FF to ATF FF will be a factor of about 0.11 for random misalignment and a factor of about 0.032 for betatron oscillation. In other words, the effect of wakefield at ILC with the designed bunch population (2×10^{10}) will be similar to that at ATF with bunch population 0.22×10^{10} for random misalignment and 0.064×10^{10} for orbit distortion.

4.2.2.8 summary and remaining issues

Confirming reliability of our calculations of wakefields and their effects is important for the design of the ILC final focus beam line.

The study of beam orbit change using wakefield sources on mover showed good agreement

between the experimental data and the calculations.

For the beam size at IP, static and dynamic effects have been studied in various ways. For static effects, reduction of wakrfield by removal of wakefield sources in the high-beta function region was confirmed, and wakefield compensation by wakefield sources on mover was also confirmed to be effective. The significant dynamic effect was shown and reduction of the effects have been demonstrated by the fast orbit feedback and data selection analysis.

Though qualitative similarity of the results of simulations and the experiments is obvious, quantitative agreement is not sufficient. Even with optimized positioning of wakefield sources on movers, we still observed intensity dependence of the beam size significantly stronger than expected from the orbit jitter effects.

One possible reason is unknown wakefield sources with different shapes of wakepotentials which cannot be compensated by prepared wakefield source on mover. Studies with different wakefield sources on mover and investigation of upstream beam line will be needed.

Effects other than the wakefield, for example, higher order chromatic or/and geometric aberrations should be also considered. Due to intra-beam scattering in the damping ring, energy spread and emittances increase as intensity increases [59]. The effect of the intra-beam scattering to IP beam size calculated from linear optics is much weaker than the observed intensity dependence. Simulations including measured multi-pole fields of magnets in the beam line show that it explains only a tiny part of the intensity dependence [60]. However, there may be unknown non-linear field errors which induce much stronger dependence and possibility of strong non-linear aberrations cannot be completely excluded. We installed octupole magnets and have started study on unknown octupolar aberrations but we cannot conclude much with the existing data.

4.2.3   Beam position stabilization with the FONT intra-train feedback system

The FONT group from the University of Oxford has developed several variations of a low-latency, intra-train feedback system for use with multi-bunch trains at ATF2. The original system was a prototype for the ILC interaction point feedback system and used hardware located near the start of the ATF2 beamline (Fig. 31). A single stripline kicker was used to correct the vertical beam orbit locally based on the position measured at a single stripline BPM. This system was upgraded to a dual-phase system by including a second stripline BPM and kicker, allowing simultaneous correction of the vertical position and the vertical trajectory angle.

An independent system for correcting the position at the ATF2 IP using a single stripline kicker installed just upstream of the IP chamber was also developed. This system used the same feedback control hardware as the existing FONT system but with the firmware modified in order to work with signals from the C-band cavity BPMs at the IP. Both the upstream stripline-based system and the IP cavity-based system will be described in this section.

4.2.3.1   Upstream feedback system

Hardware   The hardware of the upstream feedback system is depicted schematically in Fig. 32 and the longitudinal distance of the key components from the start of the ATF2 beam line are given in Table 5. P2 and P3 are stripline BPMs. The voltage pulses induced on the top and bottom striplines by the passage of an electron bunch are processed using custom analogue electronic modules; the design of these BPMs and electronics has been previously reported [67]. The stripline voltage-difference signal (Δ) depends on both the vertical position of the bunch and its charge, while the stripline voltage-sum signal (Σ) depends only on charge. The position of the bunch is derived from the ratio Δ/Σ. A beam position resolution of 291 ± 10 nm for this system in operation at ATF2 has been reported [67]. In 2016 the system was upgraded [68], resulting in an improved position resolution of 157 ± 8 nm for a beam charge of 1.3 nC (0.82×10^{10} electrons/bunch). The upgraded system was used for the results reported
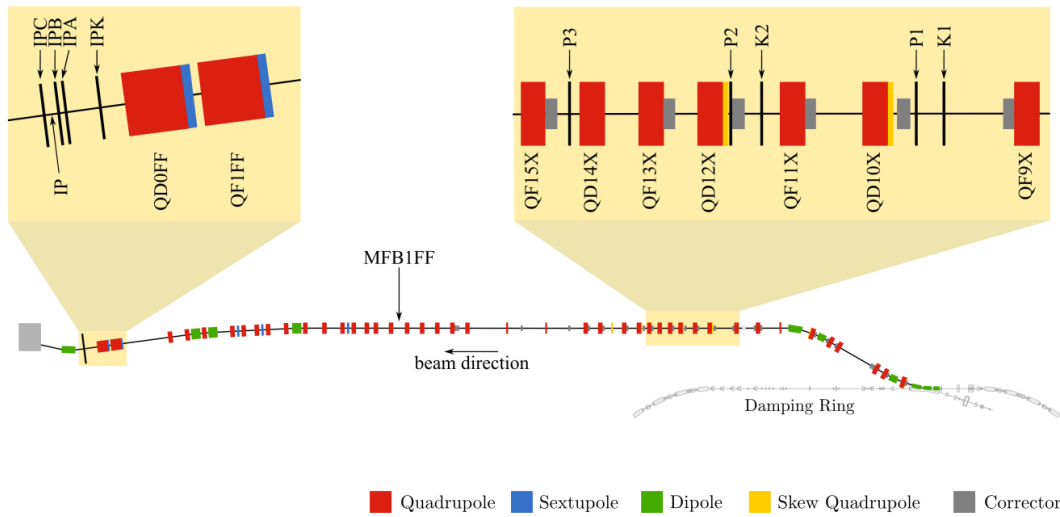
Figure 31: Schematic of the layout of the ATF2 beamline, with the regions containing the hardware used for the FONT feedback systems shown in more detail.
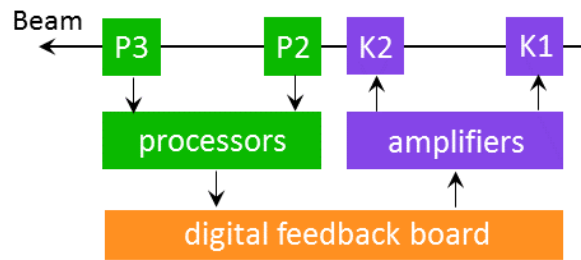

Figure 32: Schematic of the coupled-loop feedback system using BPMs P2 and P3 and kickers K1 and K2.

here.

The processed BPM signals are input to a custom-made digital feedback ('FONT5') board [13,67]. The FONT5 board features a Field-Programmable Gate Array (FPGA) along with nine analogue-to-digital converters and a pair of digital-to-analogue converters. The feedback algorithm runs on the FPGA and is able to calculate the appropriate kicker drive signals from the digitized BPM signals. The kicker drive signals are then amplified externally using bespoke ultra-fast amplifiers developed by TMD Technologies and applied to the stripline kickers K1 and K2. By design the two BPM-kicker pairs (P2,K1) and (P3,K2) are situated in the lattice at sufficiently different values of the betatron phase advance that the measurements and corrections are non-degenerate and the offset in both position and trajectory angle can be removed.

4.2.3.2 Results

The beam stability study was performed using trains of two bunches extracted from the Damping Ring with a bunch spacing of 187.6 ns, and a train repetition rate of 1.56 Hz.

Witness BPMs The stripline BPM MFB1FF is located about 25 m downstream of the feedback system (Table 5) and was instrumented with an analogue processor of the same type as used for P2 and P3. The outputs of this processor were monitored using a second FONT5 board operating purely as a

digitizer. The cavity BPMs IPB and IPC are located either side of the nominal IP (Fig. 31). These BPMs were instrumented with a completely distinct set of processing electronics [69], the outputs of which were monitored by a third FONT5 board. The operation of these BPMs for multi-bunch intra-train readout has been previously reported [63, 70–72].

Measurements Distributions of the vertical beam position recorded at each BPM are shown in Fig. 33 for a run comprising 200 beam pulses. The feedback was toggled on and off for alternate beam pulses and the distributions are shown separately for the feedback-off and feedback-on sets of pulses.

It is clear from the feedback-off data that there is a significant difference in the orbits of the two bunches. The feedback BPMs themselves are mounted on translatable mover stages and, at the start of a period of data taking, would normally be aligned so as to zero the mean of the readout position of bunch 1. In the case of a difference in the bunch orbits, the second bunch would still be stabilized by the feedback system (as long as the pulse-by-pulse positions of the two bunches were highly correlated), but the mean position of the corrected bunch would be offset from zero by the difference in mean orbit of the uncorrected bunches.

The requirement to keep the corrected trajectory of the second bunch within the dynamic range of the downstream witness BPMs (including MFB1FF, which has no mover) complicates the issue. The set of measured mean positions essentially represents the end result of an iterative process of tuning the corrected orbit of the second bunch while working within the limits imposed by the orbit difference of the uncorrected bunches and the range of the cavity BPM movers.

The performance of the feedback system in terms of the beam stability is shown in Fig. 33. Bunch 1 provides the feedback input and its position is not corrected. Bunch 2 is well corrected by the feedback as shown by the substantial reduction in the position jitter seen at the two feedback BPMs (from 1.39 µm to 0.34 µm at P2 and from 0.81 µm to 0.27 µm at P3) and also at the three downstream witness BPMs (from 71.9 µm to 17.4 µm at MFB1FF, from 19.7 µm to 4.8 µm at IPB and from 7.2 µm to 1.7 µm at IPC). Table 6 shows the measured beam position jitter at each BPM for bunches 1 and 2 with feedback off and on. The correction is limited by the resolution of BPMs P2 and P3, which was c. 200 nm for the bunch charge used (0.45×10^{10} electrons). The correction factor at all three witness BPMs is consistent with the in-loop correction of roughly a factor of 4.

Also shown in Table 6 are the predictions of a linear beam transport model of the ATF2 beam line based on MAD. The measured beam positions at P2 and P3 were extrapolated using the model to give predicted positions at MFB1FF, IPB and IPC. The predicted jitter values and respective correction factors are in good agreement with the direct measurements, implying that there are no major sources of additional beam jitter between the extraction line and the ATF2 final focus.

Table 5: Table indicating the longitudinal distance of selected beam line components from the start of the ATF2 beam line).

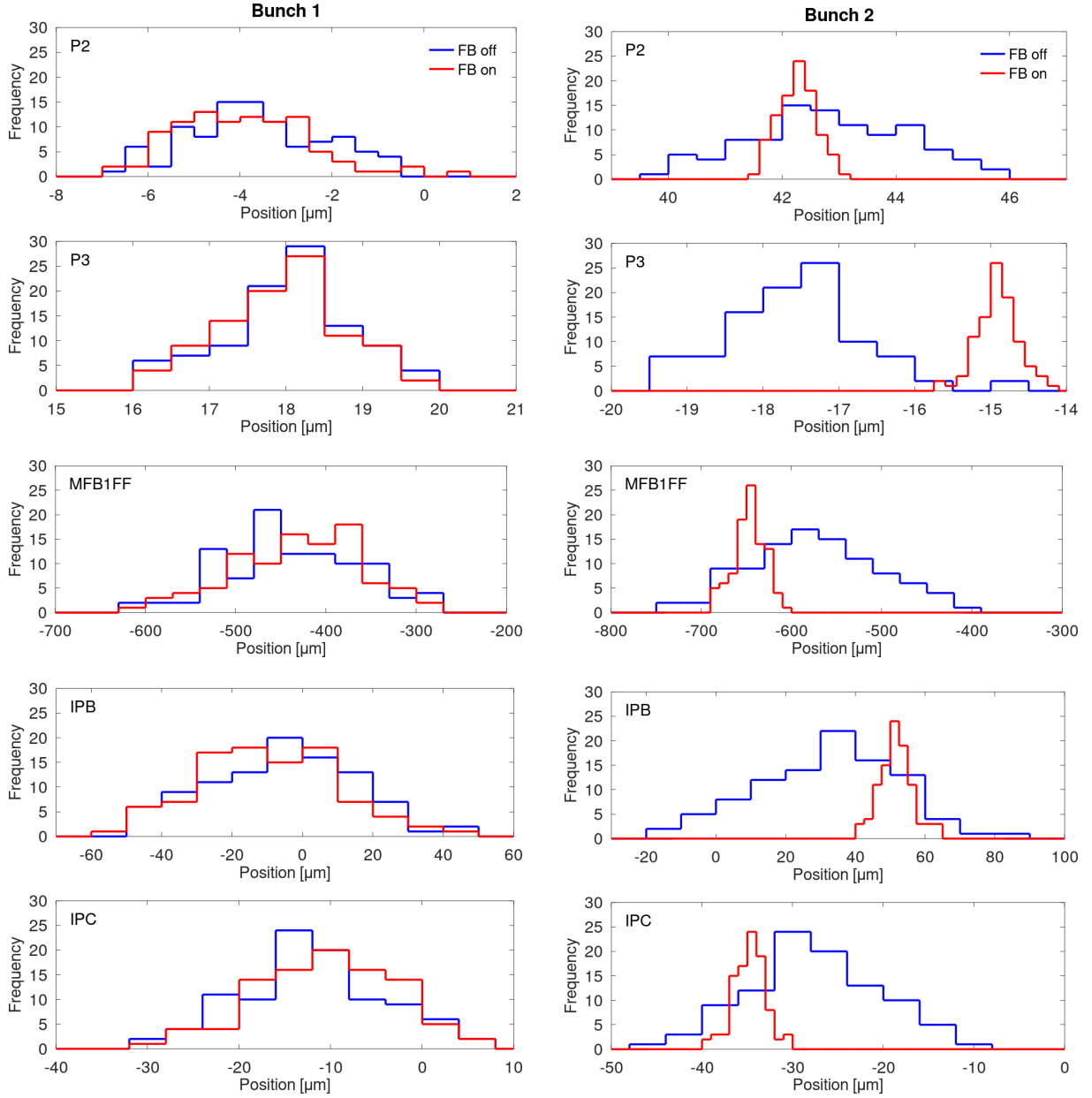| Name	Distance [m]
K1	26.672
K2	29.598
P2	30.123
P3	33.025
MFB1FF	58.534
IPB	89.212
IP	89.299
IPC	89.386

Figure 33: Distribution of position measured at each BPM (rows) for bunch 1 (left column) and bunch 2 (right column) with feedback off (blue) and on (red). Where necessary a reduced bin width is used to display the feedback-on data so as to limit the maximum frequency of a single bin for display purposes.

As the system is dual-phase, the effect of the feedback on the angular jitter of the beam is also of interest. The angular jitter of the bunch is calculated using the position measured at two BPMs and knowledge of how the beam propagates from one BPM to the other; the MAD model is used for the transfer matrix from P2 to P3. In the IP region the transfer matrix is trivially obtained as the beam propagates in a ballistic fashion from IPB to IPC.

The measured position and angle at P2 can then be propagated downstream using additional transfer matrices from the model in order to give the predicted distributions of the beam angle at each witness BPM. The angle at P3 is shown in Fig. 34 and these results, along with those at MFB1FF and in the IP region, are summarized in Table 7. The results show that the angular jitter of bunch 2 is also reduced by about a factor of 4, consistent with the position-correction analysis. Also shown in Table 7 is the
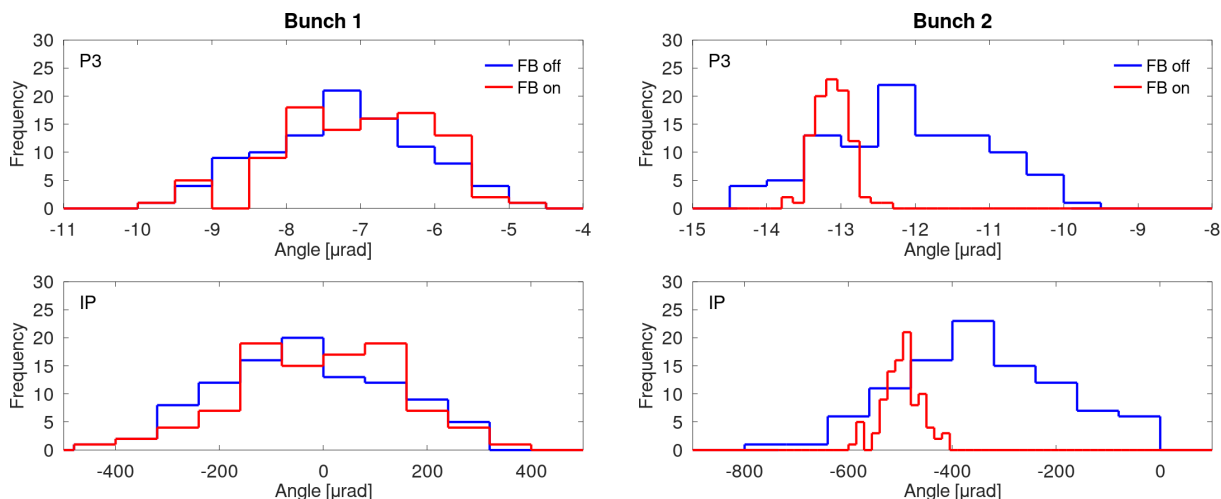
Figure 34: Distribution of angle at P3 (calculated from the position at P2 and P3) and in the IP region (calculated from the position at IPB and IPC) with feedback off (blue) and feedback on (red). A reduced bin width is used for the feedback on data where necessary to limit the maximum frequency of a single bin for display purposes.

Table 6: Vertical beam position jitter in microns for both bunches for feedback off and feedback on. The top five rows are the values measured locally. The bottom three rows are the result of tracking the P2 data downstream using the model.

	BPM	b1 FB off	b1 FB on	b2 FB off	b2 FB on
	P2	1.47±0.11	1.46±0.11	1.39±0.10	0.34±0.02
	P3	0.84±0.06	0.81±0.06	0.93±0.07	0.27±0.02
Local	MFB1FF	74.90±5.35	70.98±5.12	71.89±5.13	17.35±1.25
	IPB	20.65±1.48	19.87±1.43	19.70±1.41	4.83±0.35
	IPC	7.93±0.57	7.57±0.55	7.23±0.52	1.73±0.13
	MFB1FF	77.17±5.51	75.20±5.43	75.54±5.40	16.70±1.21
Tracked	IPB	21.77±1.56	21.21±1.53	21.31±1.52	4.71±0.34
	IPC	7.65±0.55	7.46±0.54	7.49±0.53	1.66±0.12

locally-measured beam angle in the IP region determined from the directly-measured positions at IPB and IPC; the model prediction is in good agreement with the local measurement.

The model can also be used to predict the position distribution at the IP where the vertical beam position jitter is at a minimum. For the feedback-off case, the P2 and P3 data predict a position jitter of 2.9 ± 0.2 nm at the focal point. With feedback operational, the equivalent value at the focal point is 1.2 ± 0.1 nm, which is consistent with the jitter that would be predicted when the upstream BPMs are resolution-limited. Therefore, to the extent that the beam transport model is correct, and assuming no additional jitter sources, it is possible that the FONT feedback system is correcting the beam jitter at the focal point to the level of 1 nm, thereby meeting the ATF2 beam stability goal. However, it is not possible with any known BPM technology to directly measure the beam position to the desired level of accuracy of order 1 nm, so this prediction cannot be confirmed by direct measurement. The best resolution of the cavity BPMs installed at the ATF2 IP achieved to date is c. 20 nm [71].

4.2.3.3 IP feedback system

The IP feedback system can be operated either using position information from a single BPM to provide stabilisation at that BPM, or by using position information from two BPMs to stabilise the beam at an

Table 7: Vertical beam angle jitter in microradians for both bunches for feedback off and feedback on. The top four rows are the result of tracking the P2 data downstream using the model. The final row is obtained using the IPB and IPC position data.

	BPM	b1 FB off	b1 FB on	b2 FB off	b2 FB on
	P2	1.11±0.08	1.08±0.08	1.08±0.08	0.24±0.02
	P3	1.07±0.08	1.04±0.08	1.04±0.07	0.23±0.02
Tracked	MFB1FF	29.91±2.14	29.15±2.10	29.29±2.09	6.48±0.47
	IP	168.9±12.1	164.6±11.9	165.3±11.8	36.6±2.6
Local	IP	164.1±11.7	157.5±11.4	154.5±11.0	37.4±2.7

intermediate location.

The layout of the three C-band cavity BPMs installed around the IP (IPA, IPB and IPC) is illustrated in Fig. 35 and more information is provided in Section 4.4.2.2. There is a longitudinal separation of 80.8 mm between IPA and IPB, and 174.2 mm between IPB and IPC.
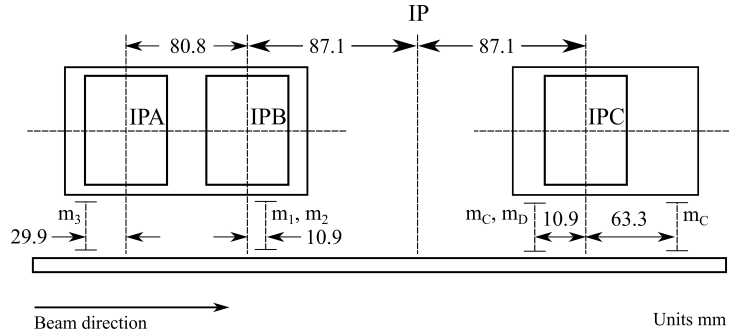

Figure 35: Schematic of the IP BPM configuration, with the IPAB mover block, on which IPA and IPB are mounted, with piezo-movers m_1, m_2 and m_3, and the IPC mover block with piezo-movers m_C, m_D and m_E, allowing for the adjustment of the BPM positions and tilts.

The cavity BPM waveforms are digitised with a FONT5 board. The feedback calculation is performed on the FPGA as before and the same hardware as for the upstream system amplifies the pulse generated on the output DAC in order to drive the stripline kicker IPK, located upstream of the BPMs (Fig. 31).

BPM alignment   The limited dynamic ranges of the BPMs necessitate good alignment of the BPMs with the beam and also the minimization of the beam jitter at the feedback BPMs. When operating with a single BPM, the best results are achieved by locating the beam waist at that BPM [64]. The beam waists in x and y can be shifted longitudinally, largely independently of each other, by adjusting the focusing strength of the quadrupoles QD0FF and QF1FF respectively [65, 66]. The mean position and angle of the beam at the waist is adjusted by transversely shifting the quadrupoles in the final focus region to generate dipole kicks. In particular, moving the vertical or horizontal position of QD0FF will affect the position, while moving QF1FF or QF7FF will adjust the angle [66].

The nominal optics configuration has a sub-1 mm β_y value at the beam waist and as a result the position jitter grows quickly with distance from the waist. In order to keep the beam within the dynamic range of a BPM while retaining a useful resolution, operation close to the beam waist is thus necessary. This requirement typically prohibits three-BPM operation with the 'nominal optics' configuration, as the jitter at the two BPMs furthest from the beam waist exceeds their dynamic ranges. For three-BPM operation, it is useful to use an optics configuration with a reduced divergence at the IP in order to reduce

the jitter off-waist. One such configuration is referred to as the 'high-beta optics' and has a vertical beta function on-waist which is a factor of 1000 larger than the nominal value.

BPM processing   The system of cavity BPMs at the IP comprises a cylindrical reference cavity, for which the dominant mode of excitation is the monopole mode [62], and three dipole cavities, from which the monopole mode is filtered so that the most strongly extracted mode is the dipole mode. The signals from the dipole cavities have position and charge information while the signal from the reference cavity is position-independent and thus provides charge normalisation.

For vertical bunch position measurements, the cavity signals are processed using a two-stage system (Fig. 36). The monopole and y-port dipole modes, both of 6.4 GHz, are frequency down-mixed to 714 MHz using a common 5.7 GHz Local Oscillator (LO) signal, thus retaining their relative phases [69]. For each of the BPMs, the monopole mode is then limited, split and mixed both in-phase and in-quadrature with the dipole signal, producing orthogonally-phased baseband I and Q signals [62].
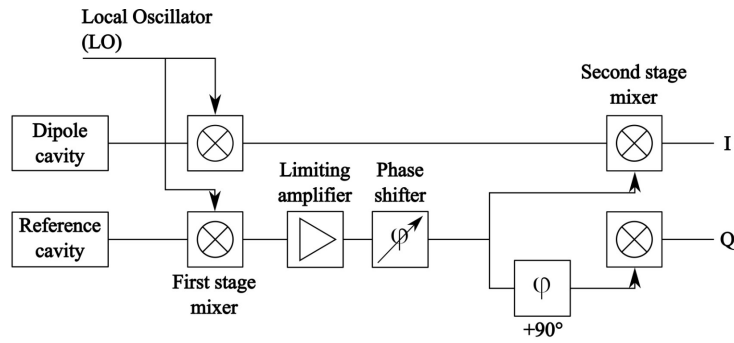

Figure 36: Simplified schematic of the FONT processing electronics [62].

Determination of the bunch position, y, is performed on the FPGA using the I, Q and charge (q) signals:

$$y = \frac{1}{k}\left(\frac{I}{q}\cos\theta_{IQ} + \frac{Q}{q}\sin\theta_{IQ}\right) \tag{18}$$

where k refers to the position calibration constant and θ_{IQ} to the IQ phase angle [62]. Each BPM is calibrated by vertically scanning the beam through a known range and measuring the corresponding response of the BPM. The beam is steered vertically by translating the final quadrupole, QD0FF (Fig. 31) [66].
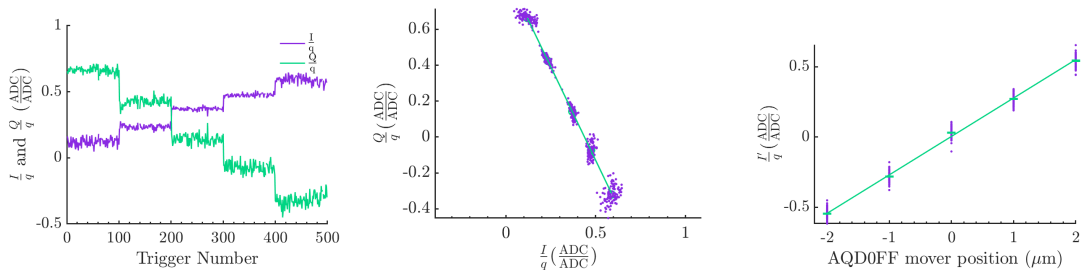

Figure 37: Normalised vertical position calibration of IPA, using an 11-sample integration range: (a) $\frac{I}{q}$ and $\frac{Q}{q}$ versus trigger number; (b) the data points show $\frac{Q}{q}$ versus $\frac{I}{q}$ and the line shows a least-squares fit to determine $\theta_{IQ} = -1.093 \pm 0.006$ radians; (c) the data points show $\frac{I'}{q}$ versus AQD0FF mover position, the error bars show the standard error on the mean values at each AQD0FF setting and the line shows a least-squares fit to determine $k = 0.184 \pm 0.002\,\mu\text{m}^{-1}$.

BPM	Pos. calibration const. (μm^{-1})	Ang. calibration const. (μrad^{-1})	Pos.-to-ang. sensitivity ($\frac{\mu m}{\mu rad}$)
IPA	0.184 ± 0.002	0.277 ± 0.003	0.0034
IPB	0.168 ± 0.002	0.253 ± 0.003	0.0032
IPC	-0.11 ± 0.001	-0.157 ± 0.002	0.0028

Table 8: BPM position and angle calibration constants and position-to-angle sensitivities.

An example calibration of IPA is shown in Fig. 37 and position and angle calibration constants for the three IP BPMs are presented in Table 8. It can be seen that IPA and IPB have similar position and angle sensitivities, whereas IPC has approximately half the sensitivity of the other two BPMs.

4.2.3.4 BPM resolution

Figure 38 shows the resolution as a function of the number of I and Q samples which were integrated. The analysis was performed on data taken in June 2017, at a bunch charge of 0.5×10^{10} and with a dipole attenuation of 10 dB. The BPM resolution is improved by more than a factor of two through sample integration, as this increases the signal-to-noise ratio and the sample-by-sample fluctuations are averaged.
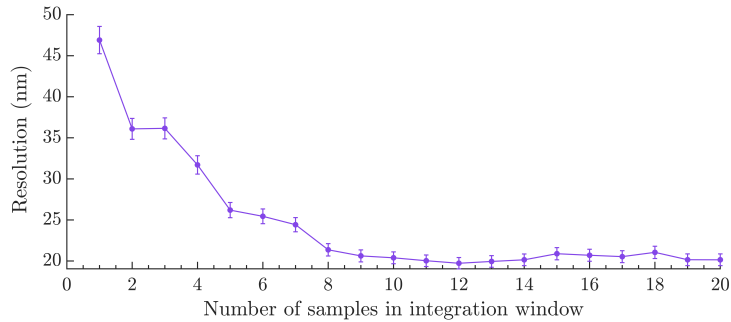

Figure 38: Resolution vs. number of samples integrated. The data points show the geometric resolution, the lines connect the data points and the error bars show the statistical uncertainty on the resolution. The location of each integration window was chosen so as to optimize the geometric resolution.

Resolution	Single-sample	11-sample
Geometric	40.6 ± 1.0	19.0 ± 0.4
IPA fitting	40.6 ± 1.0	19.2 ± 0.6
IPB fitting	40.8 ± 1.0	19.4 ± 0.6
IPC fitting	62.8 ± 1.3	17.6 ± 0.4

Table 9: The best single-sample and integrated-sample resolution measurements for the geometric method and resolution with fitting to $\frac{I'}{q}$, $\frac{Q'}{q}$ and q.

4.2.3.5 Bunch-by-bunch IP Feedback

As indicated in Fig. 39, single-BPM feedback was performed using IPC and two-BPM feedback was operated with measurements at IPA and IPC interpolated to provide beam stabilization at IPB. In this configuration, the feedback BPMs, IPA and IPC, contribute in a ratio 32:68, as determined from their
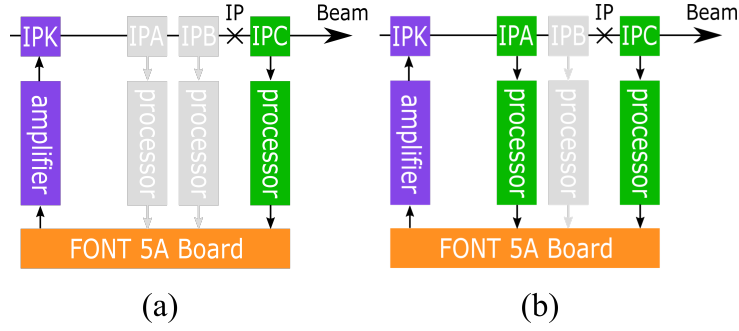
Figure 39: Diagrams of feedback loops with cavity BPMs (IPA, IPB and IPC) and a stripline kicker (IPK) for (a) single-BPM feedback with beam stabilization at IPC and (b) two-BPM feedback, with position measurements at IPA and IPC, for beam stabilization at an intermediate location.

distances from IPB, and the resolution of the interpolated measurement is:

$$\sigma_{\text{res. int.}} = \sqrt{0.32^2\sigma_{\text{res.}}^2 + 0.68^2\sigma_{\text{res}}^2} = 0.75\sigma_{\text{res}} \qquad (19)$$

where σ_{res} is the BPM resolution.

Single-BPM IP feedback The stabilization achieved using a single BPM is illustrated in Fig. 40 and the values are given in Table 10. A 10 sample integration window was used as it was empirically determined to give the best resolution. Feedback was applied to alternate bunch trains so that a comparison could be made between the subsets of data with feedback off and on. The feedback system stabilized bunch 2 to 50±5 nm.
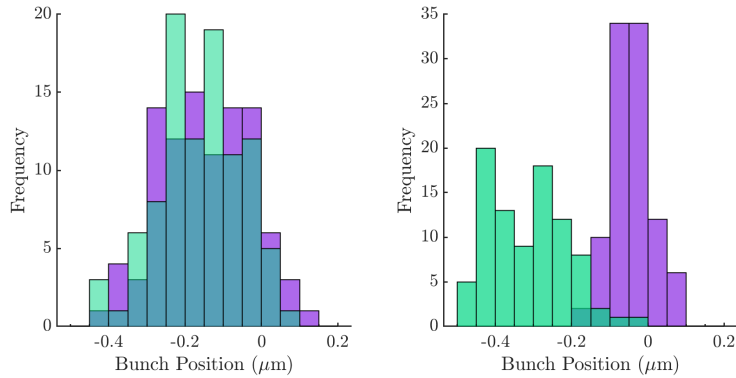

Figure 40: Distributions of bunch positions measured at IPC, for bunch 1 (left) and bunch 2 (right) with feedback off (green) and feedback on (purple).

Table 10: Position jitters and bunch-to-bunch position correlation with feedback off and on, for single-BPM feedback.

FB	Position jitter (nm)		Corr. (%)
	bunch 1	**bunch 2**	
Off	109±11	119±12	$85.1^{+2.5}_{-3.5}$
On	118±12	50±5	$-26.0^{+9.8}_{-8.8}$

45

Two-BPM IP Feedback In order to operate three BPMs simultaneously, the optics were modified to have a β_y^* value 1000 times the nominal value. This reduced the divergence at the IP so that the beam jitters at IPA and IPC were smaller making the alignment of the beam within the dynamic range of the BPMs easier.

The results from operating feedback using integration over five samples are presented in Fig. 41 and Table 11. The beam stabilization demonstrated (41±4 nm), is in excellent agreement with the predicted beam stabilization of 40 nm.
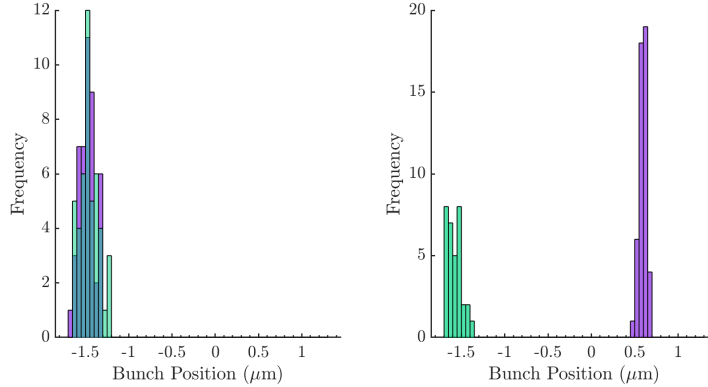

Figure 41: Distributions of bunch 1 (left) and bunch 2 (right) positions measured at IPB, with feedback off (green) and feedback on (purple). Feedback was performed in two-BPM mode, stabilizing at IPB using beam position measurements from IPA and IPC.

Table 11: Position jitters and bunch-to-bunch position correlation with feedback (FB) off and on, for 2-BPM feedback.

FB	Position jitter (nm)		Corr. (%)
	bunch 1	**bunch 2**	
Off	106±11	96±10	$91.6^{+1.8}_{-3.1}$
On	100±10	41±4	$41.3^{+9.1}_{-12.3}$

4.3 Beam tuning studies

4.3.1 Wakefield Free Steering (WFS) study

The Wakefield Free Steering finds a combination of corrector kicks that minimizes the impact of wakefields on the beam orbit. The first WFS response matrix is computed for a beam intensity of 2.0×10^9 electrons. The second WFS response matrix is computed for a beam intensity of 6.0×10^9 electrons. Figure 42 shows the convergence of the WFS correction. After 10 iterations, the norm of the difference between the vertical orbit at high intensity, 6.0×10^9 electrons (y_{HQ}) and at low intensity, 2.0×10^9 electrons, (y_{LQ}) defined as $\|y_{HQ} - y_{LQ}\| = \sqrt{\sum |y_{HQ} - y_{LQ}|^2}$, at each BPM, is decreased by more than 30%. This means that, on average, at each BPM, the impact of wakefields on the vertical orbit was decreased by 12 μm.

Figure 43 shows the impact of WFS and a Dispersion Free Steering correction (DFS) on the vertical beam size at the IP σ_y^*. DFS reduces the impact of a difference of energy on the beam orbit using the same steering magnets used for WFS. For each beam size measurement, 200 consecutive pulses are taken into account. The error bars represent the standard error for 200 pulses. The DFS and WFS
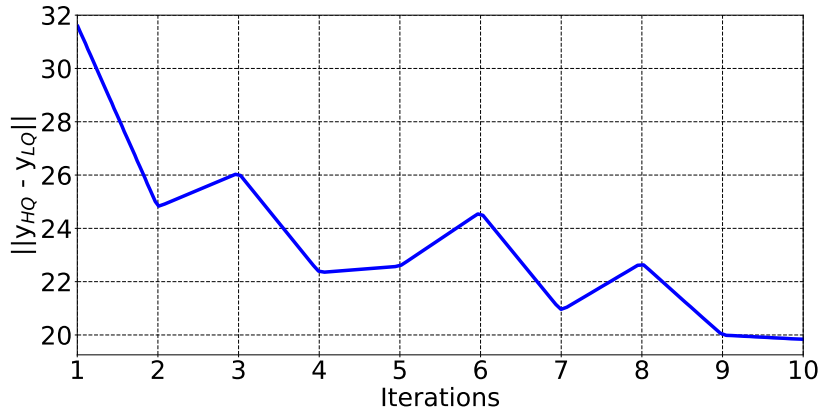
Figure 42: Norm of the difference between the vertical orbit at high intensity, 6.0×10^9 electrons (y_{HQ}) and at low intensity, 2.0×10^9 electrons, (y_{LQ}) vs. the number of iterations of the WFS correction.

corrections reduced the intensity dependence parameter from 22.39 ± 1.18 nm/10^9 e^- to 15.04 ± 2.02 nm/10^9 e^-. The intensity-dependent effects on the beam size at the IP were clearly decreased thanks to DFS and WFS.
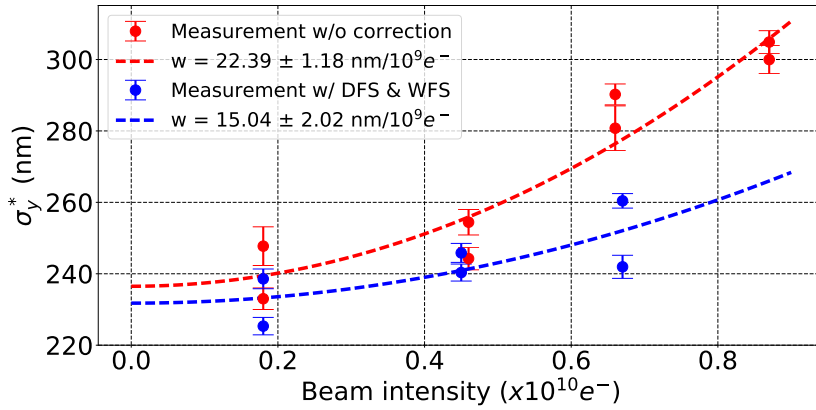

Figure 43: Measured vertical IP beam size (σ_y^*) vs. the beam intensity without correction and with DFS and WFS corrections.

4.3.2 Halo

At the future ILC, beam halo may sharply limit machine performances, cause potential component damage and activation, and has to be well controlled by an efficient collimation system. To evaluate the impact on the experiments and the collimation efficiency, a clear understanding of beam halo formation mechanisms is crucial. Measurements and characterization of beam halo at ATF have demonstrated appropriate diagnostics and provided a reliable halo model for the damping ring (DR) of the ILC.

Two sets of halo diagnostics, the diamond sensor (DS) detector installed at the post-IP and the YAG/OTR monitor located in the EXT section were developed for the experimental measurements [73–75], as illustrated in Fig. 44. The DS detector is similar to a one-dimensional (1D) wire scanner, providing a 1D beam profile by scanning a set of DS strips through the electron beam. The dynamic range of the DS detectors is above 1×10^5, i.e., the number of incident electrons can be from 1×10^3 to more than 5×10^8,

thanks to a data rescaling technique applied to the core profile. For a complementary and more flexible and faster halo diagnostics, a novel YAG/OTR monitor was constructed. It consists of four ceramic Ce:YAG screens with a central rectangular opening allow the visualization of beam core and beam halo, together with an additional OTR target that enables a supplementary observation of the dense beam core if needed. 1D full-beam distributions are acquired by moving the YAG pads using a stepping motor with micrometer precision. A high dynamic range (more than 10^5) and a high resolution (less than 10 μm, vertically) have been demonstrated at the ATF2 beamline.

The contribution to the halo of the low energy ATF DR beam from the beam-gas scattering (BGS) process was first estimated through analytical approximations followed by Monte-Carlo simulations [76, 77]. Satisfactory consistency between the predictions and measurements using both the DS detector and the YAG/OTR monitor, as well as a clear characteristic vacuum dependence, showed that the BGS process in the DR is the main driver for the vertical beam halo. The horizontal beam halo was comparable to the vertical halo, but appeared asymmetric, due to a combination of effects from the optics and extraction kicker field. In addition, the momentum tail was for the first time imaged with the YAG/OTR monitor, using a dispersion bump technique in the EXT section. The measurements showed several features consistent with the presence of Touschek scattering while also suggesting possibility of other mechanism for horizontal beam halo generation.
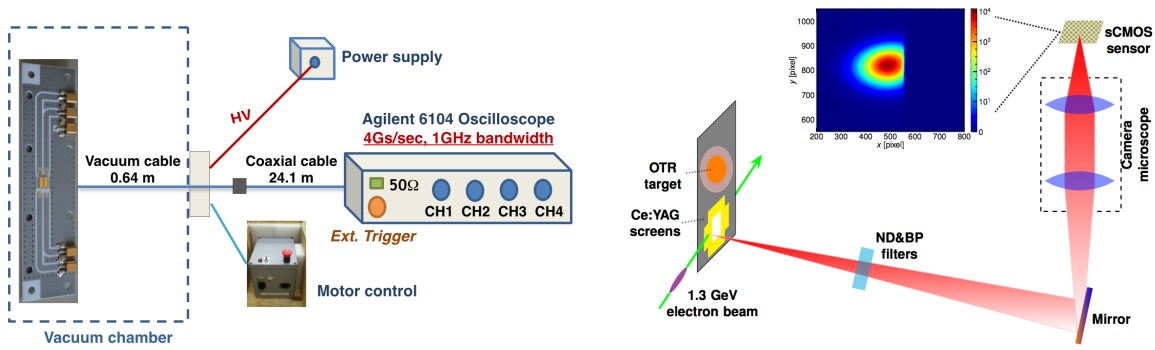

Figure 44: Schematics of DS detector (left) and YAG/OTR monitor (right) for halo diagnostics at ATF2.

Development of halo diagnostics and investigation of beam halo physics were carried out in a close collaboration between CERN, KEK and LAL for about six years (2012~2018), and led to two doctoral theses. Full simulations of beam halo from Touschek scattering are still underway, and complementary measurements of the momentum tail for different extraction times would still need to be conducted to complete the picture. Moreover, evaluation of beam halo in the presence of BGS and Touschek scattering has recently been shown to be important for the SuperKEKB main ring, and an customised implementation is under way.

4.3.3   *Ground motion feed-forward system*

The motion of the ground itself is a potential source of luminosity loss at a future linear collider. Even small misalignments of the quadrupole magnets will deflect the beam away from the ideal orbit, resulting in an increase in the emittance of the beam if not compensated for. Synchronous measurements of the motion of the quadrupoles in the ATF extraction line and the vertical beam orbit in the final focus established the potential for a pulse-by-pulse orbit feed-forward system that would use live seismometer readings to calculate the deflection to apply to the beam in order to compensate for the dynamic misalignment of the quadrupoles [78]. This novel technique is depicted schematically in Fig. 45.

A prototype system was deployed at ATF and shown to successfully eliminate the approximately 60% pulse-by-pulse correlation that existed between the vertical position of the beam in the final focus

and the vertical position of a particular quadrupole in the extraction line, reducing the observed vertical position jitter of the beam in the final focus by 15% in the process [79]. This was achieved using a single seismometer measuring the position of a quadrupole early in the extraction line to drive a single kicker located just before the entrance to the matching line, although the system was capable of operating with multiple inputs and outputs.
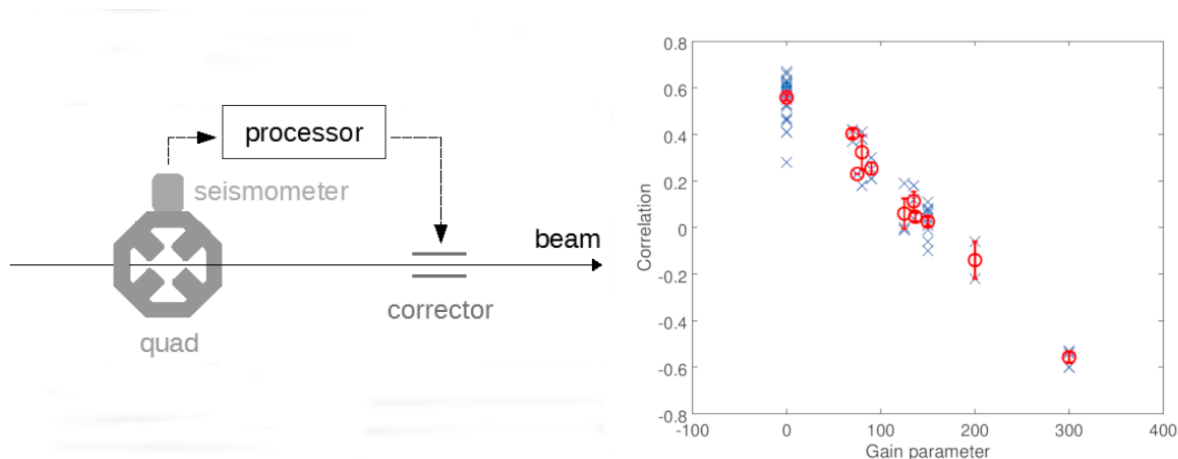

Figure 45: Left: schematic of the ground motion feed-forward system. Right: pulse-by-pulse correlation between the vertical position of the beam and that of the quadrupole as a function of the feed-forward gain parameter.

Development of the feed-forward system itself started in late 2014 but the infrastructure for taking measurements with the seismometers was in place before then. The above results demonstrating removal of the component of the beam jitter due to the quadrupole motion were taken in June 2017. The status of the ATF as a testbed for developing new diagnostics and techniques proved crucial to the success of the project. The main breakthrough that allowed correction to be achieved was the establishment of a dedicated link between the newly procured feed-forward controller and the pre-existing orbit correction hardware belonging to the intra-train feedback group of the University of Oxford. The other main benefit of operating at ATF was the high degree of autonomy afforded to the user; in particular, the ability to switch the beam on and off at will made it far easier to synchronize the seismometer data set with the beam position data set, thereby measuring the correlation between the two.

Since more than 10 years, studies of support design and vibration analysis of Final Doublet (FD), Ground Motion (GM) modelling, GM measurements all along the accelerator and Feed-Forward control experiments have been realized in ATF2. At this moment, a dozen of GM sensors are on site and they are punctually used to identify vibrations sources, evaluate transfer functions or to test the beam feed-forward control.

Taking into account the successful implementation in SuperKEKB of a "permanent GM monitoring" (http://lappweb.in2p3.fr/SuperKEKB/), acquired via a real-time setup on site and then synchronized on a cloud system to be saved in a local server and automatically treated to provide spectral analysis, with ATF2 type of GM sensors, in the short term we will plan to implement a similar permanent GM monitoring system in ATF2. For doing this we will use the already installed GM sensors at various strategic locations that will be chosen by experiments and simulations, along with the already known sensitive locations as the FD magnets (QF1 and QD0). This permanent GM monitoring will allow to evaluate more efficiently the vibrations sources in time. A very important aspect is the disturbance, which creates dynamics effects close to the IP and could induce vibrations with amplitudes beyond the desired tolerances. Furthermore, these studies will permit also to analyze in time the mechanics behaviour of the main relevant elements of the accelerator (ex: the quadrupole QD2). In fact, their vibrations could have an impact on the orbit and the beam size at the IP that are very complex to control and mitigate. The results of the analysis will also give the opportunity to envisage, if necessary at long term, the upgrade of

some magnet mechanical supports. Finally, the vibration data acquired during this period could be used to perform correlation studies in order to optimize the beam size at the IP and to extend the results for ILC.

4.3.4 Slow drift, search for sources, mitigation studies

We have observed horizontal beam orbit slowly oscillating in the final focus beam line, with about 2 minutes period, and the peak to peak amplitude roughly 1.5 of the beam size (about 600 μm at high beta-function region).

Data analysis of the beam orbit in the extraction beam line showed the origin of the orbit drift was upstream part of the extraction line, or it may be from the damping ring. The orbit in the extraction line and the orbit in the damping ring were also analyzed, but any clear correlation could not be found between them. However, because of limited resolution of the beam position monitors, possibility of the orbit drift sources in the damping ring can not be excluded.

Slow orbit feedback system was installed for stabilizing the orbit in the final focus beam line. Though the feedback is expected to cure most effects of the slow orbit drift, it could not eliminate problems completely. The performance should be limited at low beam intensity due to limited resolution of the beam position monitors. Also, it corrects orbit only in the final focus beam line and effects in the upstream region is not cured. Despite these limitations, threr is still possibility of improving the feedback system, such as optimization of time constant, choice of BPMs to be used, etc..

We have been investigating possible sources of the slow drift. Stability of applied currents of almost all magnets in the beam line was checked. Temperature of cooling water and air at various locations have been also checked. However, correlation between the orbit drift and any applied current or temperature at any location could not be found so far.

Nevertheless, temperature stability of cooling water of magnets and air in the tunnel has been improved based on long time experience, for example, modification of cooling water control scheme, optimizations of thermometer locations and additions of monitors, etc.. Though the orbit drift of time scale of a few minutes could not be reduced, the temperature stability has obviously contributed to stabilization of the damping ring circumference (and beam energy) in time scale of hours, which was another practical problem.

4.4 Beam instrumentation development

4.4.1 Fast kicker

The electron beam or positron beam is converted into a low emittance beam while circulating the damping ring. This low emittance beam is indispensable for realizing a nanometer small beam at the collision point. In the ILC, a bunch train of 1312 bunches with the bunch interval of 554 ns is generated by the electron or positron source and stored in the damping ring. These bunches have to be stored in DR by compressing the bunch interval down to 6 ns which enable the smaller 3.2 km ring compare to that of uncompressed one. After bunches becomes low emittance, they are extracted bunch by bunch from DR by recovering the bunch interval of 554 ns. These requirements will be changed for the luminocity upgrade option of ILC, i.e., a beam consists of 2625 bunches with its interval of 332 ns, then the bunch interval in DR becomes 3 ns.

The kicker requires a high repetition frequency of 2 MHz, and very fast rise/fall time of the kick field of 6 ns and 3 ns for the nominal and the luminocity upgrade option, respectively. These parameters cannot be realized by using ordinary kicker system, which consists of a pulse magnet and a pulse power supply with thyratron switch. A system using multi-units of stripline kicker and fast high voltage pulsers is the most promising candidate to realize the parameters.

One of the key technologies of the kicker is a high voltage pulser to drive the stripline. The pulser

Figure 46: Side view of the stripline kicker

requires over 5 kV of peak voltage, 1 ns rise/fall time, 2 MHz burst pulse at 1 ms duration and 5 Hz of operation to realize the ILC parameters. It is very difficult to make such a high speed, high voltage and high repetition rate switching using ordinary switching devices. A semiconductor device called drift step recovery diode (DSRD) has a very fast switching speed and high repetition rate. The pulser using DRDS switches (fabricated by FID Technology, Ltd.) meets these parameters. The beam kick test using a single unit of stripline kicker and DSRD pulser was carried out in the ATF-DR by measuring the betatron oscillation amplitude of the circulate orbit. The stripline kicker used this experiment has 30 cm long, 12 mm gap distance and 9 mm electrode width. Fig. 46 shows the picture of the stripline electrode. The measured beam kick angle as a function of time is shown in Fig. 47. The measured rise/fall time of the beam kick field was 3.0 ns each, which meets the ILC requirements. The measured peak kick angle was 90 μrad [80]. In order to inject/extract beam to/from DR, multi-units of the stripline kicker are required for ILC. The all of the stripline kicker needs to synchronize very precisely.
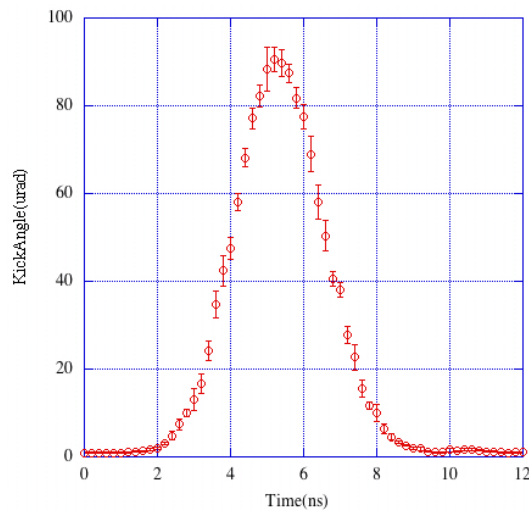

Figure 47: Beam kick angle as a function of time

A successful beam extraction was demonstrated in the beam operation from ATF-DR to ATF2 line. Two units of stripline kickers were installed for this experiment, temporarily replacing the conventional extraction kicker, which has been put offline. The striplines have 60 cm long and the gaps of the electrodes are 9 mm and 11 mm, respectively. Two pairs of 10 kV pulsers were used to drive the strip-lines. The strip-line kicker produced a 3 mrad kick angle for the 1.3 GeV beam. The pulse bump orbit and the auxiliary septum magnet were used with the stripline kicker due to geometrical restriction. Fig. 48 shows the beam trajectory with the pulse bump and the kicked beam orbits.

The stored beams in the DR are 3 trains, spaced 154 ns apart for each train with each train con-
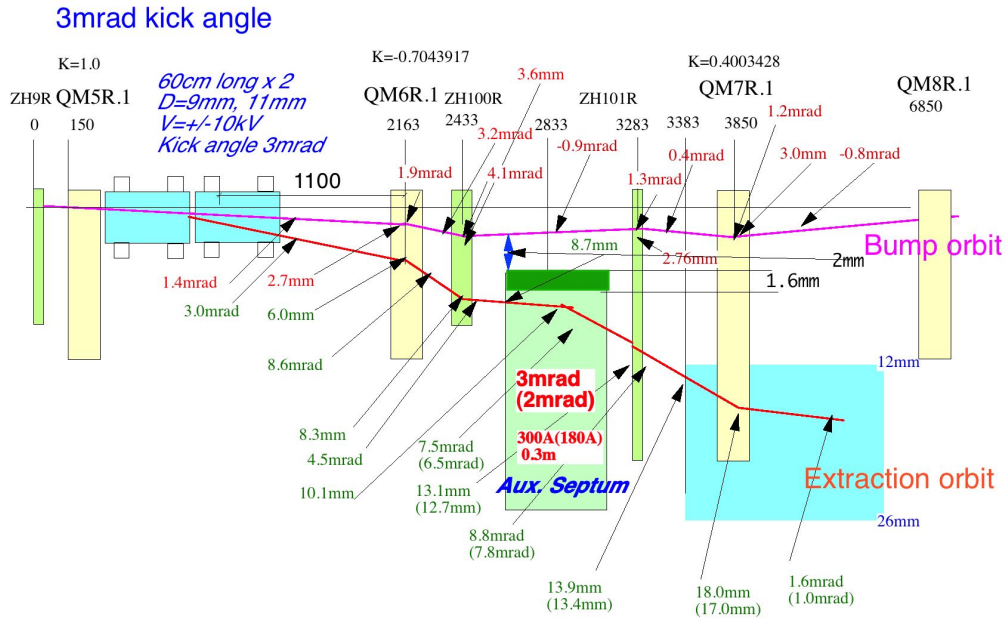
51

Figure 48: Beam extraction orbit downstream of the stripline kicker

sisting of 10 bunches with 5.6 ns bunch spacing, for a total 30 bunches. The stripline kicker kicks out bunch by bunch from the last bunch of each train with a 308 ns (302.4 ns for every three pulses) interval. Fig. 49 shows the stored beam in the DR and extracted multi-bunch beam in the ATF2 beam line. The stability of the kick angle was measured by using the BPMs in the ATF2 beam line. The measured angle jitter of the extracted beam was 1.3 μrad, which correspond to 3.5×10^{-4} of the kick angle [81].
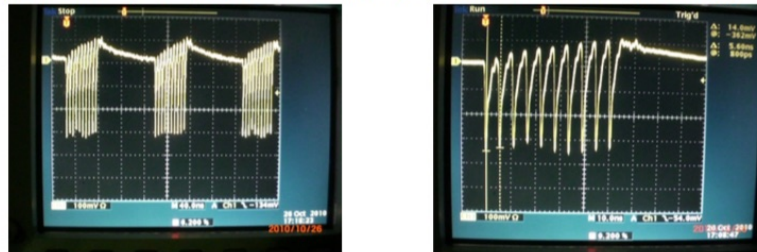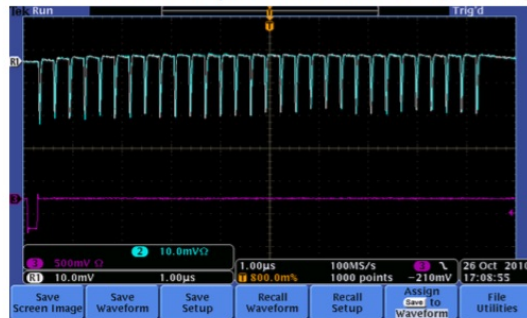

Figure 49: Observed multi-bunch beam in the DR with 5.6 ns bunch spacing and extracted bunch train in the ATF2 beam line with 308 ns (302.4) bunch spacing

4.4.2 Cavity BPMs

4.4.2.1 Cavity BPMs for the ATF2 beamline

ILC requires precision mechanical pre-alignment of thousands of magnet centres to position sensors, but the final beam to magnet concentricity of better than 100 μm, and in some cases approaching a few μm, is achieved via beam-based techniques. Success of beam based techniques depends on BPM resolution and stability, therefore a full test of the proposed high resolution Cavity BPM (CBPM) is necessary. Similarly at ATF2, methods of beam based alignment are used to measure the relative offset between the electromagnetic centres of a CBPM and the hosting quadrupole or sextupole magnet. This alignment has to be better than 1 μm for the most critical optical elements in order to achieve the ATF goal of a small beam size at the interaction point. Thus, ATF2 provides a unique and flexible facility to test the operation of high resolution cavity type BPMs.

The ATF2 cavity CBPM system shown in Fig.50 is the one of the largest installed and operating, accounting up to 41 position sensors: 34 C-band cavities with a 20 mm aperture in the extraction, matching and final focus sections [64], 4 S-band sensors in the final focus [82] and 3 small aperture extreme resolution "IP cavities" around the beam size measurement area downstream of the final doublet [83]. The main C-band cavity system operates routinely with a resolution of approximately 250 and 30 nm in CBPMs with and without 20 dB attenuators respectively at around 0.7×10^9 electrons per bunch. Each cavity is located either inside or close to a quadrupole or sextupole magnet. The main C-band cavities are physically located in adapter holders attached to the pole faces of their respective magnet. In the extraction system (from QD10X to QF21X), the quadrupoles are rigidly attached to their girder, while downstream from QF21X all quadrupoles are mounted on individual 3-axis mover systems, which are used for quadrupole alignment and BPM calibration.
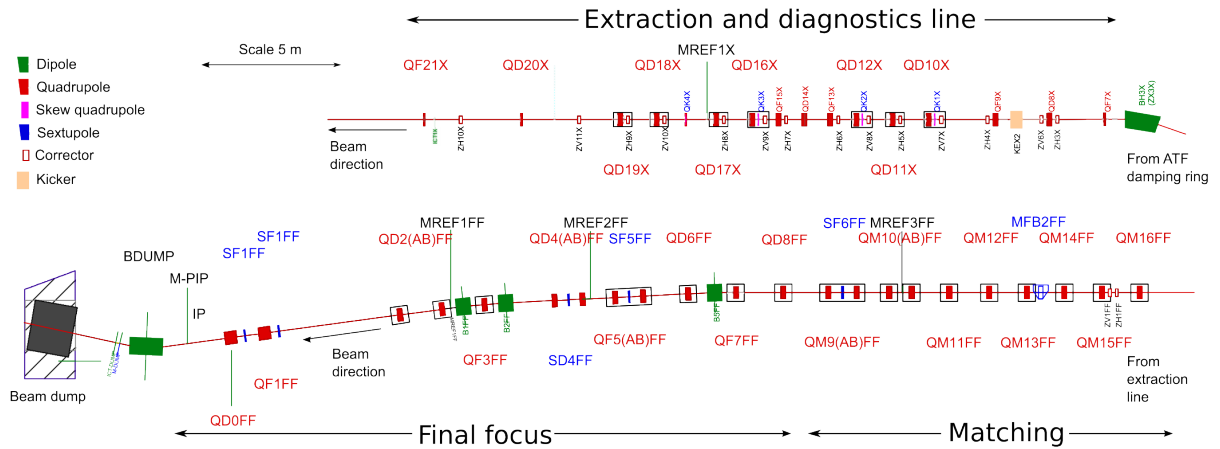

Figure 50: ATF2 beam line, highlighting the quadrupoles containing CBPMs.

The CBPM system has operated continuously during ATF2 commissioning and operation. It typically takes 4 hours to calibrate and verify the system, with the majority of time spent on executing the mover or beam motion. Each CBPM has to be calibrated individually as the determination of the processing parameters requires a precise knowledge of the introduced change of the beam position at the CBPM's location. In order to maintain a 250 nm position resolution (see Fig.51) at a beam offset by 250 μm from the cavity centre typically used for calibrations, CBPMs are required to reach a precision of 0.1%. The precision had initially been affected by the beam jitter, introducing a calibration error that reached over 10% in some cases. This issue was solved by applying machine learning methods to correlate raw CBPM readings and generate jitter-subtracted calibration data to achieve the required precision [84].

In the course of 2017–2020 operation of the ATF2, calibrations were usually performed during
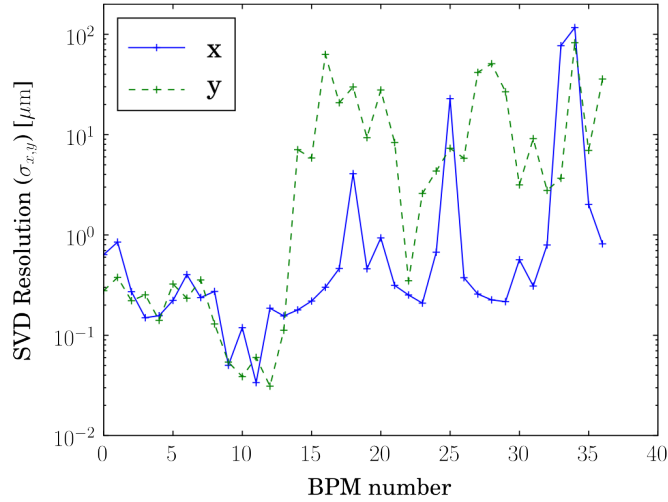
Figure 51: A typical resolution of all of the BPMs along the beam line.

machine start-up – in anticipation that beam position measurements would be required for beam tuning. Calibrations typically remained applicable for 2-3 days, after which a noticeable systematic difference would appear. Intrinsically the electronics are stable in gain and phase to $< 1\%$ and < 1 deg. over the course of one operation week. The changes have been mainly attributed to trigger timing drifts/jumps and temperature changes of the sensing cavities resulting in significant fluctuations of the signal's phase. While trigger timing issues have been mostly rectified, temperature changes are harder to compensate for due to significant hysteresis between the ambient temperature and the resulting change in cavity's resonant frequency. The use of high resolution CBPMs in future linear colliders and light sources, where hundreds to thousands of cavities are required to operate with a minimum intervention, dictates that the calibration constants remain valid for periods exceeding one week and ideally many weeks at a time. Luckily, the environment in these machines is normally tightly controlled, so a stable performance can be expected without any additional measures to control the sensor cavity's temperature.

Our ongoing studies concentrate on improving the stability of the system and studying its effect on the beam based alignment and wake kick budget [57]. Effects like beam position jitter, trigger jitter, and cavity frequency variation with temperature also are being investigated. Another important area is signal processing of closely spaced bunches, i.e. multi-bunched beam, generating overlapping signal patterns [85]. This issue is extremely relevant in the context of CBPM application in ILC due to bunch-to-bunch distance comparable to typical decay times of the sensing cavities. We have shown that individual bunch signals can be deduced from the convoluted response with a small loss of the resolution that can be compensated by using modern high speed data acquisition. This study will be summarized in an upcoming paper.

Overall, the cavity BPM system has achieved its original specifications of sub-100 nm resolution, despite being operated at a lower sensitivity. Were better alignment to magnet centres feasible, the entire CBPM system could be run in a high-resolution mode. As operating now the CBPM system is routinely used for beam tuning, including beam based alignment, optics model verification, dispersion reconstruction, and dedicated beam stability studies. The system can now provide individual bunch positions when ATF operates in two or three bunch mode.

4.4.2.2 Cavity BPMs for IP

For the study of Goal-2 which aims to demonstrate the stabilization of beam position at IP in a few nanometer, a cavity BPM with beam position resolution of a few nanometers is demanded. The development

of this advanced BPM had been conducted at the previous extraction line before constructed the ATF2 beamline. The method of resolution evaluation, which is described here and after, uses a set of three BPMs. Two of them are used to define the trajectory on remained BPM, then the position resolution of remained BPM is evaluated by comparing positions measured by itself and defined by other two. The first prototype showed a best position resolution of 8.7 nm for a single bunch beam [69].

In order to measure the position of consecutive three bunches with 150 ns spacing at ATF2, a low-Q property of cavity is required to enable a fast decay of excited signal by a bunch to avoid the overlap of a following bunch [86, 87]. After the study of low-Q protype BPM at the middle of the ATF2 beamline, three low-Q BPMs were fabricated as shown in Fig.52. Each BPM was designed with a rectangular-shape single cavity which enabled measurements of beam position in vertical and horizontal independently. The first block consists of two cavities and each cavity are located at 8cm and 16cm upstream of the IP, and the second block consists of single cavity which is located at 8cm downstream of the IP as shown in Fig.53. They are mounted on movers described below and installed in a large vacuum chamber at IP (Fig.54).
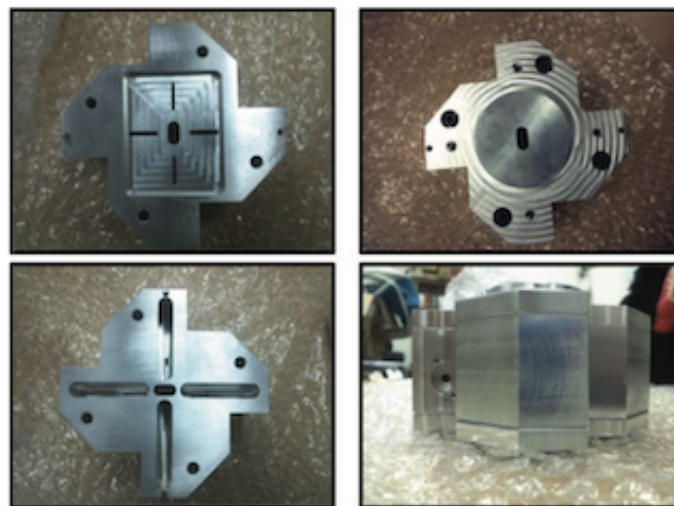

Figure 52: Fabricated one block Low-Q IP-BPM (BPM-C). Sensor cavity part (left up). Wave guide part (left down). Cavity covers with flange (right up). Side view after stacking (right down).
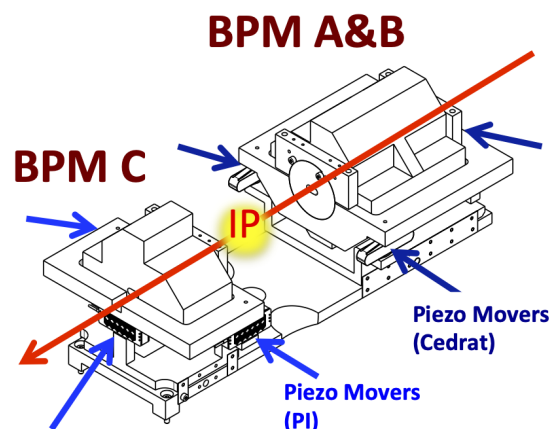

Figure 53: Layout of the three Cavity BPMs at ATF2-IP.

These BPMs must be very well aligned with respect to the beam, at the few micron level, to fully
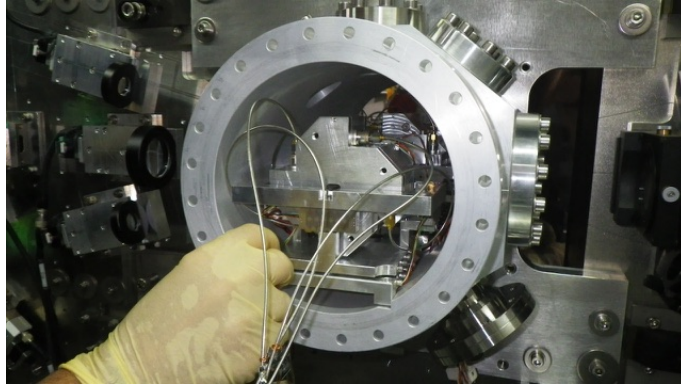
Figure 54: IPBSM installed in the vacuum chamber at IP. BPM is mounted on the mover cradle.

exploit their fine resolution. The mechanical positioning system has been developed to enable such a precise alignment [88]. It is based on a set of six piezo actuators with nanometer range displacement resolution. Due to the expected resolution of the piezo actuators, this system also brings a functionality, the possibility to calibrate the BPMs by mechanically scanning the beam. A set of eight piezo-movers bought from two companies (PI and Cédrat) are used for lateral and vertical adjustments in the range of about 230 / 300μm, respectively. Strain gauges are used for readback and feedback, with a precision of 10^{-4} over the full range. A set of in-vacuum PT100 thermal gauges are included on the IP-BPM cradles for temperature monitoring. The control and readout electronics are located outside the accelerator shield, after about 25m of cables.

The installed BPMs had lower-than-design loaded Q values and decay times about 10 ns. Short decay times reduce the likelihood of signal contamination between pulses when measuring multi-bunch trains, which in typical two-bunch operation at the ATF2 have a $\sim$280 ns separation. However, the very short signal length reduced sensitivity to position offsets. The BPMs were modified to incorporate an indium seal between the cavity body and side covers to raise the loaded Q. Spacers were also added under the cavity feedthroughs to reduce external coupling. These modifications increased the decay times to 25 ns to restore the system's position sensitivity.

Resolution studies were performed with the reinstalled BPMs at a charge of $\sim$1 nC in single-bunch mode. The signal processing in the FONT digitiser board was upgraded so as to allow for real-time sample integration to improve the operational BPM resolution. Sample integration can be used operationally with an integration window of up to fifteen samples. The best geometric resolution measured for the IP BPM system was $\sim$20 nm, which was consistently reproducible by integrating over multiple samples of the digitised waveform [63]. To achieve the best resolution with the IP BPM system it was demonstrated that good position and angular alignment of the BPMs are required [70].

4.4.3   Collimator

The reduction and control of the beam halo is a crucial aspect of the Future High-Energy Linear Colliders (FLC) to enable the ambitious luminosity configuration of the order of $10^{34} - 10^{35}$cm^{-2} s^{-1} and reduce the background in the experiments.

In the framework of the FLC collimation system, beam halo collimation studies have been realized in ATF2. The main source of beam halo population in the ATF/ATF2 beamline was demonstrated to be the beam gas scattering in the DR [73, 77, 89]. The beam halo formed in the ATF DR goes into the ATF2 beamline and hits some beamline components producing undesired background photons. The control of the background photons is especially important at the end of the beamline since many of them are generated in the beam pipe of the last bending magnet (BDUMP) and may limit the precision of the nanometer vertical beam size measurements using the IPBSM monitor.

There was no dedicated beam halo collimation system at the ATF2 although some apertures and a Tapered Beam Pipe (TBP) installed in the FFS were intercepting some of the beam halo particles. Because of available space constraints only single collimators were considered in the study. Based on the standard requirements for designing a collimation system [90] and considering a location where we have at least 0.6 m different locations for a single betatron and energy collimator have been considered. The detailed study is described in [91–93]. In 2016 as result of this study, a single vertical collimator was designed and installed at the ATF2, in the FFS between QM10BFF and QM11FF in 0.8 m available free space with a high β-function location and with a phase advance difference with respect to the BDUMP magnet (the main collimation target of the study) close to an integer ($\Delta\mu=n\pi$). The design is inspired on a first ILC spoiler's prototype [94], based on the wakefield studies, the stopping power and the temperature rise calculation, the final chosen parameters of the collimator jaws are summarized in Table 12. The

Material	a [mm]	$\alpha(°)$	L_F [mm]	h [mm]
Cu	3-12	3	100	12

Table 12: Optimized jaw parameters for the vertical collimator.

complete system before and after installation in ATF2 is shown in Figure 55. The system is retractable in order to be able to adjust the collimation depth required without introducing intolerable wakefields for different ATF2 beam operation modes and experiments.
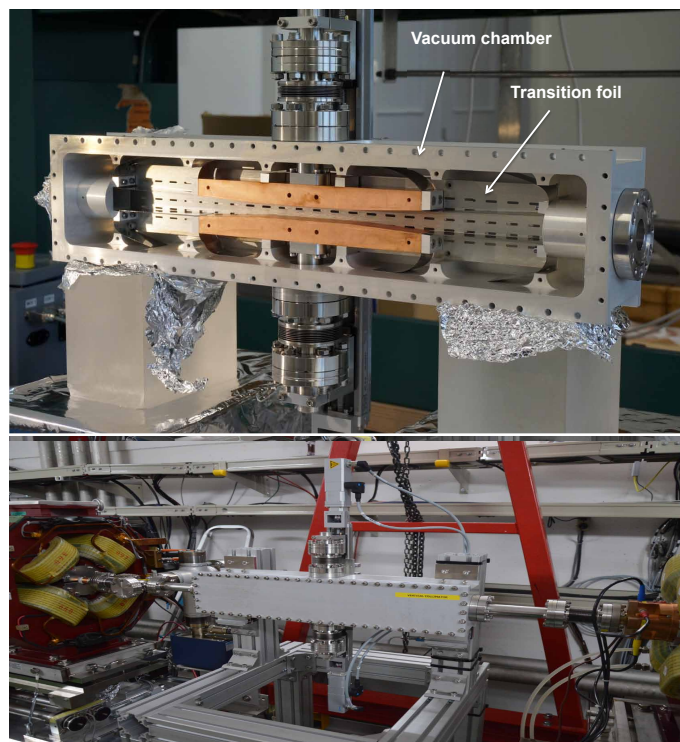
Figure 55: Vertical collimator in the construction process (top) and installed at ATF2 (bottom).

A measurement campaign was carried out during two run periods in spring 2016 to characterise the efficiency of the vertical collimator for different intensities, DR vacuum pressures and optics. Furthermore, the efficiency of the collimator was measured in comparison to the effect of the TBP working as a kind of collimator with a fixed half aperture of 8 mm. During these measurements the energy was 1.3 GeV and the machine was operated with the ($10\beta_x \times 1\beta_y$) optics [95]. In order to quantify the efficiency

57

of the collimator the "Relative background photons reduction", Δb, has been calculated as:

$$\Delta b = 100 \times \left(1 - \frac{b^{w\ coll}}{b^{w/o\ coll}} \right) \qquad (20)$$

where $b^{w\ coll}$ is the background monitor signal in arbitrary units with the vertical collimator closed to a given half aperture, a_y, and $b^{w/o\ coll}$ corresponds to the background monitor signal with the vertical collimator opened to its maximum half aperture of 12 mm. In Fig. 56 the "Relative background photons reduction", Δb, measured as a function of the vertical collimator half aperture is shown. The measured
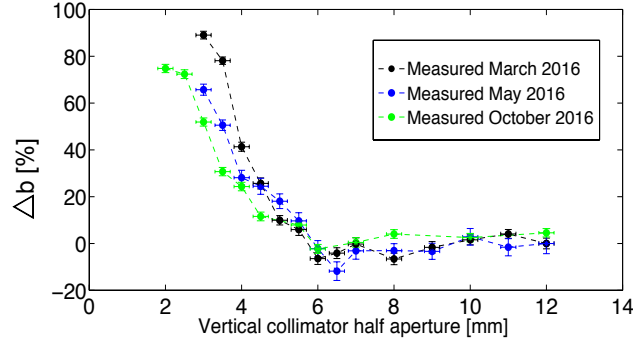

Figure 56: Measured relative background photons reduction, Δb, in the Post-IP region in the 2016 runs for a beam intensity of 0.7-0.8 $\times 10^{10}$.

reduction of background photons in the Post-IP was between 30-40% for a 4 mm collimator half aperture and between 60-80% for a 3 mm half aperture. These measurements are consistent with the BDSIM simulations.

A detailed wakefield study has been also performed in the same period, to optimize the geometry of the collimator jaws and to evaluate the impact of the collimator on the orbit and the beam size at the IP. For the ATF2 prototype, laying in the inductive and long, geometric and resistive wakefield regimes respectively, the analytical and numerical estimations were completed with a measurement campaign contributing to the understanding of agreement between measurements and simulation. The measured vertical collimator wakefield kick is about 21% higher than the analytical estimations and 8% higher than the CST PS numerical simulations.

In February 2017, in order to perform new wakefield experiments a C-BPM was placed at the location of the TBP, used in the past as a collimator, and the vertical collimator has been operated successfully since then as main device to reduce backgrounds at ATF2. Furthermore beinfgthe design of the system inspired by a preliminary design made for the ILC spoilers and because of that, the experience in the design, the wakefield studies, measurements and operation of the system are of great importance towards the design of the FLC collimation system, in particular for the ILC.

This project had been led by IFIC team with the collaboration in the construction and integration of LAL and KEK teams. A PhD thesis has been framewored in this project [91].

4.4.4 Laser wire

For future linear electron-positron collider such as the International Linear Collider (ILC), measurement of the particle beam emittance is essential for achieving and maintaining the required nanometer level final focus beam sizes if their target luminosity is to be reached. A laserwire is a beam profile monitor based on Compton scattering of laser photons from the electrons or positrons in the particle beam. The scattered photons have a high energy and travel nearly parallel to the particle beam and can be detected after a bend in the beam line that deflects the charged particle beam. As the laser focus is scanned

transversely across the particle beam, the rate of Compton-scattered photons is modulated yielding a laserwire scan. With knowledge of the laser size at its focus, the laserwire scan can be deconvolved to give the electron beam profile. As the Compton cross section is very small, a high power pulsed laser source must be used and only a small fraction of the bunch particles are scattered. To demonstrate the desired micrometer size profiles, the laserwire system was constructed in extraction line of the ATF [96] and then repositioned in the matching section of the ATF2 extraction line at a virtual image point of the final focus in the vertical dimension [97], Fig. 57.
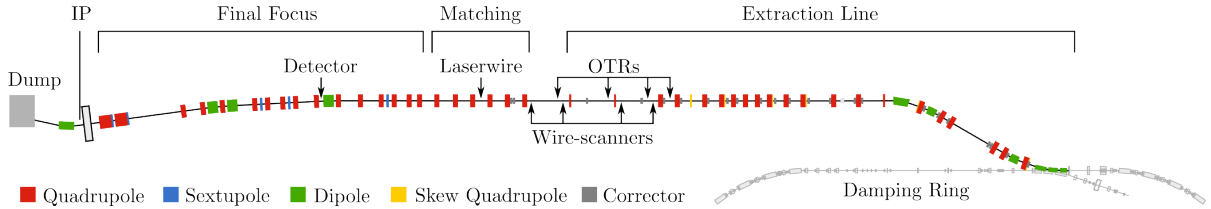

Figure 57: Schematic of the ATF2 extraction line showing the location of the laserwire system as well as the detector located immediately behind the first dipole magnet after the laserwire interaction point.

The laser system consists of a Q-switched Nd:YAG amplifier seeded by a 357 MHz mode-locked oscillator, synchronized with the ATF RF. The laser output parameters were as follows: energy per pulse $\sim$ 150 mJ, wavelength 532 nm and pulse duration 70.8 ± 0.6 ps at 3.12 Hz repetition rate. For the proof-of-principle experimental study a special electron beam optics set was developed to create an approximately $1 \times 100~\mu$m (vertical $\times$ horizontal) electron beam at the laserwire location, Fig. 58.
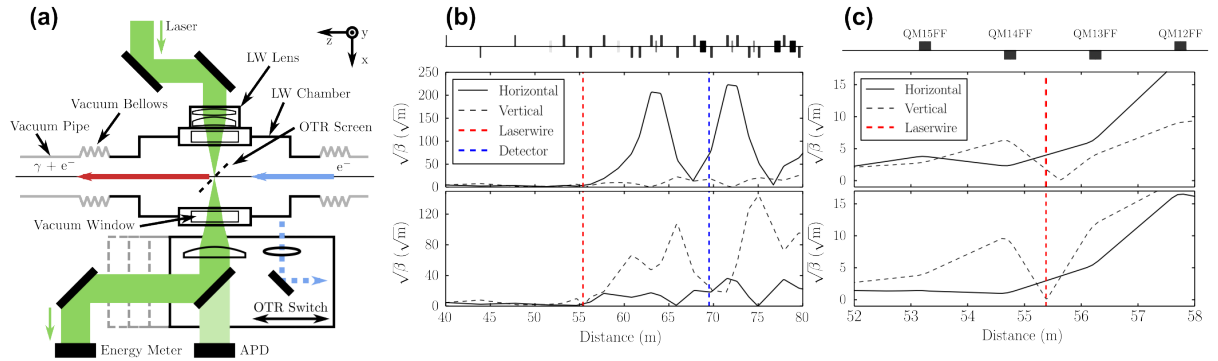

Figure 58: Schematic of the laserwire interaction point (*a*). Electron beam amplitude functions about the laserwire interaction point for normal ATF2 operation (top) and for laserwire operation (bottom) (*b*). Zoon-in of the laserwire interaction region (*c*).

The precise characterization of the laser propagation allows the non-Gaussian laserwire scan profiles caused by the laser divergence to be deconvolved. After the laser is transported to the laserwire interaction point, it is directed into a custom-made vacuum chamber with high damage threshold vacuum windows on either side to allow the laser beam to enter and exit, Fig. 58,*a*. The vacuum chamber can be moved 3 mm in both the horizontal and vertical axes. A kinematic lens mount attached to the vacuum chamber is used to mount the laserwire lens, which allows precise control of the lens separation from the vacuum window as well as its angle. This is imperative as the vacuum window is an integral part of the lens optical design. The laserwire lens ($f = 56.6$ mm) consists of two radiation-hard fused silica elements that are designed to correct geometric aberrations, Fig. 59,*a*. The Nd:YAG laser source provides narrow bandwidth laser pulses with transverse profile shown at Fig. 59,*b* and measured M^2 shown at Fig. 59,*c* that are easily accommodated by the 2 nm acceptance bandwidth of the lens negating

any chromatic aberrations. By moving the vacuum chamber, the attached lens and therefore the laser focus also move. Optical position encoders provide 50 nm accuracy on the chamber position measurement. The laserwire detector is placed after the $BH5X$ dipole magnet in the ATF2 lattice, which is the first bend after the LWIP and constitutes a bend of $2.927°$.
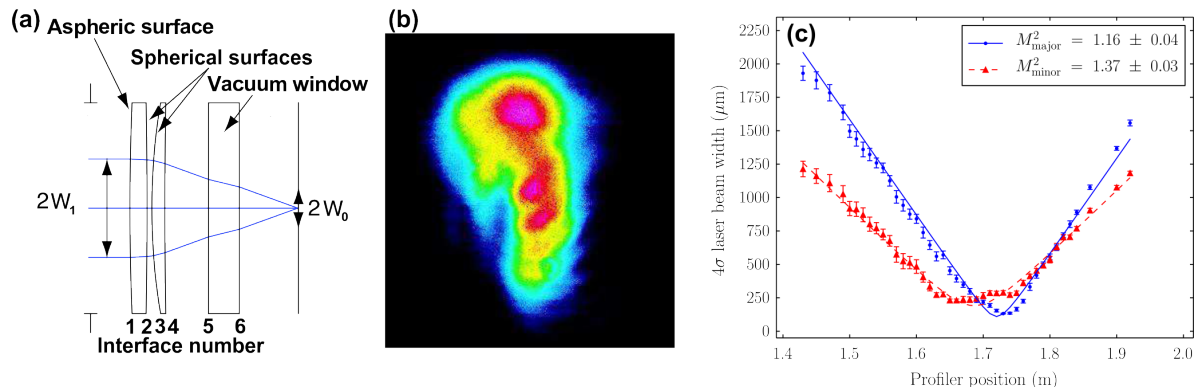

Figure 59: Diagram of the final focus lens (*a*). Input laser profile measured at the end of the laser diagnostic line with telescope actuator at 12.5 mm (*b*). Measured 4σ widths of the laser beam through the focus created with a $f = 1.677$ m lens (*c*). The M^2 model is shown for each intrinsic axis of the laser propagation, which were found to be rotated to the extrinsic lab axes by $-17.4°$.

The box-shaped vacuum pipe in the dipole has an aluminum window 26 mm in diameter and 200 μm in thickness at the end that allows the Compton-scattered photons from the laserwire to be detected. The detector consists of a $4 \times 4 \times 0.6$ cm^3 ($x \times y \times z$) lead sheet that acts as a converter of photons to electron-positron pairs, followed by a $4 \times 4 \times 5$ cm^3 block of SP15 Aerogel. The Aerogel acts as a Cherenkov radiator for the electron-positron pairs and the Cherenkov light is guided in a light tight pipe, internally coated with aluminumized mylar, to a shielded photomultiplier tube out of the accelerator plane. Synchrotron radiation background was expected to be negligible as the synchrotron photon energy at the peak of its spectrum is ~ 0.3 keV, which is insufficient to generate electron-positron pairs in the lead converter plate.
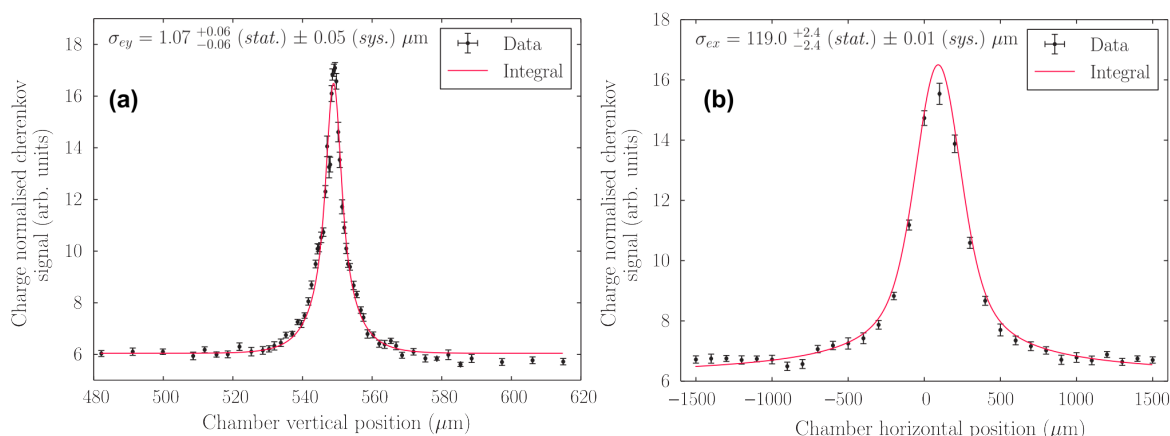

Figure 60: Vertical laserwire scan with nonlinear step size and the smallest measured electron beam size (*a*). Horizontal laserwire scan for the smallest vertical scan (*b*).

The laserwire was operated in a series of experimental runs during January and February 2013. The detector background level, laser propagation, and electron beam properties were all characterized

60

before performing laserwire scans. The laserwire system has demonstrated a high resolution, effectively noninvasive method of measuring the transverse profile of a high charge density, low emittance electron beam such as that at a future linear electron-positron collider. A minimum vertical electron beam size of 1.07 ± 0.06 μm was measured with a corresponding horizontal beam size of 119.0 ± 2.4 μm, Fig. 60. A single quadrupole scan as used to measure the vertically projected geometric emittance of 82.56 ± 3.04 pm rad. Simultaneous fitting of the data from the horizontal and vertical laserwire scans using the overlap integral model was demonstrated in the presence of Rayleigh range effects and was shown to provide an accurate measurement of both the horizontal and the vertical electron beam sizes. This has demonstrated that Rayleigh range effects do not preclude the use of a laserwire to measure a high aspect ratio beam. Furthermore, an alignment method capable of finding collisions between the laser and electron beam was developed. The laserwire was successfully operated with a low electron bunch population of 0.2×10^{10} and will easily scale to 2×10^{10}. We have identified a series of improvements and studies, which could improve this diagnostic, reduce systematic uncertainties, and improve ease of engineering for a future laserwire. Overall, a diagnostic for a future linear collider such as the ILC has been demonstrated, capable of measuring an electron beam size of 1 μm. Also, the use of a fibre-based laser system as a suitable laser source for a laser-wire was studied at Oxford. The test fibre laser system was constructed to investigate the suitability of high efficiency and excellent spatial quality fibre laser to be used for future laser-wire monitors with high resolution and high repetition intra-train scanning [98].

4.4.5 *Optical radiation monitors*

In particle accelerators, the measurement of the transverse beam profile is a key diagnostics required for optimization of the accelerator performance and beam parameters stability. Polarization radiation appeared as a result of dynamic polarization of a medium by charged particles beam. In this case the electron filed interacts with electron shell of each atom of the medium creating dipoles, which oscillates generating a variety of different radiation types belonging to polarization radiation family.

The ATF2 has two sets of OTR systems at present, one is a multi-OTR system for beam diagnostics of the ATF2 beamline, the second is an R&D station consisting of monitors for optical transition radiation, optical diffraction radiation and Cherenkov diffraction radiation. Previously another OTR monitor was also installed (written in Sec. 4.3.2), but it was removed during the Wakefield survey of the ATF2 beamline.

4.4.5.1 *multi-OTR system*

A multi-Optical Transition Radiation (mOTR) system made of four stations is being used routinely for transverse beam size measurement and emittance reconstruction in the extraction line of ATF2, providing diagnostic support during the ATF2 tuning operation [99–101]. Furthermore it is also an excellent tool for fast transverse coupling correction. Figure 61 shows the schematic of an OTR station. The system was prepared by a cooperation of IFIC, University of Valencia and SLAC. Aluminized kapton 2 μm thick is used for the target, which has withstand beam intensity of 1×10^{10} electrons per pulse and spot sizes of about 200 μm in horizontal and 60 μm in vertical. The center of the target is 1.5 mm from the center of the beam pipe. So with this set up the beam intercepts the target just lowering the whole OTR body by 1.5 mm. In the measuring configuration the beam remains almost centered within the beam pipe. The optical device with achromat lens features a working distance of about 55 mm and provides a resolution of 10%.

4.4.5.2 *Sub-micrometer resolution optical transition radiation monitor.*

Optical transition radiation (OTR) refers to the emission of broadband electromagnetic radiation when a charged particle crosses a boundary between two media with different dielectric properties, i.e. vacuum-metal interface. OTR arises as a result of interaction of the electron field with the metal atoms. OTR
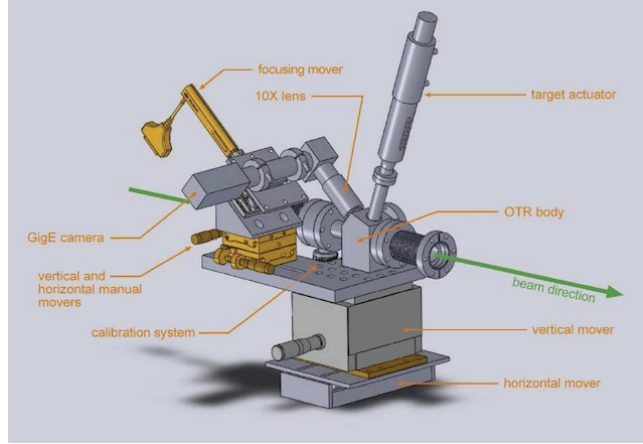
Figure 61: Schematic of the OTR station: The four OTR stations have the same configuration.

screens have become very popular because of several advantages including relatively high photon yield (e.g. 1 photon per 100 electrons); large emission angles simplifying the imaging geometry; and temporally instantaneous emission enabling time resolved measurements. In conventional OTR monitors the image generated on the surface of a metallic screen corresponds to the beam profile that can be measured with resolution of the order of 10 micron.
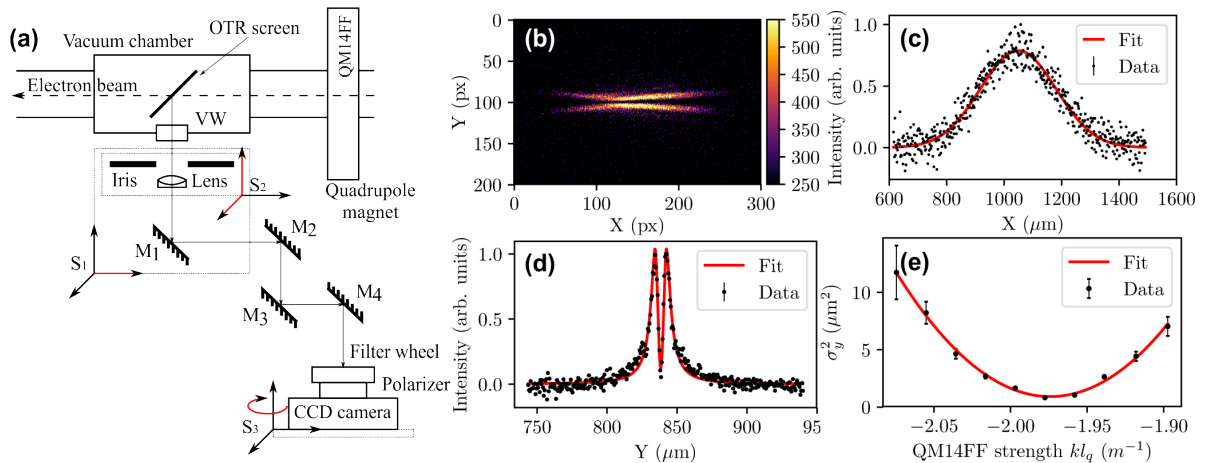

Figure 62: Schematic of the OTR setup (*a*), typical OTR image (*b*). An example horizontal (*c*) and vertical (*d*) projection along with the associated fits; (*e*) - the measured beam size squared as a function of effective quad strength. The red line represents the parabolic fit used to extract the emittance.

At ATF2 we have demonstrated that the OTR source (point-spread function, PSF) generated by a single electron is not uniform but has a crater-like shape with a zero at the center [102]. If the beam size is smaller than the OTR PSF, the beam size can be measured with sub-micrometer resolution. The experiment has been performed at ATF2 extraction beam line [103]. The experimental setup is shown in Fig. 62,*a*. The particle beam crossed an aluminized silicon plate placed at a 45 degree angle with respect to the electron beam propagation direction. OTR propagated at a 90 degree through a focusing optics and delivered to a CCD camera by a system of mirrors. A typical OTR image is shown in Fig. 62,*b*. Horizontal projection (Fig. 62,*c*) provides direct measurement of the horizontal beam size. From the gaussian fit the horizontal beam size is $132.0 \pm 0.3 \ \mu$m. The vertical projection (Fig. 62,*d*) represents the vertical OTR PSF. Its visibility, the ratio of min intensity divided by max intensity, is used to extract vertical beam size. The minimal measured beam size was $0.91 \pm 0.05 \ \mu$m. The measurements were

crosschecked by simulations performed with SAD code and measured by the laser wire system [97]. From the quadrupole scan (Fig. 62,e) the vertical emittance is 59.3 ± 4.2 pm rad.

4.4.5.3 Non-invasive optical diffraction radiation micron-scale beam size monitor.

Optical diffraction radiation (ODR) is a member of polarization radiation family and appears when a fast charged particle moves in the vicinity of a medium (e.g. moves through the slit in a screen). At ATF/ATF2 we have directly observed and performed detailed investigation of ODR properties from both a single edge target [104] and from a slit target [105]. To achieve the best resolution for beam size measurements we have switched the detection system to near ultra-violet spectral range [106]. Figure 63,a illustrates
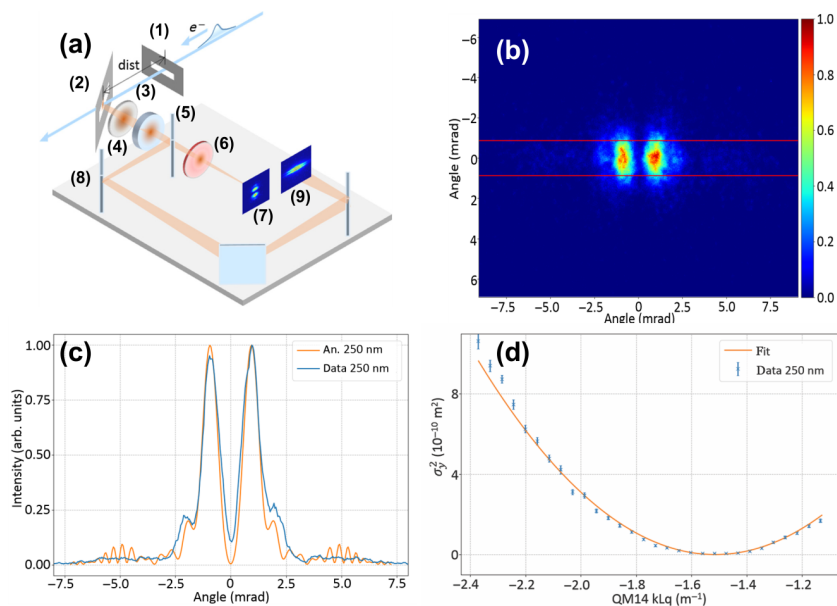

Figure 63: Schematic drawing of the optical instrument (*a*): mask slit (1), target slit (2), polarizer (3), lens (4), optical beam splitter (5), mirrors (8), filter wheel (6). Both images (9) and the angular distribution (7) of the ODR intensity of the electron bunches are recorded. Vertically polarized ODR at 250 nm from a 49.57 μm -wide slit (*b*). Projection of vertical polarization component (*c*); Square of the beam size measured with ODR for UV light (250 nm) as a function of the quadrupole magnetic strength. A parabolic fit is shown as a solid orange line (*d*).

a schematic drawing of the experimental arrangement. A charged particle beam moved through a slit in a conducting screen. Imaging part was used to measure the beam size with OTR (to cross check the ODR measurement) and to centre the beam in the slit for ODR measurement. The angular distribution arrangement was used for beam size measurement as the visibility of the angular distribution depends on the beam size. A typical UV-DR angular pattern of the vertical polarization component is depicted in Fig. 63,b. The vertical projection of the angular pattern is shown in Figure 63,c. The beam size as a function of the quadrupole field strength is shown in Figure 63,d. The resolution for the beam size measurements was 3 μm. The vertical beam emittance extracted from the quadrupole scan was 32 ± 5 pm rad. Both OTR and ODR technologies can be applied simultaneously to measure low intensity pilot beams using OTR and highly intense beam using ODR.

4.4.5.4 Cherenkov diffraction radiation as a promising technique for beam diagnostics.

Cherenkov effect refers to the emission of broadband electromagnetic radiation from a fast charged particle travelling inside a dielectric with the speed greater than the speed of light inside the medium. Since the discovery in 1934 a numerous range of applications have been developed for radiation generation, particle detection and identification. Cherenkov radiation can be generated when the charged

particle moves in the vicinity of and parallel to a dielectric interface. Due to finite boundaries of a radiator and the lack of direct interaction with the medium the phenomenon was called Cherenkov diffraction radiation (ChDR). On top of non-invasive nature, ChDR has two key advantages in comparison with OTR
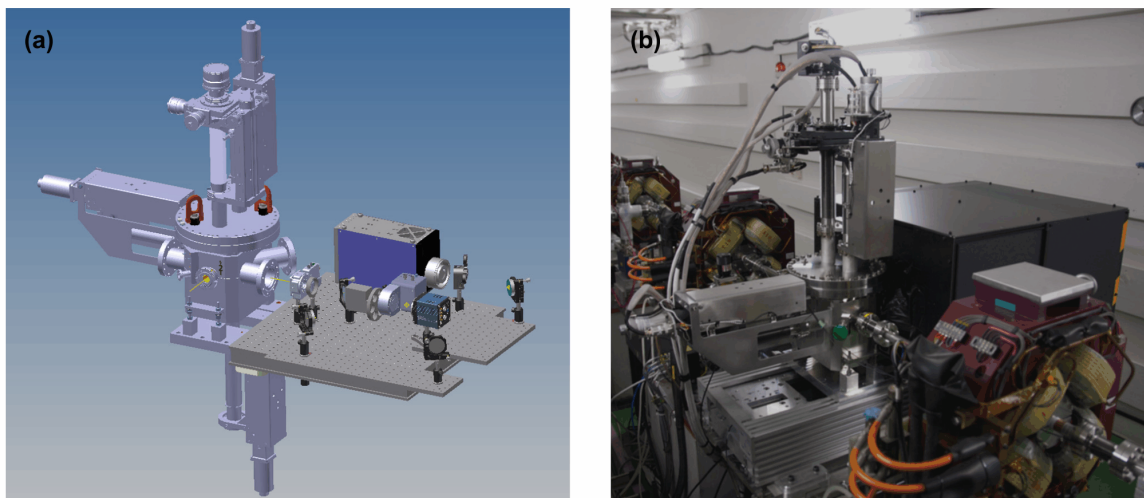

Figure 64: Schematic illustration of the tank and optical instrument (*a*), and the tank and optical instrument installed in the extraction line of ATF2 (*b*).

and ODR: the photon yield is proportional to the length of the radiator and its direction angle is defined by the dielectric properties of the medium and defined as $\cos\theta = 1/\beta n$, where n is the refractive index. The ChDR phenomenon has a potential to be applied for transverse beam size, position, bunch length and arrival time diagnostics. Moreover, coherent part of the spectrum can be applied for generation of intense THz radiation beams, drive-witness acceleration scheme and for introducing energy chirp. Despite of the great potential for beam instrumentation a detailed theoretical and experimental investigations are needed. The direct observation of incoherent ChDR in optical wavelength range and its detailed investigation have been performed in Refs. [107, 108]. The research has clearly demonstrated its basic characteristics. In [109] we have applied coherent ChDR in millimeter wavelength range for longitudinal beam size and profile diagnostics. At ATF2 facility we have proposed to reuse the equipment used for OTR/ODR studies (see Fig. 64) and investigate ChDR characteristics as a tool for transverse beam size, emittance and position diagnostics. An extremely low emittance beam of ATF2 can challenge any diagnostics equipment and demonstrate its strengths and weaknesses. The experimental work was performed in frame of international collaboration spanning KEK, CERN (Switzerland), RHUL, Daresbury Laboratory and Diamond LS (UK), TPU and Belgorod University (Russia).

5 Utilization of ATF/ATF2 beam for R&D beyond Linear Colliders

ATF is a test accelerator for technology development, which is flexible in operation and can provide the opportunity to perform R&D not only for LC technology development but also for other technology development using electron beam. Therefore, we first sought potential interest in the application and use of ATF electron beams from the Japanese accelerator community. Here, we will provide a beam for these R&Ds while the preparation of their experimental equipment is expected by their resources. Some ideas were submitted by interested people. We expect that overseas researchers will also have the some interests when we spread the inquiry widely. The proposals obtained can be grouped into two categories. The first is that the experimental setup can be implemented relatively easily, just like installing the setup at the beamline. The other is proof of principle experiments, some of which require further development of experimental equipment.

5.1 Proposals that can be implemented relatively easily

Development of SuperKEKB Fast Kicker:

The SuperKEKB, which is advancing high luminosity experiments, added a damping ring to the low energy section of the injector linac for highly efficient beam injection to the SuperKEKB ring. Stable extraction of the low emittance beam from the damping ring is important for increasing a performance of SuperKEKB. Two bunches separated by 90 ns are extracted from the damping ring simultaneously. The Beam Control Group of SuperKEKB is planning to use a fast kicker to correct the orbit of the second bunch. However, since their injector linac and damping ring are operating continuously for the injections into the SuperKEKB and Photon Facility, the available R&D beam time is very limited. With its low emittance beam and high precision cavity BPM, the ATF2 beamline is expected to be an ideal test bench for the development of SuperKEKB fast kicker.

Development of SuperKEKB OTR Monitor:

R&D at ATF2 beamline is proposed because the R&D is not timely conducted by the limited beam time for study and also limited access to the beamline when the SuperKEKB is running. On the other hand, it is much flexible at ATF.

Test of advanced beam control by new betatron feedback scheme, AC multiple magnets, and ultra-fast quadrupole kicker

Betatron feedback is the key for stable high average and/or bunch current beams of rings. Its conventional scheme calculates the kick with the turn-by-turn beam position data taken with a single BPM, and the coupling between the kick and the positions limits the maximum stable feedback gain. New scheme that calculates the kick with one turn position data at multiple location in the ring is proposed to eliminate this coupling to achieve higher gain. Also, feedback for the relative motion of the bunch head and tail (HT) was proposed for single-bunch instabilities. The HT motion is extracted with the difference of the parity of the BPM signals of the center of mass motion and of the HT motion, and the different kicks for the head and tail is produced efficiently with new driving technique or with low Q cavity kicker.

The strengths of non-linear and coupling resonances depend on betatron tunes of a ring. If a resonance is excited with an AC multipole or an AC skewed magnet, the constraints on the tunes are eliminated, and the resonance is produced just by the AC magnet. With this, the pulsed multipole magnet injection scheme can be replaced by resonance injection driven by a weaker AC magnet. And AC skewed quadrupole magnet drives x-y coupling and enlarge bunch volume to reduce intra-bunch scattering, with the switching-off the coupling with nano second skew quadrupole kicker just at the neighborhood timing of the injected bucket.

Nano-second pulsed quadrupole kicker for the injection to narrow aperture is developed with minimizing the effect on the stored beam to a nano second duration, much shorter than with a pulsed quadrupole magnet of which pulse length is hundreds nano seconds.

The ATF damping ring is the unique machine in the world for the test of new concept and devices like shown above, because of its high-quality beam, the high-performance instruments and its variety of operation modes.

Accelerator Control System:

Test and demonstration of the accelerator control system, White Rabbit (WR), developed by CERN for the future large accelerator is proposed. It is based on the synchronization between control nodes in $O(100 \text{ ps})$ accuracy. Delivery of the timing signals and RF clocks, the distributed DAQ will be investigated with the beam. ATF will be a suitable start point at KEK and bring a knowledge and experience to improve the control of KEK accelerators.

Detector R&D on the radiation resistance:

Test of the radiation resistance of detector by using low energy electron beam at the ATF LINAC

is proposed. The electron beam which energy from 80 to 100 MeV will be injected into a target and the beam spread by the multiple scattering hits the detector. Total amount of beam electrons demanded is from 10^{11} to 10^{15} and it corresponds to from 3 sec to 90 hours. The present study is conducting at the linac of Tohoku university, where 3-hours travel from KEK, because of less availability of other electron accelerator occupied by physics users. Researchers want to do R&D at ATF where the experiment can be done by adding a shield for the test stand.

Among the detectors which may be tested, there is a special interest in the radiation tolerance of diamond sensors and of a new generation of cooled silicon sensors. Single crystal CVD diamond sensors are currently used at SuperKEKB and foreseen at future colliders such as ILC or CLIC. Significant data on radiation damage exists using protons and neutrons, but not electrons.

Gamma-ray source for user application:
A gamma ray source based on the Laser-Compton scattering (LCS) is in function for the user application at the Spring8 NewSUBARU storage ring (1.5 GeV). It supplies gamma ray from $2 \sim 33$ MeV by changing laser wavelength and has an available flux of 10^7 photons/sec. The mono-energetic polarized gamma-ray beam is used for fundamental study of physics and engineering. On the study of photo-nuclear reaction, the reaction cross sections are measured to improve its data base that is used for designing an electron accelerator. Data on energy and angular distribution of particles from the reaction as a function of polarization are useful to update theoretical model implemented in a particle transport simulation code.

The optical cavity system that realizes high density laser pulses was developed at ATF DR (1.3 GeV) for the R&Ds of polarized positron source and the laser wire monitors. It produced gamma rays by LCS about 10^8 photons/sec and energy of $10 \sim 30$ MeV [110]. Therefore ATF has a potential to conduct R&Ds which need gamma rays.

Performance evaluation of ultra-short period undulator:
Synchrotron light sources with shorter wavelengths are always demanded to expand research fields in photon science. The undulator magnets with a very short a few mm-period length has been developed to bring the high energy radiation and realize the compact photon source. Recently the undulator magnet with 4 mm-period length was developed by KEK and tested at 50 MeV linac in Tohoku university [111]. Next step of the development is the performance evaluation, demonstration of the higher average brightness, by using the ring accelerator. Since a vertical gap of the developed undulator magnet is very short, 1 to 3 mm in operation while 20 mm in standby, it is difficult to test in the light-source rings where several experiments are conducting simultaneously. The ATF DR is capable to conduct this R&D and make contribution for the compact light source in future.

5.2 Proposals: the proof of principle experiments
Demonstration of seed FEL (CHG) utilizing extremely low vertical emittance:
In generally, the conventional scheme of FEL does not work for the beams in a storage ring by their long bunch lengths, even when the beam emittances are as small as those for linear accelerators. However, a novel scheme has been proposed to compress the beam density of the beam in the storage rings [112]. The idea is that the micro bunch structures are generated by applying the smaller energy modulation than the intrinsic energy spread to the beams in storage rings. The energy modulation is produced by a laser light in a specially designed dogleg layout. In this method, the extremely small vertival emittance is essential, and the vertical emittance of the ATF beam is enough small to produce the micro bunch beam structure. Since we will be able to confirm the method to product the micro bunch structure only by installing the dogleg and the laser in the ATF beamline, the proof of principle is proposed in the ATF extraction line to confirm the possibility of the future seed FEL in the storage ring.

Polarized gamma-ray beam generation assuming ILC:

As for an application of ILC beam, a polarized gamma-ray generation by a beam which energy of around 75 GeV has been discussed in the researchers group for ILC applications. It will bring a development, for example, on the hadron photoproduction experiment. To generate polarized gamma rays, high-energy electrons are passed through a thin plate of diamond crystal (thickness 20-50 μm), and coherent bremsstrahlung is generated by adjusting the passage angle with a precision automatic stage. In this case, a high-quality (low emittance) electron beam is required. Therefore, ATF is expected as the only place in Japan to promote the development of these coherent bremsstrahlung generation and the detectors before the ILC started. Using the existing electron beam extraction line, ATF2, a series of preparatory experiments are envisioned, including the development of new technologies for the future.

Electron beam focusing by active plasma lens:

Development of the plasma lens has been conducted, for example, for the plasma accelerators. A plasma-filled capillary is realized in a channel filled with a gas, and applying the current of several 100 A between electrodes at the end of a channel [113]. Researchers of Osaka University has been developed a plasma channel, 1 mm in diameter, 50 mm long and driven by a relatively high current, order of kA. They propose a development of the electron beam focusing by the plasma lens, which expects a focal length of 27 mm for 1.3 GeV ATF beam. The ATF2 beam can be used to pass the plasma channel and results of focusing will be measured by the beam profile monitor.

Test of the Lorentz invariance with high-precision photon beam:

Some types of the theory of quantum gravity introduce quantized space and time, resulting in the violation of the Lorentz invariance in the sense of a non-linear dispersion relation of light propagating in vacuum. A sub-picosecond photon beam generated by the inverse Compton scattering of an electron nano-beam and a very short laser pulse will provide a unique opportunity to make a test of the Lorentz invariance on the Earth's surface at the precision of $10^{-5} \sim 10^{-6}$ which corresponds to the search for new physics in the TeV energy region. A nano-beam of electron at ATF2 is considered to be the best suited facility for such a high-precision experiment concerning fundamental physics.

Strong-field QED experiments:

Following past experimental studies at SLAC, Michigan University, Osaka University and BNL there is an idea to perform a strong–field QED experiment for detailed investigation of collisions between the 1.28 GeV electrons and a 250 TW laser ($\lambda = 800$ nm, 25 fs). With the present advances in laser technology, and stable nano–beam availability at ATF2, new experiments to measure non–perturbative QED approaching the Schwinger critical field value can be considered. In addition to non–linear effects of Compton scattering with multiple photon absorption, the energy loss in the laser pulse, i.e. the radiation damping can be observed. Thus, the precise measurement can verify the strong QED in uncharted territory. The ATF2 nano beam is also unique for the Unruh radiation experiment [114] which is generated by quantum effect near the event horizon, which is similar to Hawking radiation. Therefore, it has received much attention for possible experimental verification from a broad international physics community [115]. The experimental condition when an electron is accelerated in the laser high electric field and radiates in the same direction can be realized at ATF2 with the major upgrade of the timings system, electron beam diagnostics (BSM monitor), incorporation of the 250 TW laser transport line and its final–focus system, development of the ultra–precise detectors, and several tens meter extension of the accelerator tunnel downstream of ATF2 IP.

Bibliography

[1] The International Linear Collider: Technical Design report (TDR) (2013),
https://ilchome.web.cern.ch/publications/ilc-technical-design-report .

[2] The International Linear Collider Machine Staging Report 2017", KEK 2017-3, DESY 17-180, CERN-ACC-2017-0097 (2017),
https://arxiv.org/ftp/arxiv/papers/1711/1711.00568.pdf .

[3] CLIC Conceptual Design Report (CDR), Volume 1 (2012),
http://project-clic-cdr.web.cern.ch/CDR_Volume1.pdf .

[4] "UPDATED BASELINE FOR A STAGED COMPACT LINEAR COLLIDER", CERN–2016–004 (2016),
http://dx.doi.org/10.5170/CERN-2016-004 .

[5] "The Compact Linear Collider (CLIC) - Project Implementation Plan", CERN–2018–010-M (2019),
https://arxiv.org/abs/1903.08655 .

[6] F. Hinode *et al.*, "ATF, Accelerator Test Facility, Design and Study Report", KEK Internal 95-4,
https://ilc.kek.jp/ATF/Pub/KEK-I-95-4.pdf .

[7] ATF2 Collaboration, "ATF2 Proposal", CERN-AB-2005-035, CLIC-Note-636, DESY-05-148, DESY-2005-148, ILC-ASIA-2005-22, JAI-2005-002, KEK-REPORT-2005-2, SLAC-R-771, UT-ICEPP-2005-02,
https://cds.cern.ch/record/855957/files/cer-002539108.pdf .

[8] ATF2 Group, "ATF2 Proposal Vol.2", DESY-06-001, CERN-AB-2006-004, ILC-ASIA-2005-26, JAI-2006-001, KEK-REPORT-2005-9, SLAC-R-796, UT-ICEPP-05-04,
https://arxiv.org/pdf/physics/0606194.pdf .

[9] P. Raimondi and A. Seryi, "Novel Final Focus Design for Future Linear Colliders", *Physical Review Letters*, **86**, 3779 (2001),
https://doi.org/10.1103/PhysRevLett.86.3779 .

[10] V. Balakin *et al.*, "Focusing of Submicron Beams for TeV-Scale e^+e^- Linear Colliders", *Physical Review Letters*, **74**, 2479 (1995),
https://doi.org/10.1103/PhysRevLett.74.2479 .

[11] R. Tomas, "Overview of the Compact Linear Collider", *Phys. Rev. ST Accel. Beams* **13**, 014801, (2010),
https://doi.org/10.1103/PhysRevSTAB.13.014801 .

[12] ATF2 Technical Review, ILC-GDE, April 3-4 (2013),
https://agenda.linearcollider.org/event/5973/ .

[13] Apsimon, R. J. *et al.* "Design and operation of a prototype interaction point beam collision feedback system for the International Linear Collider", *Phys. Rev. Accel. Beams* **21** 122802 (2018),
https://doi.org/10.1103/PhysRevAccelBeams.21.122802

[14] D.R. Bett et al, "A sub-micron resolution, dual-phase, bunch-by-bunch beam trajectory feedback system and its application to reducing wakefield effects in single-pass beamlines", submitted to Phys. Rev. Accel. Beams (2020) .

[15] KEK, "KEK-ILC Action Plan (rev. 2018)",
https://www.kek.jp/en/newsroom/KEK-ILC_ActionPlan_Addendum-EN%20%281%29.pdf .

[16] KEK, "Recommendations on ILC Project Implementation", October 1 (2019),
https://www2.kek.jp/ilc/en/docs/Recommendations_on_ILC_Project_
Implementation.pdf .

[17] International Linear Collider (ILC) Advisory Panel, MEXT, "Summary of the ILC Advisory Panel's Discussions to Date after Revision", July 4 (2018),
https://www.mext.go.jp/component/b_menu/shingi/toushin/__icsFiles/
afieldfile/2018/09/20/1409220_2_1.pdf .

[18] "Technical issues pointed out in the report by the Science Council of Japan (written in Japanese)", translated in Sec.4 of ref. [16], original report (Dec. 19, 2018) is available below.

http://www.scj.go.jp/ja/info/kohyo/pdf/kohyo-24-k273.pdf .

[19] C. Belver-Aguilar *et al.*, "Stripline Design for the Extraction Kicker of Compact Linear Collider Damping Rings", *Phys. Rev. ST Accel. Beams* **17**, 071003 (2014), https://doi.org/10.1103/PhysRevSTAB.17.071003 .

[20] J. Holma and M. J. Barnes, "Prototype Inductive Adders With Extremely Flat-top Output Pulses for the Compact Linear Collider at CERN", *IEEE Trans. Plasma Sci.*, Vol 46., No 10, Oct. (2018), https://doi.org/10.1109/TPS.2018.2836310 .

[21] B.J.A. Shepherd *et al.*, "Tunable high-gradient permanent magnet quadrupoles", *JINST* 9 T11006 (2014) https://iopscience.iop.org/article/10.1088/1748-0221/9/11/T11006/pdf .

[22] C. Adolphsen *et al.*, "Design of the ILC crab cavity system", *EUROTEV-REPORT-2007-010* (2007), https://doi.org/10.2172/915387 .

[23] M. Liepe, "Review on progress in RF control systems", in presentation given at *12th International Workshop on RF Superconductivity* (2005), http://www.lepp.cornell.edu/public/SRF2005/talks/thursday/ThA08_talk_srf2005.pdf .

[24] D. J. Scott *et al.*, "Demonstration of a High-Field Short-Period Superconducting Helical Undulator Suitable for Future TeV-Scale Linear Collider Positron Sources", *Physical Review Letters*, **107**, 174803 (2011), https://link.aps.org/doi/10.1103/PhysRevLett.107.174803 .

[25] T. Nakanishi *et al.*, *Nucl. Instrum. Meth.*, **A455**, 109 (2000), https://doi.org/10.1016/S0168-9002(00)00715-4 .

[26] K. Kubo *et al.*, "Extremely Low Vertical-Emittance Beam in the Accelerator Test Facility at KEK", *Physical Review Letters*, **88**, 194801 (2002), https://doi.org/10.1103/PhysRevLett.88.194801 .

[27] Kiyoshi Kubo. "Simulation study of low emittance tuning of the accelerator test facility damping ring at KEK", *Phys. Rev. ST Accel. Beams* **6**, 092801 (2003), https://doi.org/10.1103/PhysRevSTAB.6.092801 .

[28] Y. Honda *et al.*, "Achievement of Ultralow Emittance Beam in the Accelerator Test Facility Damping Ring", *Physical Review Letters*, **92**, 054802 (2004), https://doi.org/10.1103/PhysRevLett.92.054802 .

[29] T. Shintake, "Proposal of a nanometer beam size monitor for e+e-] linear colliders", *Nucl. Instrum. Meth. A* **311**, 455 (1992), https://doi.org/10.1016/0168-9002(92)90641-G .

[30] Y. Yamaguchi, Master thesis at Graduate School of Science, The University of Tokyo(2010).

[31] T. Suehara *et al.*, "A nanometer beam size monitor for ATF2", *Nucl. Instrum. Meth. A* **616**, 1 (2010), https://doi.org/10.1016/j.nima.2010.02.065 .

[32] T. Yasui, Master thesis at Graduate School of Science, The University of Tokyo(2018).

[33] T. Okugi *et al.*, "Linear and second order optics corrections for the KEK Accelerator Test Facility final focus beam line", *Phys. Rev. ST Accel. Beams* **17**, 023501 (2014), https://doi.org/10.1103/PhysRevSTAB.17.023501 .

[34] T. Okugi, "Achievement of small beam size at atf2 beamline", in *Proc. of LINAC'16, East Lansing, MI, USA*, MO3A02 (2016), https://accelconf.web.cern.ch/linac2016/papers/mo3a02.pdf .

[35] G. White *et al.*, "Experimental Validation of a Novel Compact Focusing Scheme for Future Energy-Frontier Linear Lepton Colliders", *Phys. Rev. Lett.* **112**, 034802 (2014), https://doi.org/10.1103/PhysRevLett.112.034802 .

[36] K. Kubo, "Towards an International Linear Collider: Experiments at ATF2", in *Proc. of the IPAC'14*, WEZA01 (2014),
https://doi.org/10.18429/JACoW-IPAC2014-WEZA01 .

[37] S. Kuroda, "ATF2 for final focus test beam for future linear colliders", in *Proc. of the ICHEP2014* (2014),
https://doi.org/10.1016/j.nuclphysbps.2015.09.030 .

[38] N. Blaskovic Kraljevic *et al.*, "Development of a Low-latency, Micrometre-level Precision, Intra-train Beam Feedback System based on Cavity Beam Position Monitors", in *Proc. of the IPAC'16*, THPOR035 (2016),
https://doi.org/10.18429/JACoW-IPAC2016-THPOR035 .

[39] Y. Kano, Master thesis at Graduate School of Science, The University of Tokyo(2016).

[40] T. Okugi *et al.*, "Beam jitter reduction with FONT intra-train feedback at ATF2", in *Proc. of the 13th Annual Meeting of Particle Accelerator Society of Japan*, MOOL04 (2016),
https://www.pasj.jp/web_publish/pasj2016/proceedings/PDF/MOOL/MOOL04.pdf .

[41] R. Tomás *et al.*, "ATF2 Ultra-Low IP Betas Proposal", in *Proc. of the PAC'09, Vancouver, Canada*, WE6PFP024 (2009),
https://accelconf.web.cern.ch/PAC2009/papers/we6pfp024.pdf .

[42] E. Marin *et al.*, "Scenarios For The ATF2 Ultra-Low Betas Proposal", in *Proc. of IPAC'10, Kyoto, Japan*, THPE020 (2010),
https://accelconf.web.cern.ch/IPAC10/papers/thpe020.pdf .

[43] E. Marin *et al.*, "Design and high order optimization of the accelerator test facility lattices", *Phys. Rev. ST Accel. Beams* **17**, 021002 (2014),
https://doi.org/10.1103/PhysRevSTAB.17.021002 .

[44] M. Patecki *et al.*, "Towards Ultra-Low beta* in ATF2", in *Proc. of the IPAC'15, Richmond, USA*, MOBC1 (2015),
https://doi.org/10.18429/JACoW-IPAC2015-MOBC1 .

[45] M. Patecki *et al.*, "Probing half β_y^* optics in the Accelerator Test Facility 2", *Phys. Rev. ST Accel. Beams* **19**, 101001 (2016),
https://doi.org/10.1103/PhysRevAccelBeams.19.101001 .

[46] R. Tomás, "Nonlinear optimization of beam lines", *Phys. Rev. ST Accel. Beams* **9**, 081001 (2006),
https://doi.org/10.1103/PhysRevSTAB.9.081001 .

[47] M. Patecki and R. Tomás, "Effects of quadrupole fringe fields in final focus systems for linear colliders", *Phys. Rev. ST Accel. Beams* **17**, 101002 (2014),
https://doi.org/10.1103/PhysRevSTAB.17.101002 .

[48] F. Plassard, "Optics optimization of longer L* Beam Delivery System designs for CLIC and tuning of the ATF2 final focus system at ultra-low beta* using octupoles", PhD thesis, Universite Paris-Saclay, Orsay, France, (2018),
http://cds.cern.ch/record/2646086/files/CERN-THESIS-2018-223.pdf .

[49] A. Pastushenko, "Nonlinear optimization of the ultra-low beta* optics", talk at the International Workshop on Future Linear Collider, (2019),
https://agenda.linearcollider.org/event/8217/contributions/44511/attachments/34958/54033/LCWS_2019_ATF2_oct_29_10_2019__2.pdf .

[50] R. Yang *et al.*, "Tuning the ultra-low beta* optics at the KEK Accelerator Test Facility 2", *Phys. Rev. Accel. Beams* **23**, 071003, (2020),
https://doi.org/10.1103/PhysRevAccelBeams.23.071003

[51] A. Jeremie *et al.*, "Recent progress on GM studies at ATF2", talk at *the CLIC Workshop* (2018),
https://indico.cern.ch/event/656356/contributions/2832990/attachments/1587569/2510668/CLICWS2018ATF2GM_ajc.pdf

[52] T. Okugi *et al.*, "Intensity dependence of ATF2 virtual IP beam size (in Japanese)", in *Proc. of the 16th Annual meeting of particle accelerator society of Japan*, FRPI023 (2019),
https://www.pasj.jp/web_publish/pasj2019/proceedings/PDF/FRPI/FRPI023.pdf .

[53] T. Okugi *et al.*, "Intensity dependence simulation of ILC IP beam size (in Japanese)", in *Proc. of the 16th Annual meeting of particle accelerator society of Japan*, FRPI024 (2019),
https://www.pasj.jp/web_publish/pasj2019/proceedings/PDF/FRPI/FRPI024.pdf .

[54] P. Korysko *et al.*, "Intensity dependent effects at ATF2, KEK", in *Proc. of IPAC'19, Melbourne, Australia*, MOPGW086 (2019),
https://doi.org/10.18429/JACoW-IPAC2019-MOPGW086 .

[55] Kiyoshi Kubo, Alexey Lyapin, and Jochem Snuverink. "Wakefield issues for the linear colliders", *ICFA Beam Dyn. Newslett.*, Vol. 61, pp. 69–85, (2013),
https://icfa-usa.jlab.org/archive/newsletter/icfa_bd_nl_61.pdf .

[56] W. Bruns, "GdfidL: A finite difference program with reduced memory and CPU usage", in *Proc. of PAC'97, Vancouver, BC, Canada*, (IEEE, New York, 1997), p. 2651,
http://www.gdfidl.de .

[57] J. Snuverink *et al.*, "Measurements and simulations of wakefields at the Accelerator Test Facility 2", *Phys. Rev. Accel. Beams* **19**, 091002 (2016),
https://doi.org/10.1103/PhysRevAccelBeams.19.091002 .

[58] K. Kubo, "ILC new luminosity design and small beam experiments at ATF", in *Talk at the Asian Linear Collider Workshop, ALCW2018, Fukuoka, Japan* (2018),
https://agenda.linearcollider.org/event/7826/contributions/41272/ .

[59] K. Kubo *et al.*, "Extremely low vertical emittance beam in accelerator test facility at KEK", *Phys. Rev. Lett.* **88**, 194801 (2002),
https://journals.aps.org/prl/pdf/10.1103/PhysRevLett.88.194801

[60] M. Patecki *et al.*, "Contribution of Optical Aberrations to Spot-size Increase with Bunch Intensity at ATF2", in *Proc. of IPAC'15, Richmond, USA*, MOPJE065 (2015),
https://accelconf.web.cern.ch/IPAC2015/papers/mopje065.pdf

[61] O. Blanco Garcia, "Beam dynamics in the final focus section of the future linear collider", (2015), PhD thesis, Orsay, LAL (2015),
https://inspirehep.net/literature/1429601 .

[62] N. Blaskovic Kraljevic, "Development of a high-precision low-latency position feedback system for single-pass beamlines using stripline and cavity beam position monitors", D.Phil. thesis, University of Oxford (2015),
https://ora.ox.ac.uk/objects/uuid:0286d951-d177-4d3a-8bce-a50e6ccb8645 .

[63] R. Ramjiawan, "Development of feedback algorithms for future linear colliders", D.Phil. thesis, University of Oxford (2019),
https://ora.ox.ac.uk/objects/uuid:1c17df3b-35ce-48d1-8740-d9227b9cfe0d .

[64] Y. I. Kim *et al.*, "Cavity beam position monitor system for the Accelerator Test Facility 2", *Phys. Rev. ST Accel. Beams* **15**, 042801 (2012),
https://doi.org/10.1103/PhysRevSTAB.15.042801 .

[65] S. Bai *et al.*, "First beam waist measurements in the final focus beam line at the KEK Accelerator Test Facility", *Phys. Rev. ST Accel. Beams* **13**, 092804 (2010),
https://doi.org/10.1103/PhysRevSTAB.13.092804 .

[66] S. Liu *et al.*, "Development of Diamond Sensors for Beam Halo and Compton Spectrum Diagnostics after the Interaction Point of ATF2", in *Proc. of IPAC'13, Shanghai, China*, MOPME003 (2013),
https://accelconf.web.cern.ch/IPAC2013/papers/mopme003.pdf .

[67] Apsimon, R. J. *et al.* "Design and performance of a high resolution, low latency stripline beam

position monitor system", *Phys. Rev. ST Accel. Beams* **18** 032803 (2015),
https://doi.org/10.1103/PhysRevSTAB.18.032803 .

[68] N. Blaskovic Kraljevic *et al.* "Optimisation of a high-resolution, low-latency stripline beam position monitor system for use in intra-train feedback", in *Proc. of IPAC'17, Copenhagen, Denmark*, TUPIK110 (2017),
https://doi.org/10.18429/JACoW-IPAC2017-TUPIK110 .

[69] Y. Inoue *et al.*, "Development of a high-resolution cavity-beam position monitor", *Phys. Rev. ST Accel. Beams* **11**, 062801 (2008),
https://doi.org/10.1103/PhysRevSTAB.11.062801 .

[70] Bromwich, T. "Development of high-resolution cavity beam position monitors for use in low-latency feedback systems", D.Phil. thesis, University of Oxford (2018),
https://groups.physics.ox.ac.uk/font/thesis/thesisBromwich.pdf .

[71] T. Bromwich *et al.*, "Performance of Nanometre-Level Resolution Cavity Beam Position Monitors at ATF2", in *Proc. of IPAC'18, Vancouver, BC, Canada*, TUZGBD5 (2018),
https://doi.org/10.18429/JACoW-IPAC2018-TUZGBD5 .

[72] R. Ramjiawan *et al.* "Development of a low-latency, high-precision, beam-based feedback system based on cavity BPMs at the KEK ATF2", in *Proc. of IPAC'18, Vancouver, Canada*, WEPAL025 (2018),
https://doi.org/10.18429/JACoW-IPAC2018-WEPAL025 .

[73] S. Liu *et al.*, "In vacuum diamond sensor scanner for beam halo measurements in the beam line at the KEK Accelerator Test Facility", *Nucl. Instrum. Meth. A* **832** 231-242 (2016),
https://doi.org/10.1016/j.nima.2016.06.122 .

[74] T. Naito, T. Mitsuhashi, "Beam halo measurement utilizing YAG: Ce screen", in *Proc. of the IBIC2015, Melbourne, Australia*, 373-376 (2016),
https://doi.org/10.18429/JACoW-IBIC2015-TUPB024 .

[75] R. Yang *et al.*, "Development of a YAG/OTR monitor for beam halo diagnostics", in *Proc. of the IBIC2018, Shanghai, China*, 429-432 (2018),
https://doi.org/10.18429/JACoW-IBIC2018-WEPB02 .

[76] R. Yang *et al.*, "Numerical investigation of beam halo from beam gas scattering in KEK-ATF", in *Journal of Physics: Conference Series, Vol.* **874**, (2017),
https://doi.org/10.18429/JACoW-IPAC2017-THPVA002 .

[77] R. Yang *et al.*, "Evaluation of beam halo from beam-gas scattering at the KEK Accelerator Test Facility", *Phys. Rev. Accel. Beams* **21**, 051001 (2018),
https://doi.org/10.1103/PhysRevAccelBeams.21.051001 .

[78] J. Pfingstner *et al.*, "Mitigation of ground motion effects in linear accelerators via feed-forward control", *Phys. Rev. ST Accel. Beams* **17**, 122801 (2014),
https://doi.org/10.1103/PhysRevSTAB.17.122801 .

[79] D.R. Bett *et al.*, "Compensation of orbit distortion due to quadrupole motion using feed-forward control at KEK ATF", *Nucl. Instrum. Meth. A* **895** 10-18 (2018),
https://doi.org/10.1016/j.nima.2018.03.037 .

[80] T. Naito *et al.*, "Development of a 3ns rise and fall time strip-line kicker for the international linear collider", *Nucl. Instrum. Meth. A* **571**, 599-607 (2007),
https://doi.org/10.1016/j.nima.2006.11.062 .

[81] T. Naito *et al.*, "Multibunch beam extraction using the strip-line kicker at the KEK Accelerator Test Facility", *Phys. Rev. ST Accel. Beams* **14**, 051002 (2011),
https://doi.org/10.1103/PhysRevSTAB.14.051002 .

[82] A. Lyapin *et al.*, "Development of the S-Band BPM System for ATF2", in *Proc. of PAC'09, Vancouver, Canada*, TH6REP025 (2009),

https://accelconf.web.cern.ch/PAC2009/papers/th6rep025.pdf .

[83] Y. Kim *et al.*, "Cavity Beam Position Monitor at Interaction Point Region of Accelerator Test Facility 2", in *Proc. of IPAC'13, Shanghai, China*, MOPWA058 (2013) https://accelconf.web.cern.ch/IPAC2013/papers/mopwa058.pdf .

[84] A. Lyapin *et al.*, "Cavity BPM system for ATF2", in *Proc. of DIPAC2011, Hamburg, Germany*, MOOC02 (2011), https://accelconf.web.cern.ch/DIPAC2011/papers/mooc02.pdf .

[85] S. T. Boogert, F. J. Cullinan, N. Y. Joshi and A. Lyapin, "Position Determination of Closely Spaced Bunches using Cavity BPMs," *Conf. Proc. C* **110904**, 1419-1421 (2011), https://accelconf.web.cern.ch/IPAC2011/papers/TUPC164.PDF .

[86] S. W. Jang *et al.*, "Development of a cavity-type beam position monitors with high resolution for ATF2", in *Proc. of IPAC'13, Shanghai, China*, MOPME058 (2013), https://accelconf.web.cern.ch/IPAC2013/papers/mopme058.pdf .

[87] S. W. Jang *et al.*, "Development of a Low- Q Cavity-Type Beam Position Monitoring System," *IEEE Trans. Nucl. Sci.* **64**, no.8, 2353-2360 (2017) https://doi.org/10.1109/TNS.2017.2718033 .

[88] P. Bambade *et al.*, "In Vacuum High Accuracy Mechanical Positioning System of Nano Resolution Beam Position Monitor at the Interaction Point of ATF2", in *Proc. of IPAC'13, Shanghai, China*, TUOCB203 (2013), https://accelconf.web.cern.ch/IPAC2013/papers/tuocb203.pdf .

[89] S. Liu *et al.*, "Status of Diamond Detector Development for Beam Halo Investigation at ATF2", in *Proc. of IPAC'14, Dresden, Germany*, THPME092 (2014), https://doi.org/10.18429/JACoW-IPAC2014-THPME092 .

[90] J. B. Jeanneret, "Optics of a two-stage collimation system", *Phys. Rev. ST Accel. Beams* **1**, 081001 (1998), https://doi.org/10.1103/PhysRevSTAB.1.081001 .

[91] N. Fuster-Martínez P.h.D. thesis, "Beam Halo Collimation and Induced Wakefield Studies for Future Linear Colliders: the ATF2 Case", http://roderic.uv.es/handle/10550/59295 .

[92] N. Fuster-Martínez *et al.*, "Design study and feasibility study of a transverse beam halo collimation system for ATF2", in *Proc. of IPAC'14, Dresden, Germany*, MOPRO033 (2014), https://doi.org/10.18429/JACoW-IPAC2014-MOPRO033 .

[93] N. Fuster-Martínez *et al.*, "Beam halo collimation studies and measurements at the Accelerator Test Facility ATF2", *Nucl. Instrum. Meth. A* **917** 31-42 (2019), https://doi.org/10.1016/j.nima.2018.11.128 .

[94] J. D. A. Smith, "Full Structure Simulations of ILC collimators", in *Proc. of PAC'09, Vancouver, BC, Canada*, FR5RFP041 (2009), https://accelconf.web.cern.ch/PAC2009/papers/fr5rfp041.pdf .

[95] N. Fuster-Martínez *et al.*, "Commissioning and first performance studies of a single vertical beam halo collimation system at ATF2", in *Proc. of IPAC16, Busan, South Korea*, THPOR030 (2016), https://doi.org/10.18429/JACoW-IPAC2016-THPOR030 .

[96] S.T. Boogert *et al.*, "Micron-scale laser-wire scanner for the kek accelerator test facility extraction line", *Phys. Rev. ST Accel. Beams* **13**, 122801 (2010), https://doi.org/10.1103/PhysRevSTAB.13.122801 .

[97] L. Nevay *et al.*, "Laserwire at the accelerator test facility 2 with submicrometer resolution", *Phys. Rev. ST Accel. Beams* **17**, 072802 (2014), https://doi.org/10.1103/PhysRevSTAB.17.072802

[98] L. Corner *et al.*, "Laserwire: A high resolution non-invasive beam profiling diagnostic", *Nucl.*

Instrum. Meth. A **740**, 226 (2014),
https://doi.org/10.1016/j.nima.2013.10.043 .

[99] A. Faus-Golfe *et al.*, "upgrade and systematic measurement campaign of the ATF2 multi-OTR system", in *Proc. of IPAC'13, Shanhai, China*, MOPWO023 (2013),
https://accelconf.web.cern.ch/IPAC2013/papers/mopwo023.pdf .

[100] A. Faus-Golfe *et al.*, "Multi-OTR System for ATF2", *Physics Procedia, Volume 37*, 2072-2079 (2012),
https://doi.org/10.1016/j.phpro.2012.02.525 .

[101] A. Faus-Golfe *et al.*, "Emittance reconstruction from measured beam sizes in ATF2 and perspectives for ILC", *Nucl.Instrum.Meth. A819*, 122-138 (2016),
https://doi.org/10.1016/j.nima.2016.02.064 .

[102] P. Karataev, *et al.*, "First Observation of the Point Spread Function of Optical Transition Radiation", *Phys. Rev. Lett.* **107**, 174801 (2011),
https://doi.org/10.1103/PhysRevLett.107.174801 .

[103] A. Aryshev, *et al.*, "Sub-micron Scale Transverse Electron Beam Size Diagnostics Methodology Based on the Analysis of Optical Transition Radiation Source Distribution", *Journal of Inst.* **15** P01020 (2020),
https://doi.org/10.1088/1748-0221/15/01/P01020 .

[104] T. Muto, *et al.*, "Observation of incoherent diffraction radiation from a single edge target in the visible light region", *Phys. Rev. Lett.* **90**, 104801 (2003),
https://doi.org/10.1103/PhysRevLett.90.104801 .

[105] P. Karataev, *et al.*, "Beam-Size Measurement with Optical Diffraction Radiation at KEK Accelerator Test Facility", *Phys. Rev. Lett.* **93**, 244802 (2004),
https://doi.org/10.1103/PhysRevLett.93.244802 .

[106] M. Bergamaschi, *et al.*, "Non-invasive micron-scale particle beam size measurement using Optical Diffraction Radiation in the ultra violet wavelength range", *Phys. Rev. Appl.* **13**, 014041 (2020),
https://doi.org/10.1103/PhysRevApplied.13.014041 .

[107] R. Kieffer, *et al.*, "Direct observation of incoherent Cherenkov diffraction radiation in the visible range", *Phys. Rev. Lett.* **121**, 054802 (2018),
https://doi.org/10.1103/PhysRevLett.121.054802 .

[108] R. Kieffer, *et al.*, "Generation of incoherent Cherenkov diffraction radiation in Synchrotrons", *Phys. Rev. ST Acc. Beams* **23**, 042803 (2020),
https://doi.org/10.1103/PhysRevAccelBeams.23.042803 .

[109] A. Curcio, M. Bergamaschi, *et al.*, "Non-invasive bunch length measurements exploiting Cherenkov Diffraction Radiation", *Phys. Rev. ST Acc. Beams* **23**, 022802 (2020),
https://doi.org/10.1103/PhysRevAccelBeams.23.022802 .

[110] T. Akagi *et al.*, "Development of a three dimensional four mirror optical cavity for laser-Compton scattering", *Nucl. Instrum. Meth. A* **724**, 63-71 (2013),
https://doi.org/10.1016/j.nima.2013.04.066 .

[111] S. Yamamoto *et al.*, "Light source based on a 100 mm-long monolithic undulator magnet with a very short 4 mm-period length", in *Journal of Synchrotron Rad.* **26**, 1902–1910 (2019),
https://doi.org/10.1107/S1600577519013031 .

[112] C. Feng and Z. Zhao, "A Storage Ring Based Free-Electron Laser for Generating Ultrashort Coherent EUV and X-ray Radiation", *Scientific Reports*, **7**, 4724 (2017),
https://doi.org/10.1038/s41598-017-04962-5 .

[113] J. van Tilborg *et al.*, "Active Plasma Lensing for Relativistic Laser-Plasma-Accelerated Electron Beams", *Phys. Rev. Lett.* **115**, 184802 (2015),
https://doi.org/10.1103/PhysRevLett.115.184802 .

[114] P. Chen, *et al.*, "Testing Unruh radiation with ultraintense lasers", *Phys. Rev. Lett.* **83.2**, 256, (1999),
https://journals.aps.org/prl/abstract/10.1103/PhysRevLett.83.256

[115] M. Altarelli, *et al.*, "Summary of strong-field QED Workshop", *arXiv preprint* arXiv:1905.00059, (2019),
https://arxiv.org/pdf/1905.00059.pdf

Appendix

A   The ATF International Collaboration

The ATF International Collaboration was established in 2005, to cooperate in the technical research and development of the final focus system of the future linear collider. This collaboration is based on the memorandum of understandings (MoU) [8] which was signed by representatives of the participating institutes around the world (listed in Table. A.1). These institutions cooperate with the participation of researchers from other related research laboratories and universities.

Table A.1: Institution that has concurred and signed the Memorandum of Understanding for the ATF2 project.

Region	Institution
Asia	Advanced Research Institute for Science and Engineering, Waseda University
	Department of Physics, Kyoto University
	Department of Physics, Nagoya University
	High Energy Accelerator Research Organization (KEK)
	ICEPP, the University of Tokyo
	Graduate School of Advanced Sciences of Matter, Hiroshima University
	Institute of High Energy Physics, Beijing (IHEP)
	Pohang Accelerator Laboratory (PAL)
Europe	Department of Physics and Astronomy, University College London
	Deutsches Elektronen-Synchrotron (DESY)
	European Organization for Nuclear Research (CERN)
	John Adams Institute for accelerator science
	Physics Department, Queen Mary, University of London
	Royal Holloway, University of London
	Applied Physics Department, Tomsk Polytechnie University
	Institut National de Physique Nucléaire de Physique des Particules (IN2P3)
	Instituto Nazionale di Fisica Nucleare (INFN)
North America	Fermi National Accelerator Laboratory (Fermilab)
	Laboratory for Elementary-Particle Physics, Cornall University (LEPP)
	Lawrence Berkeley National Laboratory (LBNL)
	Stanford Linear Accelerator Center (SLAC)

The organization structure is shown in Fig. A.1. The international Collaboration Board (ICB), which consists of delegates from participating institutions and directors from the international organization for linear collider which is originally the Global Design Effort (GDE) and the successor Linear Collider Collaboration (LCC), is responsible for making executive decisions. The Technical Board (TB), consisting of experts from participating institutions, advises the spokesperson in formulating the Annual Activity Plan and assessing the scientific progress. The System/Group Coordinators (SCGs) will coordinate the tasks charged to the assigned Systems or Groups, and will assist the Spokespersons and the Deputies coordinate the ATF/ATF2 research programs. The "Coordination Group", spokesperson with the Deputies and System/Group Coordinators, coordinates the details of the operation and development at ATF/ATF2 on a daily (during the beam operation period) or weekly (during the maintenance and construction period) basis. In most cases, ICB meetings are held annually at the International LC Workshop LCWS, which is held in sequence in Asia, America and Europe. At the meeting, we also discussed and extended the collaboration period. The current term is until the end of March 2021. The TB meetings have been held at various occasions such as LC workshop, ATF2 project meeting at participating institutions, CLIC workshop at CERN, etc. (Fig. A.2).
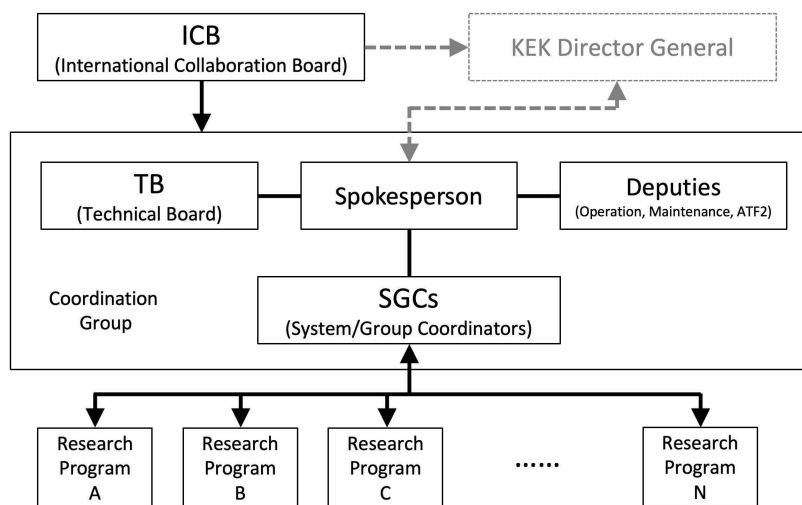
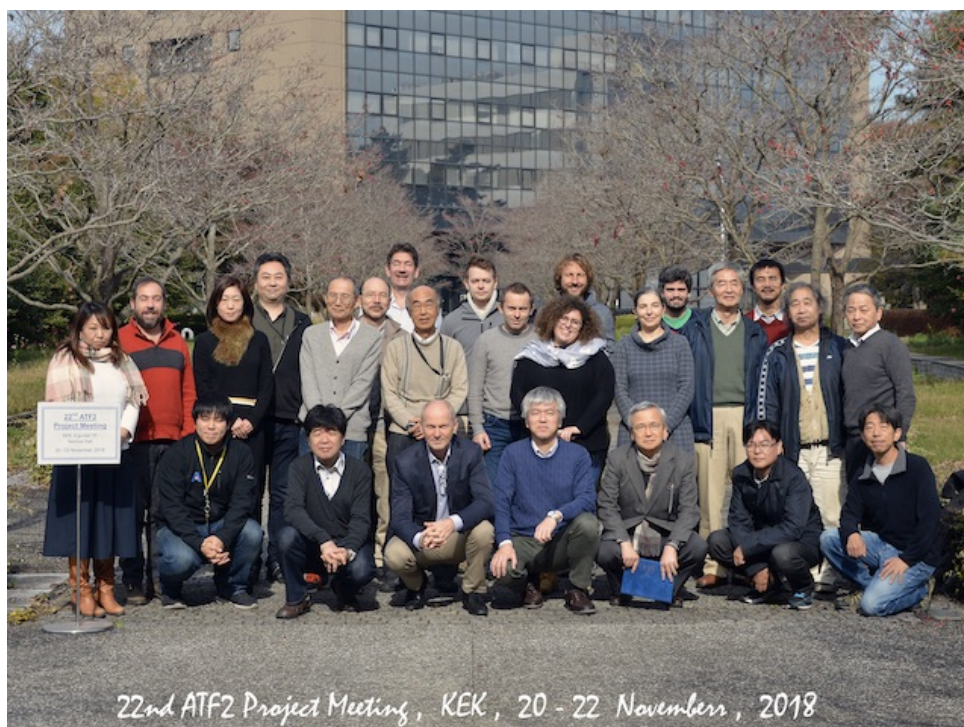**Figure A.1:** Structure of the ATF international Collaboration.

Figure A.2: Group photo of the ATF2 project meeting at KEK (2018).